NASA TN D-344




# TECHNICAL NOTE

## D-344

EXPERIMENTAL DETERMINATION OF THE PRESSURE DISTRIBUTION ON A RECTANGULAR WING OSCILLATING IN THE FIRST BENDING MODE FOR MACH NUMBERS FROM 0.24 TO 1.30

By Henry C. Lessing, John L. Troutman, and Gene P. Menees

Ames Research Center
Moffett Field, Calif.

NATIONAL AERONAUTICS AND SPACE ADMINISTRATION

WASHINGTON December 1960

NATIONAL AERONAUTICS AND SPACE ADMINISTRATION

TECHNICAL NOTE D-344

# EXPERIMENTAL DETERMINATION OF THE PRESSURE DISTRIBUTION ON A RECTANGULAR WING OSCILLATING IN THE FIRST BENDING MODE FOR MACH NUMBERS FROM 0.24 TO 1.30

By Henry C. Lessing, John L. Troutman, and Gene P. Menees

## SUMMARY

The results of an experimental investigation in a wind tunnel to obtain the aerodynamic pressure distribution on an unswept rectangular wing oscillating in its first symmetrical bending mode are presented. The wing was of aspect ratio 3 with 5-percent-thick biconvex airfoil sections. Data were obtained at $0^\circ$ and $5^\circ$ angle of attack in the Mach number range from 0.24 to 1.30 at Reynolds numbers, depending on the Mach number, ranging from 2.2 to 4.6 million per foot. The reduced frequencies, also a function of Mach number, ranged from 0.46 at $M = 0.24$ to 0.10 at $M = 1.30$.

The most important results presented are the chordwise distributions of the surface pressures generated by the bending oscillations. Similar data obtained under static conditions are also presented. The results show that the phenomena causing irregularities in the static pressure such as three-dimensional tip effects, local shock waves, and separation effects, will also produce significant changes in the oscillatory pressures. The experimental data are also compared with the oscillatory pressure distributions computed by means of the most complete linearized theories available. The comparison shows that subsonic linearized theory is adequate for predicting the pressures and associated phase angles at low subsonic speeds and low angles of attack for this wing. However, the appearance of local shock waves and flow separation as the Mach number and angle of attack are increased causes significant changes in the experimental data from that predicted by the theory. At the low supersonic speeds covered in the experimental investigation, linearized theory is completely inadequate, principally because of the detached bow wave caused by the wing thickness.

Some indication of wind-tunnel resonance was noted; however, the effects on the experimental data appear to be confined to the $M = 0.70$ results.

## INTRODUCTION

Flutter is conventionally defined (e.g., ref. 1) as a self-excited oscillation resulting from a combination of inertial, elastic, oscillatory aerodynamic damping, and temperature forces. In combination, these forces can result in unstable motion (i.e., flutter) which leads to mild or extremely severe structural failures. It is evident, then, that the subject of flutter is an extremely complex one and a reliable analysis can be made of a specific design only through the use of the most complete information about the structure, dynamics, and aerodynamics.

The present paper is concerned with only one of these fields - the oscillatory aerodynamics. The basic tool of the flutter analyst as regards aerodynamics is theory. Very little has been done with the application of experimental data to flutter calculations; instead, experimental results have been used chiefly to evaluate the accuracy of the theoretical methods. These evaluations have shown that the use of two-dimensional theory applied in a strip analysis, while yielding good results for wings of high aspect ratio, lead to inaccurate results in the case of low aspect ratio surfaces. This fact has led to the development of three-dimensional theories, two of the most complete being the subsonic kernel-function method of Watkins, Runyan, and Woolston (ref. 2), and the supersonic linearized theory of Miles (ref. 3), an analytically exact treatment applicable only to certain plan forms.

The experimental results used to evaluate theories in the past have been derived chiefly from rigid wings executing flapping, pitching, or plunging oscillations at subsonic speeds (e.g., refs. 4, 5, and 6). Mollø-Christensen (ref. 7) has obtained the oscillatory pressure amplitudes at certain points on such wings at transonic speeds. To date, only one experimental investigation has been reported with a wing performing elastic deformations (ref. 8); this investigation was conducted only at low subsonic speeds, however, and as yet no similar results are available for transonic and supersonic speeds.

The purpose of the present investigation was to develop a research technique by means of which the oscillatory pressures existing on a three-dimensional wing performing elastic deformations could be obtained throughout the subsonic, transonic, and supersonic speed ranges, and to compare the experimental results with those of the most complete theories available.

## NOTATION

The following definitions are for significant notations which will be found in the main body of the report. Notations found only in the appendices are defined therein.

| | |
|---|---|
| A | aspect ratio |
| b | semichord |

$C_{p_u}, C_{p_l}$ static-pressure coefficient on upper and lower surfaces, respectively, $\frac{p_u - p_\infty}{q}$, $\frac{p_l - p_\infty}{q}$

$C_p$ static lifting-pressure coefficient, $C_{p_l} - C_{p_u}$

$C_{p_{\alpha_h}}$ complex amplitude of oscillatory pressure coefficient per unit $\alpha_h$, $\frac{P}{q\alpha_h}$

$\zeta_h$ phase angle between oscillatory lifting-pressure coefficient magnitude and wing-tip bending magnitude, positive for pressure leading bending displacement, deg

A 3 5 4

$C_{l_{\alpha_h}}, C_{m_{\alpha_h}}$ oscillatory section lift and moment coefficients about mid-chord per unit $\alpha_h$

$\gamma_h, \gamma_{h_m}$ phase angle between wing-tip bending displacement magnitude and magnitude of oscillatory lift or moment coefficient, positive for lift or moment coefficient leading bending displacement, deg

f oscillatory frequency, cycles per unit time

H tunnel height, ft

h displacement of mid-chord line at any spanwise station, positive down

Im( ) imaginary part of a quantity - that component which is in phase with the wing-tip velocity

Re( ) real part of a quantity - that component which is in phase with the wing-tip displacement

k reduced frequency, $\omega b/V$

M Mach number

p static pressure at wing surface

P complex amplitude of oscillatory pressure at any orifice on wing surface

P' complex amplitude of oscillatory pressure at pressure cell connected to orifice at which P exists

q free-stream dynamic pressure, $\rho V^2/2$

| | |
|---|---|
| $r$ | chordwise distance from wing mid-chord to accelerometer root |
| $R$ | Reynolds number per ft |
| $t$ | time |
| $T$ | maximum wing thickness |
| $V$ | strain-gage supply voltage or free-stream velocity |
| $x$ | chordwise distance, positive downstream, measured from wing leading edge |
| $y$ | spanwise distance measured from wing root |
| $Z$ | amplitude ratio, $\frac{\lvert P' \rvert}{\lvert P \rvert}$ |
| $\alpha$ | static or mean value of angle of attack, deg |
| $\alpha_h$ | magnitude of oscillatory angle of attack at wing tip due to bending, $\frac{\lvert \dot{h} \rvert_T}{V}$, radians |
| $\rho$ | free-stream density |
| $\delta$ | phase angle between P and P', positive for P leading P', deg |
| $\omega$ | circular frequency of oscillation, $2\pi f$ |
| $\Delta$ | wing thickness-chord ratio, $\frac{T}{2b}$ |
| $\lvert\ \rvert$ | magnitude of quantity, $\lvert (\ ) \rvert^2 = [\mathrm{Re}(\ )]^2 + [\mathrm{Im}(\ )]^2$ |
| $(\dot{})$ | $\frac{d(\ )}{dt}$ |

Additional subscripts which may be attached to preceding quantities

| | |
|---|---|
| $f$ | association with forward accelerometer |
| $r$ | association with rear accelerometer |
| $i$ | component of a quantity in phase with bending displacement or resolver rotor |
| $o$ | component of a quantity out of phase with bending displacement or resolver rotor |

| | |
|---|---|
| T | value of a quantity at wing tip |
| u | value of a quantity on upper wing surface |
| l | value of a quantity on lower wing surface |
| $\infty$ | free-stream condition |

## EXPERIMENTAL INVESTIGATION

### Test Facility



The experimental investigations were conducted in the Ames 6- by 6-foot supersonic wind tunnel, which is of the closed-return, variable-pressure type capable of furnishing a continuous Mach number range from 0.70 to 2.20 by means of an asymmetric sliding-block throat. This tunnel can also be operated at M = 0.24 by halving the available compressor-drive power. In order to operate at sonic speed and to obtain more nearly uniform flow, the test-section floor and ceiling were perforated.

### Test Conditions

The pressure distributions were measured over a Mach number range from 0.24 to 1.30. The wing was oscillated at its first bending frequency, f ≈ 26.5 cycles per second, at a tip amplitude of approximately 0.2 inch, and the resulting reduced frequency range was from 0.10 to 0.46. The maximum available total pressure was maintained at each Mach number and provided Reynolds numbers from 2.2 to 4.6 million per foot. The wing angles of attack were 0° and 5°.

### Description of Apparatus

Model.- The model consisted of a semispan unswept, rectangular wing with an effective aspect ratio of 3. (The wing was provided with a rounded tip which was not included in computing this aspect ratio.) The airfoil consisted of a biconvex circular-arc section, 5 percent thick, with sharp leading and trailing edges. A photograph of the model mounted in the test section is shown in figure 1(a) and a drawing of the model giving pertinent dimensions is shown in figure 1(b).

The wing was machined from forgings of SAE 4130 steel which was heat treated to approximately Rockwell C-36 hardness. The upper and lower surfaces were machined separately and mated at the chord line to produce a monocoque structure with integral spanwise stiffening. Figure 1(c) is

a photograph of a representative cross section showing the location of the stiffeners and the resulting interior partitioning. Figures 1(d) and 1(e) show the interior sides of the upper and lower surfaces. The two halves were held together by screws through the root section, stiffeners, and leading and trailing edges. The shear loads due to wing deformation were carried by dowel pins at the root and tip, together with the shear blocks set in the spanwise stiffeners, which are visible in figure 1(e).

Wing-drive mechanism.- The drive mechanism to force the wing to oscillate in the desired structural deformation mode should be contained completely within the wing structure in order not to create flow disturbances with unknown aerodynamic effects. A unique system satisfying this requirement was developed for the present investigation and consisted of two spars extending the full spanwise length of the wing inside the channels shown in figures 1(d) and 1(e). Each spar consisted of an upper and lower half, riveted together at the wing tip as shown in sketch (a) and constrained to remain in contact over their length. Contact with the

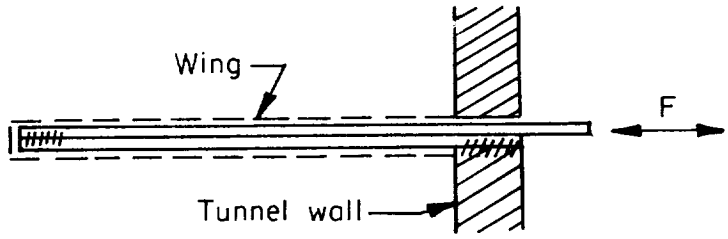


Sketch (a)

wing occurred only at the tip and 50-percent semispan station. The lower half of each spar was restricted from spanwise movement by being pinned at the wing root support in the tunnel wall. The upper half of each spar extended through the tunnel wall and was attached to an electromagnetic shaker which applied a harmonically varying force, F. The resulting alternating tension and compression in the upper spar half, coupled with the alternating compression and tension in the lower spar half, caused the spar to deflect in a manner analogous to that of a bimetallic strip. The resulting forces on the two bearing points then forced the wing to oscillate in its first bending mode, when the frequency was properly adjusted.

The bearing points were chosen from the results of an analysis which indicated that not only first bending but second bending and first and second torsion modes could also be forced by the one drive system. In practice, however, it was found that these additional modes could not be driven with sufficient amplitude to obtain data.

The wing and associated drive mechanism were mounted on the circular plate shown in figure 1(a), which allowed the angle of attack to be varied. An inflatable seal prevented leakage of atmospheric air around the plate

into the test section. It should be noted here that great care was taken to seal the interior of the wing from the free stream in the test section through the use of rubber cement on all mating surfaces and around the pressure-cell mountings. The interior was sealed from atmospheric pressure at the root by soldered lead-throughs for the orifice lines, pressure-tight plugs for the electrical connections, gaskets or rubber cement on all mating surfaces, and flexible rubber diaphragms to permit movement of the wing-drive mechanism.

Instrumentation.- The wing instrumentation was designed to furnish two types of information: the pressure distribution over the wing (either static or dynamic), and the deflection shape of the oscillating wing.

A 3 5 4

The wing pressure distribution was measured on both upper and lower surfaces approximately at the 90-percent, 70-percent, and 50-percent semispan stations and at the root. Ten 0.030-inch-diameter orifices were distributed along the chord at each of these stations on each surface. The orifice positions are shown and tabulated in figure 3(b). (The wing orifices were staggered and the root orifices were offset as shown in this figure in order to accommodate the instrumentation for an alternate pressure-measuring system at these stations. This instrumentation, consisting of flat, electrical resistance pressure cells 1/4 inch in diameter, was installed, and is visible in the photographs of figures 1(a), 1(d), and 1(e). The particular pressure cells designed for this experiment proved to be unreliable in early tests and were subsequently abandoned.)

The pressure at each orifice was piped out of the wing through the root lead-throughs inside plastic or stainless-steel tubing (I.D. = 0.042 in.) which was connected to the manifold of a model 48-D Scanivalve. This is a commercially available electromechanical pressure switch, capable of sequentially exposing 48 pressure lines to a single pressure-sensing device. Two such units were used in order that the pressure data from corresponding orifices on the upper and lower surfaces might be read simultaneously. The pressure-sensing devices used were commercially available differential pressure cells of the unbonded strain-gage type. The complete specification of an oscillatory pressure requires the determination of its two components, and in the method to be described presently for that determination, it was useful to revise the Scanivalve unit as supplied by the manufacturer in order to accommodate two independent pressure cells. As can be seen in figure 1(f) the modification resulted in an arrangement which permitted the pressure to be fed simultaneously to the face of each of the two pressure cells housed in the block. The interior diameters in the modified Scanivalve arrangement were held constant in order to prevent loss in signal strength.

The limited range of the high-sensitivity pressure cells used when obtaining the dynamic data made it necessary to equalize the static pressure on both sides of each cell diaphragm. For this purpose a bleed-filter consisting of a 5-inch length of stainless-steel hypodermic tubing (I.D. = 0.008 in.) was mounted in the top of the tee and was connected to the reference-pressure outlet of each cell mounted in its block as shown

in figure 1(f). This length of bleed tubing was found to furnish an acceptable response time to a representative step change in static pressure while satisfactorily filtering out the oscillatory part of the pressure signal. When the static-pressure data were obtained, one less sensitive pressure cell was used in each block, and it was referenced to the static pressure at the tunnel wall. This provision is also indicated diagramatically in figure 1(f).

Because of the chordwise rigidity of the wing it was assumed that any oscillatory motion was completely determined by the plunging and pitching oscillations of each of its cross sections. It was further assumed that the first symmetrical bending and torsion modes of oscillation could be adequately determined from a description of the motion at four spanwise stations. Accordingly, eight cantilever-beam-type accelerometers were located in cutouts along the extreme fore and aft stiffening spars at the 95-, 75-, 55-, and 35-percent semispan stations, and the oscillating wing motion was determined from their independent outputs.

A 3 5 4

All accelerometers were bolted to the stiffeners of the lower wing panel and are visible in figure 1(e). Two complete strain-gage bridges were bonded to each tip accelerometer beam, permitting both acceleration components to be measured simultaneously at that station while only one such bridge was bonded to each of the inboard accelerometer beams. Thus, for the inboard accelerometers, the method for component determination described below simply required sequential determination of one component and then the other. The electrical leads from the accelerometers were run along the wing cavities to cannon plugs in the root section.

All stainless-steel tubing and wiring was bonded to the wing interior with PRC 1221 cement which when dry had a rubber-like consistency and thus could flex with the wing without cracking. No fatiguing of either the bonding or the elastic properties of the cement was encountered during the test.

Electronic circuitry; method for component determination.- The electronic circuitry was designed to perform a harmonic analysis of the information provided by each element of instrumentation (whether pressure cells or accelerometer) and to respond only to the components of the complex amplitude of the fundamental. (The term fundamental as used here refers to that harmonic term which is of the same frequency as that of the gage power. In the oscillatory tests this frequency was the natural frequency for the first bending mode of the wing while in the static tests it was zero.)

The essential features of the electronic circuitry used are shown in sketch (b) for the oscillatory test case. The principle of operation

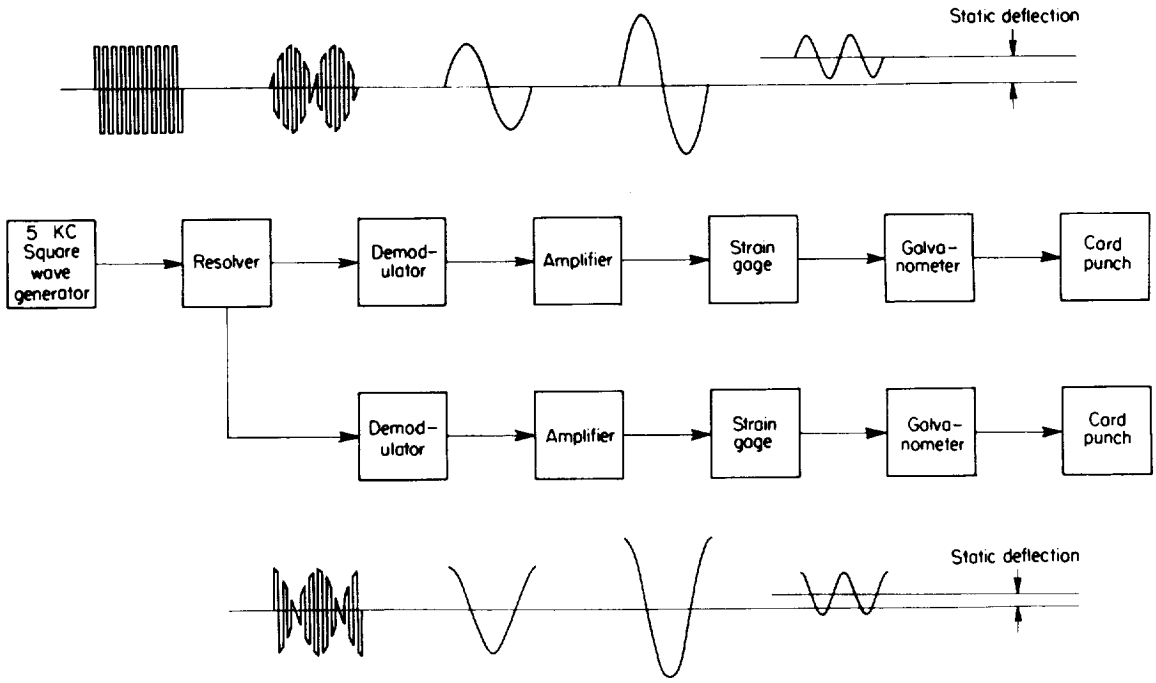


Sketch (b)

of the circuit is as follows: the output of a 5-kilocycle square-wave generator is passed through a resolver driven by the alternator supplying power to the electromagnetic shakers which force the wing motion. After subsequent demodulation this produces two alternating voltages at the wing-drive frequency such that one voltage is in phase and the other is out of phase with the angular position of the resolver rotor. After amplification, these voltages are used to power the strain-gage bridges in the various accelerometers and pressure cells in use. (The voltages were applied sequentially to the single bridge of each accelerometer at the 35-, 55-, and 75-percent semispan stations and simultaneously to the remaining gages.)

When the wing is oscillating the resulting pressures (or accelerations) impose a time-varying deformation on the various strain gages. If each gage is powered by an alternating voltage at this same frequency, then its output is essentially proportional to the product of the voltage signal and the resistance changes in the bridge associated with the deformations.

Thus, if the gage is undergoing sinusoidal deformations of the form

$$B \sin (\omega t + \epsilon)$$

(where $\epsilon$ is the phase angle between the gage deformation and the angular position of the resolver rotor) and is powered by the two voltages delivered by the resolver in the form

$$V_i = V \sin \omega t$$

$$V_o = V \sin \left( \omega t + \frac{\pi}{2} \right)$$

then the gage output voltages are, respectively,

$$v_i = K B \sin (\omega t + \epsilon) V \sin \omega t$$

$$= K \frac{VB}{2} [\cos \epsilon - \cos (2\omega t + \epsilon)]$$

and

$$v_o = K B \sin (\omega t + \epsilon) V \sin \left( \omega t + \frac{\pi}{2} \right)$$

$$= K \frac{BV}{2} [\sin \epsilon + \sin (2\omega t + \epsilon)]$$

Here $K$ is a general bridge constant depending on the type of bridge in use, its resistance, and the choice of units of $B$. Thus, the output of the strain gage is proportional to one-half the amplitude of the quantity to be measured, the frequencies are twice the frequency of operation, and each of the resultant voltages has a time-invariant component.

As shown in sketch (b), each output voltage is used to drive a galvanometer element which has an undamped natural frequency much less than $2\omega$ so that it is essentially unable to respond to the oscillatory part of the signal. However, the galvanometer is capable of responding with a deflection $G$ to the component of the strain-gage signal which is time-invariant. The result is a static indication of the in-phase and out-of-phase components of the harmonically varying quantity.

This method is more fully described in reference 9, where it is shown that such a system is capable of filtering unwanted harmonics from the data. However, tunnel turbulence and the occurrence of leading-edge separation when the wing was set to an angle of attack caused fluctuations in the strain-gage outputs which reduced the accuracy of the pressure data.

## Instrument Calibration

Accelerometers.- The calibration constants which had to be determined for each accelerometer were, from appendix A, $K_h$ and $K_\theta$, the galvanometer deflections per unit linear acceleration and per unit angular acceleration about the accelerometer root. These constants were determined after the accelerometers had been installed in the wing in order that all pertinent factors, such as root fixity, were accounted for.

The mode shape of the oscillating wing was determined for purposes of calculating the accelerometer constants by means of a stand which held depth micrometers with spring-supported conical tips fastened to the spindles. The tips provided accurate positioning of the contact point and minimized the danger of damage to both the wing and the micrometer. Contact between wing and micrometer was indicated by a battery-powered circuit which produced an audible signal in a pair of earphones. The torsion mode was excited by means of opposed eccentric weights attached to the shaft of a small electric motor mounted on the wing tip. A pure torsional moment was produced in this manner with no accompanying force tending to disturb the wing in bending, and since the elastic axis lay on the line of mass centers, no bending was caused by inertia coupling. In order that all quantities might be referenced directly to the tip amplitude, the outputs of the 95-percent semispan accelerometers were calibrated in terms of the tip deflection rather than the deflection of the 95-percent semispan station.

The accelerometer calibration showed that $K_\theta$ was negligible with respect to $rK_h$ in determining a torsional component of motion at the first bending frequency, and was consequently set equal to zero in the data-reduction equations used in the investigation. The calibration also showed that no torsional motion was present when the wing was driven in the first bending mode. This important result was later found to be true during the wind-on test also. This was to be expected, considering the mass symmetry of the wing about the mid-chord line mentioned previously, and the fact that the torsional resonant frequency was approximately 110 cycles per second as compared to the first bending frequency of approximately 26 cycles per second.

Pressure cells.- The static sensitivities of the pressure cells were obtained by means of a precision manometer. The calibration constants so obtained were used directly in the static-pressure-distribution test. No basic difference in the static or dynamic cell sensitivities existed since the resonant frequency of the pressure cells was several orders of magnitude greater than the test frequency. The dynamic calibration constants denoted as $K_i$ and $K_o$ in appendix A differed from the static constants because the dynamic data were obtained by powering the cells with an alternating voltage rather than a constant voltage. The root mean square of the alternating voltage was maintained at a value equal to the constant voltage used during calibration; the effect of this change, coupled with

the factor 1/2 noted in the section on Instrumentation, resulted in a dynamic calibration constant equal to $\sqrt{2}$ times the static constant when expressed in the units of $K_i$ and $K_o$ given in appendix A.

## Test Procedure

The data presented for each test condition were obtained in three distinct stages; the static test, the oscillatory test, and the orifice-tube calibration. Data from each of these phases were automatically entered on punched cards and the results appropriate to each phase were computed electronically.

Static test.- The static-pressure distribution was obtained by powering one of the cells in each Scanivalve unit with a constant voltage. Each cell was referenced to the static pressure at the wall of the test section, so that its output for each orifice was directly proportional to the static-pressure difference between the wing orifice and the tunnel wall. Adjustments to free-stream conditions yielded the static-pressure coefficients.

A 3 5 4

Oscillatory test.- The wing was driven in resonance at its first bending frequency in order to obtain the maximum available tip amplitude of motion (approximately 0.2 inch for all test conditions). The pressure cells in the Scanivalves were connected to the bleeds as described in the section on instrumentation so that no static-pressure difference existed across the cell diaphragm. The cell outputs, corresponding to the oscillatory-pressure amplitude, were recorded for each orifice. Simultaneous readings of the accelerometer outputs were also recorded, and these data, together with the data obtained as described in the next section, yielded the mode shape and oscillatory-pressure distribution when combined in the equations of appendix A.

Orifice-tube calibration.- The calibration was performed by means of the fixture shown in figure 1(g) which clamped to the wing and simultaneously covered all orifices at a given span station. A similar fixture was used in the calibration of the root orifices. At most test conditions the oscillating pressures experienced by the pressure cells in the Scanivalves were not representative of either the magnitude or phase angle of the pressures existing on the wing surface because of the attenuation and phase characteristics of the tubing which transmitted the pressures to the cells. It was experimentally determined that the tube characteristics were functions primarily of the frequency and static pressure existing in the tube, and essentially independent of the amplitude of oscillating pressure for the values experienced during the investigation.

The tube characteristics could also be affected by the introduction of foreign particles into the wing orifice and by necessary maintenance work on the Scanivalve. To minimize the possibility of such occurrences affecting the data, a calibration was made immediately after each

oscillatory test. In the calibration the absolute static pressure, as determined from the static test, and the frequency, as determined from the oscillatory test, were matched for each orifice location and an average value of oscillating-pressure amplitude was applied at the orifice.

The calibration fixture consisted of a chamber which applied the same conditions to all orifices on the upper or lower surfaces of the wing. Sealing around each orifice was accomplished by clamping on the rubber grommets visible in the photograph. The static pressure was set to the value corresponding to the particular orifice being calibrated. The oscillating-pressure amplitude, supplied by a piston-cylinder arrangement mounted on an electromagnetic shaker, was indicated by the two pressure cells mounted in each half of the fixture as shown. It was experimentally determined that there was no attenuation or phase shift introduced by the calibration fixture, so that the pressure cells in the fixture gave a true indication of the oscillating pressure existing at each orifice.

The data obtained from the calibration were reduced to the form of amplitude ratio, Z, and phase angle, $\delta$, and were used in the data-reduction equations of appendix A. A plot showing the variation of these quantities with static pressure, typical of the orifices at the 90-percent semispan station, is presented in figure 2. Although the investigation was conducted at the maximum tunnel pressure available, the decrease in static pressure with increasing Mach number caused an increasing loss of system accuracy because of the resulting attenuation. Because of this effect the maximum Mach number at which reasonably accurate data could be obtained was 1.30.

## RESULTS AND DISCUSSION

### Static Data

The pressure distributions obtained under static conditions are presented in figure 3 for angles of attack of $0^\circ$ and $5^\circ$. (These angle of attack values are nominal in that the tunnel stream angle varied across the span, generally becoming more negative toward the root as can be seen from the zero angle of attack data.) The data are given in the form of the chordwise distributions of the surface pressure coefficients (upper and lower) and the lifting pressure coefficient at the four instrumented stations. In general, the static data agree with those of other biconvex airfoil and rectangular wing studies (e.g., refs. 10 and 11) and require little comment.

For the transonic speed range (M = 0.9 - 1.10), the local surface Mach numbers were computed from equation 11.4 of reference 12 and the results are presented in figure 4. These data show that for Mach numbers 1.0 and 1.1, the Mach number freeze condition (see, e.g., ref. 9) existed

over the entire surfaces at both angles of attack, while at 0.9 Mach number a significant freeze occurred only at 5° angle of attack and then was confined to the leading edge of the upper surface.

Unsteady static pressures occurred at the root station over both surfaces and were most significant near the leading edge. These were attributed to the effects of a turbulent wall boundary layer. In addition, certain unsteady pressure phenomena which were encountered during the oscillatory tests are believed to have their origin in the static environment of the wing, and the relevant features will be pointed out here.

First, at Mach number 0.9, the presence and location of the shock wave terminating the region of local supersonic flow should be noted as seen in figures 3(g) and 3(h). Although it is not shown in figures 4(e) through 4(h), there were also shock waves terminating a small region of supersonic flow near the leading edge of the upper surface at $M = 0.7$ for $\alpha = 5°$. Small changes in the location of these shock waves were constantly occurring as a result of slight changes in the flow conditions.

A 3 5 4

Second, although the effective semiwedge angle of the airfoil at the leading edge was approximately 7°, and thus the upper surface of the wing leading edge was at approximately a 2° negative angle of attack with respect to the free stream, the $\alpha = 5°$ data of figure 3 indicate that the induced upwash raised the effective flow angle sufficiently to require the flow to expand over the upper leading-edge surface. Because of the sharpness of the leading edge, a small region of separated flow probably existed for most test conditions. However, the data of figure 3 indicate the possible separated region to be confined to the region ahead of the 5-percent chord under static conditions.

Finally, at 5°, for Mach numbers 0.9, 1.0, and 1.1, the local Mach number plots (fig. 4(e) through 4(h)) show that the flow over the upper surface of the wing was almost entirely supersonic; therefore, the wing tip may be expected to have a domain of influence on the upper surface similar to that of a purely supersonic wing, and the associated abrupt changes in the pressure at the boundary of this region. The approximate location of this curved boundary line for $M = 1.1$ was computed from the local Mach number data of figure 4, and is shown in figure 5; as a result of the transonic Mach number freeze over the tip portion of the upper surface, this boundary-line position is also applicable for $M = 0.9$ and 1.0. The correspondence of its location with the position of the slight peaks nearest the leading edge in the static-pressure distributions of figures 3(h), 3(k), and 3(n) at the three outboard stations shows that the peaks mark the boundary of the tip domain of influence. The boundary-line location for $M = 1.3$ was computed in a similar manner and is also shown in figure 5. However, for this Mach number, the tip effect, in terms of peaks in the pressure distribution, was so small that it was negligible statically and unnoticeable dynamically.

## Dynamic Data

Mode shape.- The mode shape, normalized with respect to the tip amplitude, is shown in figure 6 for both wind-off and wind-on conditions. The wind-off curve was obtained by means of depth micrometers as described previously. The wind-on data were obtained through use of the accelerometer equation (A4) of appendix A. Data are missing from the 35-percent-station accelerometers because of an electrical failure at this station in the early stages of the investigation.

Chordwise pressure distributions, $\alpha = 0^{\circ}$.- Figure 7 presents the result of applying equations (A11) to the data for $M = 0.24$ to give the components of the chordwise surface pressure distributions per unit tip angle of attack, in phase and out of phase with the wing bending deflection. Application of equations (A12) to these data yields the in-phase and out-of-phase components of the chordwise distribution of lifting-pressure coefficient as shown in figure 8. Finally, equations (A13) yield the chordwise distribution of the lifting-pressure coefficient amplitude and phase angle shown in figure 9, the form in which most of the dynamic results of this investigation are presented.



The pressure distribution for $M = 0.24$ (fig. 9(a)) appears smooth, but as the Mach number increases, various irregularities in the data occur, as is evident in the succeeding parts of figure 9. The general deterioration in smoothness can be attributed to the inherent loss in system accuracy with increasing Mach number discussed previously. However, certain of these irregularities are isolated enough to demand an explanation based on the physical characteristics of the flow.

The first of the isolated irregularities is the sharp break in the phase-angle distribution at $M = 0.70$ (fig. 9(b)), particularly at the two outboard stations. Because of the associated small pressure amplitudes, these jumps of nearly $180^{\circ}$ are probably partially accounted for by the inherent inaccuracies in the phase-angle computations for small pressure amplitudes, but their consistent nature may be due to possible tunnel resonance effects which will be considered later.

In the $M = 0.9$ data (fig. 9(c)), this jump is still present and is accompanied by sharp peaks in the pressure amplitude distribution over the aft portion of the chord. The static-pressure data show that the terminating shock wave is also in this vicinity, and the pressure peaks are attributed to the movement of the shock with the wing motion. The amplitude of the peak is roughly a measure of the harmonic content of the oscillations in static pressure associated with this shock motion, which is superposed on that arising from the oscillatory angle of attack. Two sets of data are also shown for this Mach number, and the poor repeatability in the neighborhood of the shock is further evidence of the sensitivity of the shock location to slight changes in the flow conditions.

Chordwise pressure distribution, $\alpha = 5^{\circ}$.- The components of the chordwise pressure distribution on the upper and lower surfaces are shown in figure 10 for $M = 0.24$; also shown for comparison are the corresponding data for $\alpha = 0^{\circ}$ from figure 7. The radical change in the pressure distribution at the leading edge of the upper surface is apparently the result of the unsteady pressures associated with the changing chordwise extent of the leading-edge separation mentioned previously, caused by the additional increment in angle of attack furnished by the wing oscillations. As shown in figure 11(a), the phase angles were relatively unaffected by the separation.

At a Mach number of 0.70 (fig. 11(b)), both the amplitude and phase angle of the pressure coefficient exhibit leading-edge irregularities, but these may not result entirely from flow separation. As mentioned previously, local supersonic flow occurred over the leading edge at $M = 0.70$ when at angle of attack, and movement of the shock terminating this region could have caused increased pressure amplitudes in the same manner as that described for $M = 0.90$ at $0^{\circ}$. Because of the reduced angle of attack associated with bending oscillations (as compared with that for $M = 0.24$) and also the increased Reynolds number, it is doubtful if significant leading-edge separation occurred except perhaps near the tip. This appears to be the case for the data of Mach numbers 0.90, 1.0, and 1.1 (figs. 11(c), (d), and (e)) which show a large pressure-amplitude peak at the 90-percent semispan station. The data also show pressure amplitude peaks at the three-tenths and mid-chord points of the 70- and 50-percent semispan stations, respectively. The similarity of the data for these three Mach numbers is evidence of the Mach number freeze shown in figure 4. As discussed previously, the freeze held only over the forward portion of the chord at $M = 0.90$. Although not presented herein, the separate surface data show that the peaks occurred on the upper surface only; the coincidence of their locations with those of the abrupt changes in static pressure which were previously shown to define the boundaries of the tip domain of influence suggests that the peaks are the result of the movement of this boundary line with the wing motion. As can be seen, relatively small (but well defined) changes in static pressure at the boundary may produce a surprisingly large pressure-amplitude peak in the immediate neighborhood of the boundary. However, the diminishing of the peak at the 50-percent station when the flow is accelerated from $M = 1.0$ to $M = 1.1$, attests that this neighborhood is extremely small, and the peak might not be detected unless there were an orifice located there.

A 3 5 4

Section lift and moment distributions, $\alpha = 0^{\circ}$.- The oscillatory aerodynamic section lift and moment coefficients were obtained by numerically integrating the lifting pressure coefficient distributions for each Mach number corresponding to those of figures 8(a) through 8(d) for $M = 0.24$. It was assumed that these pressure distributions varied linearly between adjacent chord points, and the necessary leading- and trailing-edge values were selected by inspection for each spanwise station. A trapezoidal scheme of integration, consistent with these assumptions, was then utilized to obtain the in-phase and out-of-phase components of both

the section lift and the section moment coefficients per unit effective tip angle of attack. From this information, the magnitude and phase angle of the oscillatory section coefficients were computed and the results are shown in figure 12. Of particular interest are the rerun results of figures 12(c) and 12(f) which show remarkable agreement considering the approximate nature of the integrations and the general erratic character of the original pressure distributions.

Although there is some question as to the quantitative accuracy of the results, definite trends with increasing Mach number are in evidence. Among these are the decrease in the section lift phase angle from approximately 120° at M = 0.24 to 55° at M = 1.3, although at each Mach number this phase angle is relatively constant across the span. One of the most remarkable features of these data is the gradual flattening of the distribution of the section lift coefficient amplitude, until at M = 1.3 (fig. 12(f)) it is almost elliptical. It might be expected that at least the out-of-phase component would retain some evidence of the mode shape and have its maximum somewhere in the vicinity of the wing tip as it would theoretically for a parabolically twisted wing in steady linearized supersonic flow at M = 1.3; but figure 12(f) shows that the maximum oscillatory lift is produced at the root section where the wing deflection is zero. Similarly, for the section moment distribution, the most striking effect of compressibility is the decreasing of the root phase angle from 75° at M = 0.24 to -75° at M = 1.3, while the phase angles for the three outboard stations are relatively unaffected.

A 3 5 4

Because of the general irregularity of the pressure distributions for $\alpha = 5°$, no attempt was made to integrate them and obtain the associated section lift and moment coefficients.

## Comparison With Theory

Of the many oscillating wing theories developed during the last ten years (see ref. 13 for a fairly complete survey) only two furnish the lifting-pressure distribution on a deforming wing of moderate aspect ratio, and both of these assume the conditions for linearized flow. For subsonic flow, there is the approximate kernel function approach of references 2, 14, and 15 which has recently culminated in a usable program for the IBM 704 electronic computer, and for pure supersonic flow there is the analytically exact potential obtained by Miles (ref. 3). The latter has also been developed into a usable program for this report (appendix B). Mollø-Christensen (ref. 7) and Miles (ref. 16) have investigated the necessary conditions under which unsteady linearized flow theory is valid, and reduced them to the following:

1. $\Delta$, $M\Delta$, $k\Delta$, $kM\Delta \ll 1$
2. $A^{-1} \gg \Delta^{1/3}$
3. $|M^2 - 1| \gg \Delta^{2/3}$
4. $k \gg \Delta^{2/3}$

} any one or more of these

where $\Delta$ is the thickness ratio of the wing.

From the values of the appropriate test parameters, it is seen that although condition 1 was always met, conditions 2 and 4 were never met, while condition 3 would require either $M \gg 1.065$, or $M \ll 0.930$. Therefore, in general, it would not be expected that the results of these linearized theories should agree well with those obtained experimentally, except possibly at $M = 0.24$, 0.70, and 1.30. With the reservations dictated by these considerations, the comparison between experimental results and those of the above linearized theories will be examined in more detail.

For the subsonic speeds, the computing program requires the selection of control points on the plan form at which the downwash (as determined by the mode shape) is to be specified. Twelve control points were chosen; the 1/4-, 1/2-, and 3/4-chord points at the 20-, 40-, 60-, and 80-percent semispan stations.

At $M = 0.24$, $\alpha = 0$, the agreement between the theoretical and experimental pressure distributions is good (figs. 7, 8, and 9(a)). The data were obtained at the greatest static pressure of any data of the investigation, so that the phase lag and attenuation of the orifice tubes were at their minimum values. There was also no evidence of stream fluctuation, so that these data are the most reliable of all that were obtained in the oscillatory testing. The good agreement between theory and experiment shows that linearized theory is adequate to describe the flow at this Mach number. The comparison between theory and experiment in the form of section lift and moment coefficients (fig. 12(a)) shows considerably more discrepancy than would be expected on the basis of the pressure distribution comparison. The primary cause of the discrepancy has been traced to the pressures assumed to exist at the leading edge; whereas the experimental data were extrapolated to pressures considered reasonable on a physical basis, the theory, of course, assumes the usual subsonic singularity. Therefore, if a more realistic handling of the leading-edge pressures could be incorporated into the theory, better agreement with the experimental values of lift and moment would undoubtedly result.

At $M = 0.70$, $\alpha = 0$ (figs. 9(b) and 12(b)), although the pressure amplitudes are in fair agreement, the phase angles are not, particularly near the three-quarter chord line, while the lift amplitudes show a noticeable decrease from their values at $M = 0.24$. The latter circumstance suggests the possibility of wind-tunnel resonance rather than violation of the limits for application of linearized theory. If the

resonance induced by a bending wing in a rectangular test section is considered to be primarily a two-dimensional problem, the theory of reference 16 is applicable for predicting the combination of Mach number and reduced frequency at which resonance could occur. The slotted floor and ceiling construction of the test facility necessitate considering an effective tunnel height somewhere between 6 and 18 feet. A plot of the appropriate test parameters is given in figure 13, with critical resonance curves from reference 17, based on tunnel heights of 6, 12, and 18 feet. As can be seen from the figure, resonance at $M = 0.7$ could indeed occur, for an effective tunnel height of approximately 13 feet, and this is believed to furnish a partial explanation for the above-mentioned discrepancies.

A 3 5 4 At $M = 0.9$ (fig. 9(c)), the agreement is poor, particularly in the vicinity of the shock waves over the afterportion of the chord. This is to be expected, since linearized theory is unable to account for the presence or the effects of these shock waves. The poor agreement is also evident in the lift and moment plots of figure 12(c).

For $M = 1.0$, the theoretical subsonic coefficients evaluated at $M = 0.99$ have been used for comparison. Although the amplitudes of the pressure coefficients are in better agreement than they were at $M = 0.90$, the corresponding phase angles are not (fig. 9(d)), nor are the section-lift and section-moment coefficients (fig. 12(d)). The requirement for the application of linearized theory is clearly invalidated at this Mach number and good agreement could not be expected.

For $M = 1.10$ and 1.30 (figs. 9(e), 9(f), 12(e), and 12(f)), there is little or no resemblance between the results of the experiment and those predicted by Miles linearized theory for parabolic bending, even in the plan-form regimes in which the latter is formally applicable (see appendix B). The discrepancies here are primarily accounted for by the nonlinear effects (detached bow wave) associated with the thickness of the wing, and partially by the over-all loss in system accuracy discussed earlier in the text. For $M = 1.30$, it is evident that the condition for linearized flow theory ($M \gg 1.065$) remains unsatisfied, while the general repeatability evidenced in the rerun data provides a measure of the reliability of these data.

## CONCLUSIONS

An experimental investigation was made in which the pressure distributions on an unswept rectangular wing of aspect ratio 3 oscillating in its first symmetrical bending mode were obtained over the Mach number range 0.24 to 1.30. From the results of the investigation, the following conclusions can be made:

1. Large effects on the oscillatory pressure distribution can be caused by the presence of static phenomena, such as local shock waves, flow separation, and finite span effects.

2. The results of linearized theory compared favorably with those obtained experimentally for $M = 0.24$ at $\alpha = 0^{\circ}$ where the flow was essentially incompressible and inviscid. However, the agreement deteriorated at transonic speeds and at angle of attack where the important effects of thickness, local shock waves, and separation could not be adequately described by linearized theory.

3. The comparison of the experimental and theoretical results tends to confirm the Miles and Mollø-Christensen criteria for the application of linearized flow theory.

4. Some evidence of wind-tunnel resonance was noted; however, the effects on the experimental data appeared to be confined to the $M = 0.70$ results.

5. The experimental method for obtaining the oscillatory pressure distributions developed in this investigation in general gave satisfactory results. The upper range of Mach numbers was limited by the increasingly poor frequency response characteristics of the pressure-measuring equipment.

Ames Research Center
National Aeronautics and Space Administration
Moffett Field, Calif., July 26, 1960

# APPENDIX A

## OSCILLATORY TEST DATA REDUCTION EQUATIONS

### Accelerometer Equations

In the following equations, the outputs of the accelerometer strain-gage bridges, which in reality are alternating voltages, are given the symbol G which, from the section on Instrumentation, indicates a static galvanometer deflection. No confusion should be caused, however, since it was shown that the static deflection is directly proportional to the amplitude of the alternating quantity, after scaling by the appropriate constants. All constants are taken to be included in the factors $K_h$ and $K_\theta$.

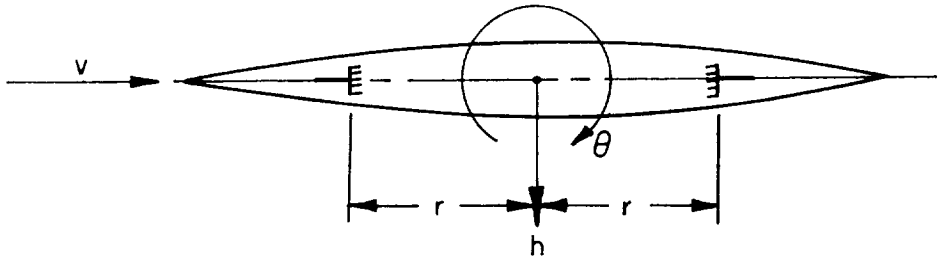


Sketch (c)

Consider the accelerometer geometry shown in sketch (c). Assume harmonic wing motion of bending and torsion. As a result of the chordwise rigidity, the motion of each cross section is completely specified by

$$h = |h| \sin \omega t$$

$$\theta = |\theta| \sin (\omega t + \Omega)$$

For each of these motions, by virtue of the high natural frequency of the accelerometers, the total output of the strain-gage bridges is directly proportional to the amplitude of the motion in question and may be taken to be in phase with it.

These outputs are as follows:

| | a. due to bending | b. due to torsion |
|---|---|---|
| forward accelerometer | $K_{h_f}\|h\|\omega^2$ | $(rK_{h_f} + K_{\theta_f})\|\theta\|\omega^2$ |
| rear accelerometer | $K_{h_r}\|h\|\omega^2$ | $(rK_{h_r} + K_{\theta_r})\|\theta\|\omega^2$ |

where

$K_{h_f}$ forward accelerometer galvanometer deflection per unit linear acceleration

$K_{h_r}$ rear accelerometer galvanometer deflection per unit linear acceleration

$K_{\theta_f}$ forward accelerometer galvanometer deflection per unit angular acceleration about forward accelerometer root

$K_{\theta_r}$ rear accelerometer galvanometer deflection per unit angular acceleration about rear accelerometer root

For the combined motion, the rotating vector diagrams for the forward and rear accelerometers are shown in sketches (d) and (e):

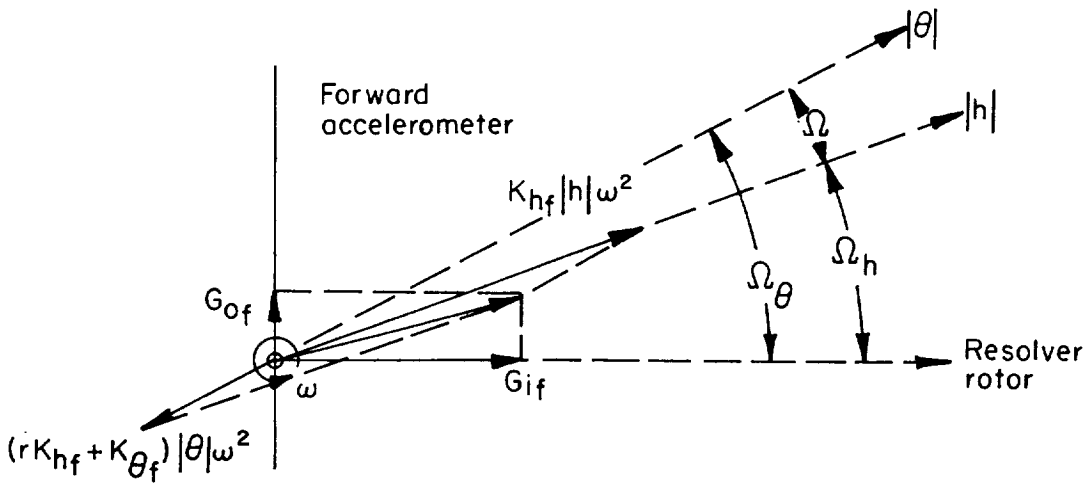


Sketch (d)

A 3 5 4

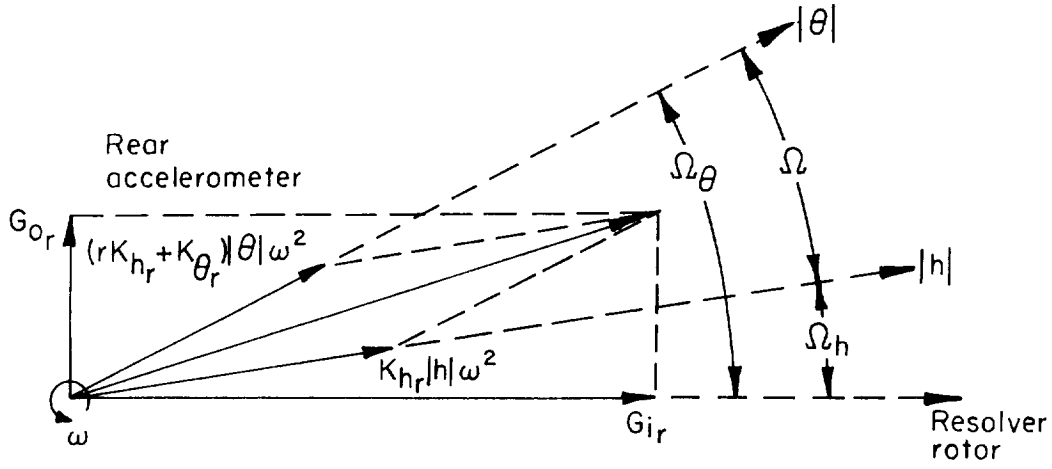


Sketch (e)

For the forward accelerometer,

$$\left.\begin{aligned} G_{i_f} &= K_{h_f}|h|\omega^2\cos\Omega_h - (rK_{h_f} + K_{\theta_f})|\theta|\omega^2\cos\Omega_\theta \\ G_{o_f} &= K_{h_f}|h|\omega^2\sin\Omega_h - (rK_{h_f} + K_{\theta_f})|\theta|\omega^2\sin\Omega_\theta \end{aligned}\right\} \quad (A1)$$

For the rear accelerometer,

$$\left.\begin{aligned} G_{i_r} &= K_{h_r}|h|\omega^2\cos\Omega_h + (rK_{h_r} + K_{\theta_r})|\theta|\omega^2\cos\Omega_\theta \\ G_{o_r} &= K_{h_r}|h|\omega^2\sin\Omega_h + (rK_{h_r} + K_{\theta_r})|\theta|\omega^2\sin\Omega_\theta \end{aligned}\right\} \quad (A2)$$

where $G_i$ and $G_o$ are the galvanometer deflections proportional to the strain-gage signals in phase and out of phase with the resolver rotor. In actual practice in-phase and out-of-phase components were indicated by a separate strain-gage bridge or else the two components were read consecutively; with either procedure there was the possibility of different sensitivities $K_h$ and $K_\theta$ for the two components. To indicate the possibility of different sensitivities for the in-phase and out-of-phase components, equations (A1) and (A2) are rewritten as

$$\left.\begin{aligned} G_{i_f} &= K_{h_{f_i}}|h|\omega^2\cos\Omega_h - (rK_{h_{f_i}} + K_{\theta_{f_i}})|\theta|\omega^2\cos\Omega_\theta \\ G_{o_f} &= K_{h_{f_o}}|h|\omega^2\sin\Omega_h - (rK_{h_{f_o}} + K_{\theta_{f_o}})|\theta|\omega^2\sin\Omega_\theta \\ G_{i_r} &= K_{h_{r_i}}|h|\omega^2\cos\Omega_h + (rK_{h_{r_i}} + K_{\theta_{r_i}})|\theta|\omega^2\cos\Omega_\theta \\ G_{o_r} &= K_{h_{r_o}}|h|\omega^2\sin\Omega_h + (rK_{h_{r_o}} + K_{\theta_{r_o}})|\theta|\omega^2\sin\Omega_\theta \end{aligned}\right\} \quad (A3)$$

Equations (A3) can be solved for the following quantities at each of the four accelerometer stations:



(a) Bending amplitude

$$|h| = \frac{1}{\omega^2}\left\{\left[\frac{(rK_{h_{r_i}} + K_{\theta_{r_i}})G_{i_f} + (rK_{h_{f_i}} + K_{\theta_{f_i}})G_{i_r}}{2rK_{h_{f_i}}K_{h_{r_i}} + K_{h_{f_i}}K_{\theta_{r_i}} + K_{h_{r_i}}K_{\theta_{f_i}}}\right]^2 + \left[\frac{(rK_{h_{f_o}} + K_{\theta_{f_o}})G_{o_r} + (rK_{h_{r_o}} + K_{\theta_{r_o}})G_{o_f}}{2rK_{h_{f_o}}K_{h_{r_o}} + K_{h_{f_o}}K_{\theta_{r_o}} + K_{h_{r_o}}K_{\theta_{f_o}}}\right]^2\right\}^{1/2} \quad (A4)$$

(b) Phase angle between resolver rotor and bending amplitude

$$\Omega_h = \tan^{-1}\left\{\frac{\left[\frac{(rK_{h_{f_o}} + K_{\theta_{f_o}})G_{o_r} + (rK_{h_{r_o}} + K_{\theta_{r_o}})G_{o_f}}{2rK_{h_{f_o}}K_{h_{r_o}} + K_{h_{f_o}}K_{\theta_{r_o}} + K_{h_{r_o}}K_{\theta_{f_o}}}\right]}{\left[\frac{(rK_{h_{r_i}} + K_{\theta_{r_i}})G_{i_f} + (rK_{h_{f_i}} + K_{\theta_{f_i}})G_{i_r}}{2rK_{h_{f_i}}K_{h_{r_i}} + K_{h_{f_i}}K_{\theta_{r_i}} + K_{h_{r_i}}K_{\theta_{f_i}}}\right]}\right\} \quad (A5)$$

(c) Torsion amplitude

$$|\theta| = \frac{1}{\omega^2}\left[\left(\frac{K_{h_{f_i}}G_{i_r} - K_{h_{r_i}}G_{i_f}}{2rK_{h_{f_i}}K_{h_{r_i}} + K_{h_{f_i}}K_{\theta_{r_i}} + K_{h_{r_i}}K_{\theta_{f_i}}}\right)^2 + \left(\frac{K_{h_{f_o}}G_{o_r} - K_{h_{r_o}}G_{o_f}}{2rK_{h_{f_o}}K_{h_{r_o}} + K_{h_{f_o}}K_{\theta_{r_o}} + K_{h_{r_o}}K_{\theta_{f_o}}}\right)^2\right]^{1/2} \quad (A6)$$

(d) Phase angle between resolver rotor and torsion amplitude

$$\Omega_\theta = \tan^{-1}\left\{\frac{\left[\dfrac{K_{h_{f_o}}G_{o_r} - K_{h_{r_o}}G_{o_f}}{2rK_{h_{f_o}}K_{h_{r_o}} + K_{h_{f_o}}K_{\theta_{r_o}} + K_{h_{r_o}}K_{\theta_{f_o}}}\right]}{\left[\dfrac{K_{h_{f_i}}G_{i_r} - K_{h_{r_i}}G_{i_f}}{2rK_{h_{f_i}}K_{h_{r_i}} + K_{h_{f_i}}K_{\theta_{r_i}} + K_{h_{r_i}}K_{\theta_{f_i}}}\right]}\right\} \tag{A7}$$

(e) Phase angle between bending and torsion

$$\Omega = \Omega_\theta - \Omega_h \tag{A8}$$

A 3 5 4

Pressure-Measurement Equations

Consider the harmonic pressure variation of amplitude $|P|$ and phase angle $\lambda_h$ occurring on the surface of the wing at a particular orifice, where $\lambda_h$ is measured with respect to the wing-tip position. Because of the attenuation and phase characteristics of the pressure line connecting the orifice at the wing surface with the pressure cells outside the tunnel, the pressure cells experience a pressure of amplitude $|P'|$ which lags the pressure at the orifice by the phase angle $\delta$. As mentioned previously in the text, all aerodynamic quantities are made dimensionless with respect to the wing-tip angle of attack amplitude. The necessary geometry is indicated in the rotating-vector diagram of sketch (f).

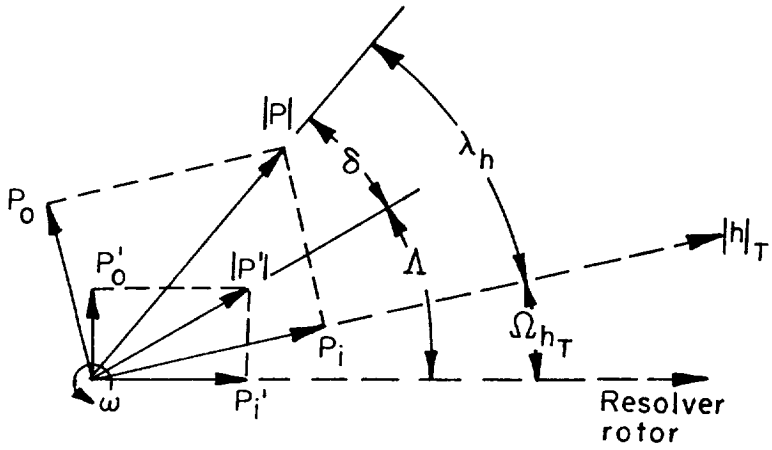


Sketch (f)

The amplitude and phase angle of the tip motion are indicated by the subscript T.

Denote by the symbol Z the ratio of the pressure amplitude $|P'|$ experienced by the pressure cells to the pressure amplitude $|P|$ existing on the wing surface. Then

$$|P| = \frac{|P'|}{Z}$$

and

$$\lambda_h = \Lambda + \delta - \Omega_{h_T}$$

Now

$$P_i = |P|\cos\lambda_h$$

$$= |P|\cos(\Lambda + \delta - \Omega_{h_T})$$

$$= \frac{|P'|}{Z}\left[\frac{P_i'}{|P'|}\cos(\Omega_{h_T} - \delta) + \frac{P_o'}{|P'|}\sin(\Omega_{h_T} - \delta)\right]$$

or

$$P_i = \frac{1}{Z}\left[P_i'\cos(\Omega_{h_T} - \delta) + P_o'\sin(\Omega_{h_T} - \delta)\right]$$

and similarly,

$$P_o = \frac{1}{Z}\left[P_o'\cos(\Omega_{h_T} - \delta) - P_i'\sin(\Omega_{h_T} - \delta)\right]$$

Now

$$P_i' = K_i G_i \qquad P_o' = K_o G_o$$

where

$K_i$ in-phase component of pressure amplitude per unit galvanometer deflection

$K_o$ out-of-phase component of pressure amplitude per unit galvanometer deflection

Then

$$\left.\begin{aligned} P_i &= \frac{1}{Z}\left[K_iG_i\cos(\Omega h_T - \delta) + K_oG_o\sin(\Omega h_T - \delta)\right] \\ P_o &= \frac{1}{Z}\left[K_oG_o\cos(\Omega h_T - \delta) - K_iG_i\sin(\Omega h_T - \delta)\right] \end{aligned}\right\} \tag{A9}$$

The amplitude of the wing-tip angle of attack is given by

$$\alpha_h = \frac{|\dot{h}|_T}{V} = \frac{\omega|h|_T}{V} \tag{A10}$$

A
3
5
4

Dividing equations (A9) by (A10) and by the dynamic pressure $q$ gives the component of the surface pressure coefficient in phase and out of phase (hereafter denoted by Re( ) and Im( )) with the bending amplitude.

$$\left.\begin{aligned} \mathrm{Re}(C_{p_{\alpha_h}}) &= \frac{V}{Z\omega q|h|_T}\left[K_iG_i\cos(\Omega h_T - \delta) + K_oG_o\sin(\Omega h_T - \delta)\right] \\ \mathrm{Im}(C_{p_{\alpha_h}}) &= \frac{V}{Z\omega q|h|_T}\left[K_oG_o\cos(\Omega h_T - \delta) - K_iG_i\sin(\Omega h_T - \delta)\right] \end{aligned}\right\} \tag{A11}$$

where $Z$ and $\delta$ are found as indicated in the text.

Equations (A11) were developed for a general orifice on either the upper or lower wing surface. The data for $M = 0.24$ obtained by means of these equations are shown in figure 7 as $\mathrm{Re}\left(C_{p_{\alpha_h}}\right)_u$, $\mathrm{Re}\left(C_{p_{\alpha_h}}\right)_l$ and $\mathrm{Im}\left(C_{p_{\alpha_h}}\right)_u$, $\mathrm{Im}\left(C_{p_{\alpha_h}}\right)_l$, the subscripts $u$ and $l$ denoting upper and lower wing surface.

The real and imaginary components of the lifting-pressure amplitude are given by

$$\left.\begin{aligned} \mathrm{Re}\left(C_{p_{\alpha_h}}\right) &= \mathrm{Re}\left(C_{p_{\alpha_h}}\right)_l - \mathrm{Re}\left(C_{p_{\alpha_h}}\right)_u \\ \mathrm{Im}\left(C_{p_{\alpha_h}}\right) &= \mathrm{Im}\left(C_{p_{\alpha_h}}\right)_l - \mathrm{Im}\left(C_{p_{\alpha_h}}\right)_u \end{aligned}\right\} \tag{A12}$$

and are shown for $M = 0.24$ in figure 8.

The magnitude and phase angle with respect to bending amplitude of the lifting-pressure coefficient are given by

$$\left.\begin{aligned} |C_{p_{\alpha_h}}| &= \left\{[\mathrm{Re}(C_{p_{\alpha_h}})]^2 + [\mathrm{Im}(C_{p_{\alpha_h}})]^2\right\}^{1/2} \\ \zeta_h &= \tan^{-1}\frac{\mathrm{Im}(C_{p_{\alpha_h}})}{\mathrm{Re}(C_{p_{\alpha_h}})} \end{aligned}\right\} \tag{A13}$$

The data are presented in this form for all Mach numbers in figure 9.

Integration of equations (A12) with respect to dimensionless chordwise coordinates gives

$$\left.\begin{aligned} \mathrm{Re}(C_{l_{\alpha_h}}) &= \int_0^1 \mathrm{Re}(C_{p_{\alpha_h}})\,d\xi \\ \mathrm{Im}(C_{l_{\alpha_h}}) &= \int_0^1 \mathrm{Im}(C_{p_{\alpha_h}})\,d\xi \\ \mathrm{Re}(C_{m_{\alpha_h}}) &= \int_0^1 \mathrm{Re}(C_{p_{\alpha_h}})(\bar{\xi} - \xi)\,d\xi \\ \mathrm{Im}(C_{m_{\alpha_h}}) &= \int_0^1 \mathrm{Im}(C_{p_{\alpha_h}})(\bar{\xi} - \xi)\,d\xi \end{aligned}\right\} \tag{A14}$$

where $\xi = x/2b$ and $\bar{\xi}$ is the center of moments ($\bar{\xi} = 0.5$) from which

$$\left.\begin{aligned} |C_{l_{\alpha_h}}| &= \left\{[\mathrm{Re}(C_{l_{\alpha_h}})]^2 + [\mathrm{Im}(C_{l_{\alpha_h}})]^2\right\}^{1/2} \\ \gamma_h &= \tan^{-1}\frac{\mathrm{Im}(C_{l_{\alpha_h}})}{\mathrm{Re}(C_{l_{\alpha_h}})} \\ |C_{m_{\alpha_h}}| &= \left\{[\mathrm{Re}(C_{m_{\alpha_h}})]^2 + [\mathrm{Im}(C_{m_{\alpha_h}})]^2\right\}^{1/2} \\ \gamma_{h_m} &= \tan^{-1}\frac{\mathrm{Im}(C_{m_{\alpha_h}})}{\mathrm{Re}(C_{m_{\alpha_h}})} \end{aligned}\right\} \tag{A15}$$

Figure 12 gives the results for all Mach numbers at zero angle of attack in this form computed from numerical integrations corresponding to equations (A14).

# APPENDIX B

## APPLICATION OF MILES' THEORY FOR SUPERSONIC RECTANGULAR OSCILLATING WINGS

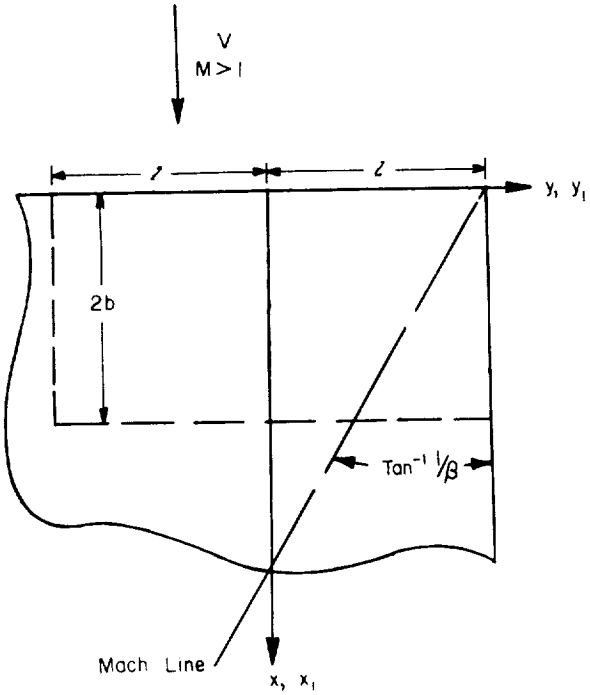


Sketch (g)

In reference 3 Miles considers the linearized problem of an infinitesimally thin quarter-infinite lifting surface having one straight edge parallel and another normal to the stream, undergoing harmonic oscillations of frequency $\omega$. For ease of reference, the surface and an appropriate coordinate system is shown in sketch (g).

A 3 5 4

By use of the Laplace transformation, he obtained the exact linearized expression for the complex amplitude of the perturbation velocity potential on this surface. With suitable identifications, and with the signs of exponentials reversed for more conventional phase interpretation, this expression is as follows:

$$\bar{\Phi}(x_1,y_1,k) = \frac{l}{\pi m_1}\int_0^{x_1} e^{-iMk_1\nu_1}\,d\nu_1 \int_{\left|\frac{\nu_1}{m_1}-\bar{y}\right|}^{\frac{\nu_1}{m_1}+\bar{y}} \frac{\bar{w}(x_1-\nu_1,\,1-\eta_1,\,k)\,d\eta_1}{\sqrt{(\nu_1/m_1)^2-(\bar{y}-\eta_1)^2}}$$

$$-\frac{k_1 l}{\pi m_1}\int_0^{x_1}\nu_1 d\nu_1 \int_{\nu_1}^{x_1} e^{-iMk_1\mu_1}\,\frac{J_1\left(k_1\sqrt{\mu_1^2-\nu_1^2}\right)d\mu_1}{\sqrt{\mu_1^2-\nu_1^2}} \int_{\left|\frac{\nu_1}{m_1}-\bar{y}\right|}^{\frac{\nu_1}{m_1}+\bar{y}} \frac{\bar{w}(x_1-\mu_1,\,1-\eta_1,\,k)\,d\eta_1}{\sqrt{(\nu_1/m_1)^2-(\bar{y}-\eta_1)^2}} \qquad \text{(B1)}$$

where

$$k_1 = \frac{2kM}{\beta^2} \qquad x_1 = \frac{x}{2b} \qquad y_1 = \frac{y}{l} \qquad \bar{y} = 1 - y_1$$

$$\beta^2 = M^2 - 1 \qquad J_1 = \text{first-order Bessel function} \qquad \bar{\Phi} = \Phi e^{-i\omega t} \qquad m_1 = \frac{\beta A}{2} \qquad \text{(B2)}$$

and where $l$ and $2b$ are reference lengths in the spanwise and streamwise directions, respectively; $\bar{w}(x_1,y_1,k)$ is the downwash amplitude resulting from a wing deformation prescribed by

$$H(x,y,t) = l\bar{H}(x_1,y_1)e^{i\omega t} \qquad \text{(postive down)} \tag{B3}$$

and related to it through the equation

$$\bar{w}(x_1,y_1,k) = -\frac{VA}{2}\left[\frac{\partial \bar{H}}{\partial x_1}(x_1,y_1) + 2ik\bar{H}(x_1,y_1)\right] \tag{B4}$$



The superposition and lift cancellation techniques of supersonic steady flow can be used to obtain from (B1) the potential at all points on a finite rectangular plan-form lifting surface performing either symmetrical or antisymmetric oscillations, such as that indicated by the dashed lines in sketch (g), providing the Mach line from one wing tip does not intersect the side edge of the opposite wing panel (i.e., $\beta A \geq 1$).

From this potential, with

$$\Delta p = \overline{\Delta p}e^{i\omega t} = 2\rho\left(\frac{\partial \Phi}{\partial t} + V\frac{\partial \Phi}{\partial x}\right)$$

defining the lifting pressure, the expressions for that pressure, the section lift, and the section moment distributions are obtained (after some integration by parts) as follows:

$$\frac{\overline{\Delta p}}{q}(x_1,y_1,k) = 2A\left(\frac{\partial \frac{\bar{\Phi}}{Vl}}{\partial x_1} + 2ik\frac{\bar{\Phi}}{Vl}\right) \tag{B5}$$

$$\bar{c}_l(y_1,k) = \frac{\bar{L}(y_1,k)}{2qb} = 2A\left[\frac{\bar{\Phi}}{Vl}(1,y_1,k) + 2ik\int_0^1 \frac{\bar{\Phi}}{Vl}(x_1,y_1,k)\,dx_1\right] \tag{B6}$$

$$\bar{c}_{ma_1}(y_1,k) = \frac{\bar{M}_{a_1}(y_1,k)}{4qb^2} = (a_1 - 1)\bar{c}_l(y_1,k) + 2A(1 + 2ik)\int_0^1 \frac{\bar{\Phi}}{Vl}(x_1,y_1,k)dx_1$$

$$- 4ikA\int_0^1 x_1 \frac{\bar{\Phi}}{Vl}(x_1,y_1,k)dx_1 \qquad (B7)$$

where the vanishing of the potential at the wing leading edge has been used, and $x_1 = a_1$ is the moment axis.

Even for elementary deformation modes, the analytical integration of equations (B1) and (B5) through (B7) has not been accomplished as yet, and in order to facilitate numerical evaluation, it is convenient to consider the following classes of mode shapes.

A 3 5 4

For symmetric modes:

$$\bar{H}(x_1,y_1) = \bar{H}_n^{(S)}(x_1,y_1) = + |y_1|^n(A_n x_1 + B_n)$$

for all $y_1$, $n = 0, 1, 2 \ldots$

For antisymmetric (rolling) modes:

$$\bar{H}(x_1,y_1) = \bar{H}_n^{(A)}(x_1,y_1) = + |y_1|^{n-1}(A_n x_1 + B_n)y_1$$

$$n = 1, 2 \ldots \qquad (B8)$$

It is seen that this choice of mode shapes limits subsequent application to wings undergoing chordwise rigid deformations for which the spanwise variation is expressible in a power series in $y_1 = \frac{y}{l}$.

Upon substitution of equations (B8) and (B1) into equations (B5) through (B7) it is possible (after some interchanging of the orders of integration) to carry out all except the final two integrations exactly, but numerical methods are necessary in order to complete these. Series methods are applicable to the inner integrals since their integrands consist of certain products of Bessel, trigonometric, and algebraic functions, and as the resulting integrated functions are well behaved, Gauss' method is employed to effect the outer integration.

This work and the subsequent combinations necessary to obtain the final answers was programmed for the IBM 704, and this program was used

in obtaining the supersonic theoretical results presented in this report. The input information required is the specification of the Mach number $M$, the true reduced frequency $k = \frac{\omega b}{V}$, the aspect ratio $A = \frac{l}{b}$, the moment axis $a_1$, and the mode shape as reflected in its general classification (symmetric or antisymmetric), the choice of $n$, and the coefficients $A_n$ and $B_n$. In its present form, the program is only applicable to the aerodynamic situations for which $\beta A \geq 2$, i.e., those for which each tip Mach line is entirely contained on its wing panel.

The program furnishes the pressure distribution at any specified points on the plan form, and the section lift and pitching moment for any designated spanwise stations. Since the various integrands are essentially nonsingular, the required series expressions and integrations are straightforward and it is believed that the final answers are in error by no more than 1 percent.

## REFERENCES


1. NACA Subcommittee on Vibration and Flutter: A Survey and Evaluation of Flutter Research and Engineering. NACA RM 56I12, 1956.

2. Watkins, Charles E., Runyan, Harry L., and Woolston, Donald S.: On the Kernel Function of the Integral Equation Relating the Lift and Downwash Distributions of Oscillating Finite Wings in Subsonic Flow. NACA Rep. 1234, 1955. (Supersedes NACA TN 3131)

3. Miles, John W.: A General Solution for the Rectangular Airfoil in Supersonic Flow. Quart. Appl. Math., vol. 11, no. 1, 1953.

4. Woolston, Donald S., Clevenson, Sherman A., and Leadbetter, Sumner A.: Analytical and Experimental Investigation of Aerodynamic Forces and Moments on Low-Aspect-Ratio Wings Undergoing Flapping Oscillations. NACA TN 4302. 1958.

5. Widmeyer, Edward, Jr., Clevenson, Sherman A., and Leadbetter, Sumner A.: Some Measurements of Aerodynamic Forces and Moments at Subsonic Speeds on a Rectangular Wing of Aspect Ratio 2 Oscillating About the Midchord. NACA TN 4240, 1958.

6. Laidlaw, W. R.: Theoretical and Experimental Pressure Distributions on Low-Aspect-Ratio Wings Oscillating in an Incompressible Flow. M.I.T. Aeroelastic and Structures Res. Lab. Rep. 51-2 (Contract NO a(s) 52-576-6), Sept. 1954.

7. Mollø-Christensen, Erik L.: An Experimental and Theoretical Investigation of Unsteady Transonic Flow. Sc.D. Thesis, M.I.T., 1954.

8. Epperson, Thomas B., Pengelley, C. Desmond, Ransleben, Guido E., Jr., and Younger, Dewey G., Jr.: (Unclassified Title) Nonstationary Airload Distributions on a Straight Flexible Wing Oscillating in a Subsonic Wind Stream. WADC TR 55-323, Jan. 1956 (Confidential Report).

9. Lessing, Henry C., Fryer, Thomas B., and Mead, Merrill H.: A System for Measuring the Dynamic Lateral Stability Derivatives in High-Speed Wind Tunnels. NACA TN 3348, Dec. 1954.

10. Knechtel, Earl D.: Experimental Investigation at Transonic Speeds of Pressure Distributions Over Wedge and Circular-Arc Airfoil Sections and Evaluation of Perforated-Wall Interference. NASA TN D-15, 1959.

11. Croom, Delwin R.: Low-Subsonic Investigation to Determine the Chordwise Pressure Distribution and Effectiveness of Spoilers on a Thin, Low-Aspect-Ratio, Unswept, Untapered, Semispan Wing and on the Wing With Leading- and Trailing-Edge Flaps. NACA RM L58B05, 1958.

12. Liepmann, H. W. and Roshko, A.: Elements of Gasdynamics. John Wiley and Sons, Inc., 1957, pp.342-346.

13. Garner, H. C., and Acum, W. E. A.: Note on Some Recent Papers on Oscillating Wings. British ARC 18952, January, 1957. Title Unclassified, Contents Confidential.

14. Runyan, Harry L.,and Woolston, Donald S.: Method for Calculating the Aerodynamic Loading on an Oscillating Finite Wing in Subsonic and Sonic Flow. NACA Rep. 1322, 1957. (Supersedes NACA TN 3694)

15. Watkins, Charles E., Woolston, Donald S., and Cunningham, Herbert J.: A Systematic Kernel Function Procedure for Determining Aerodynamic Forces on Oscillating or Steady Finite Wings at Subsonic Speeds. NASA TR R-48, 1959.

16. Miles, John W.: The Potential Theory of Unsteady Supersonic Flow. Cambridge University Press, 1959.

17. Runyan, Harry L.,and Watkins, Charles E.: Considerations on the Effect of Wind-Tunnel Walls on Oscillating Air Forces for Two-Dimensional Subsonic Compressible Flow. NACA Rep. 1150, 1953. (Supersedes NACA TN 2552)

A-25671

(a) Photograph of model mounted in test section.

Figure 1.- Model and auxiliary apparatus details.

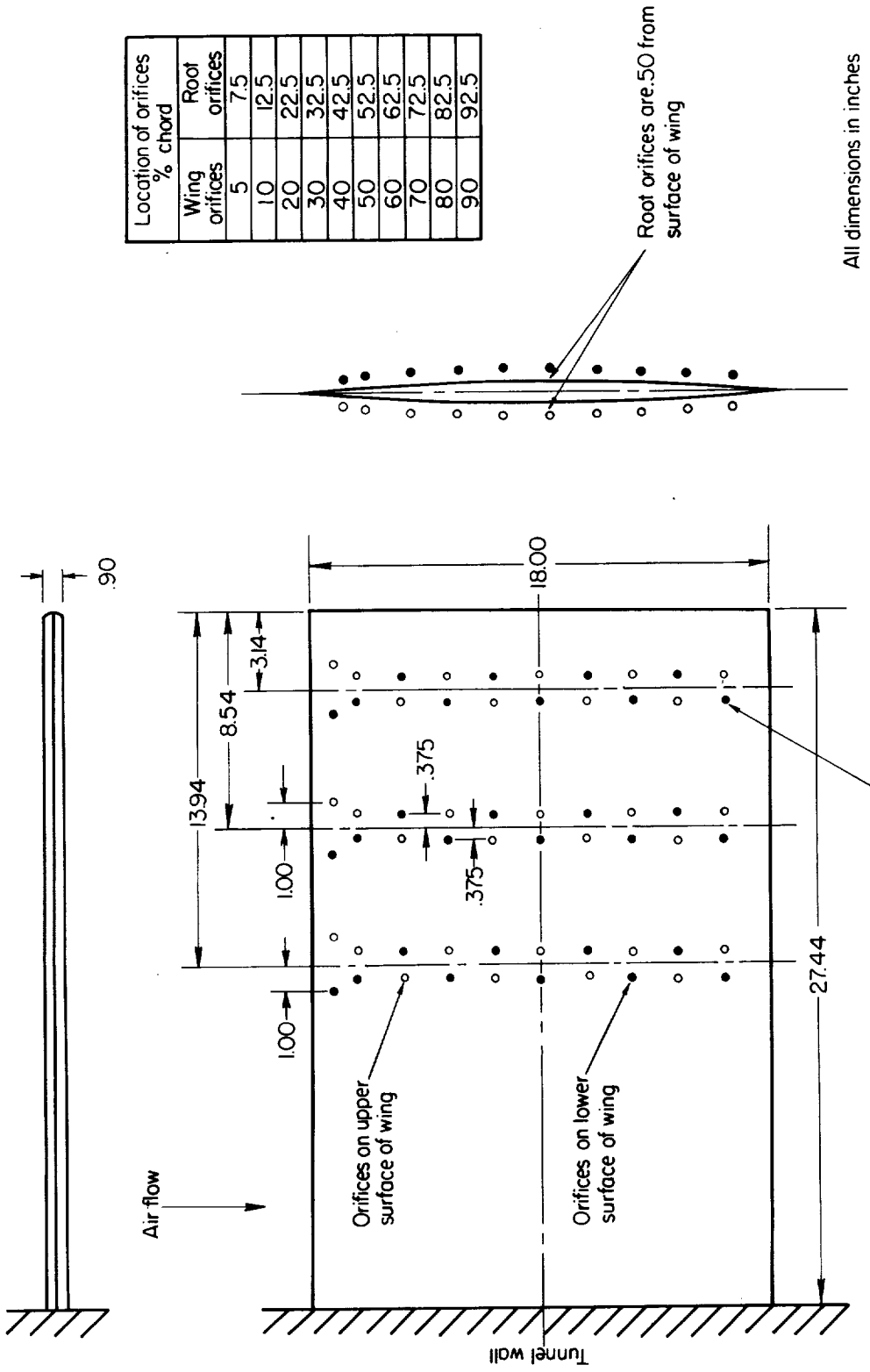


(b) Dimensional sketch of model.

Figure 1.- Continued.

A-25914

(c) Cross section of wing.

Figure 1.- Continued.


(d) Interior of upper surface of wing. A-23510

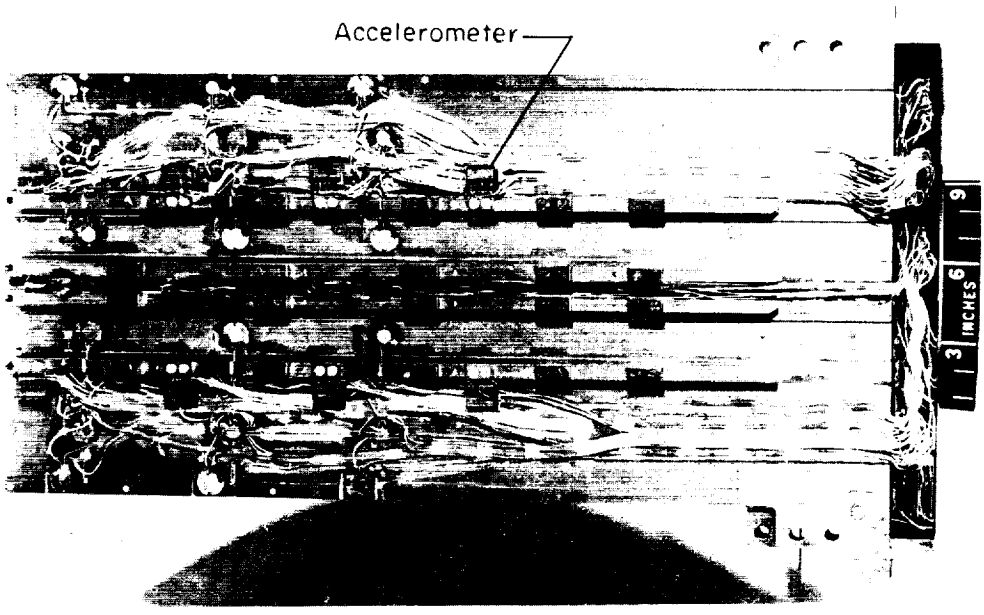


A-23509

(e) Interior of lower surface of wing.

Figure 1.- Continued.

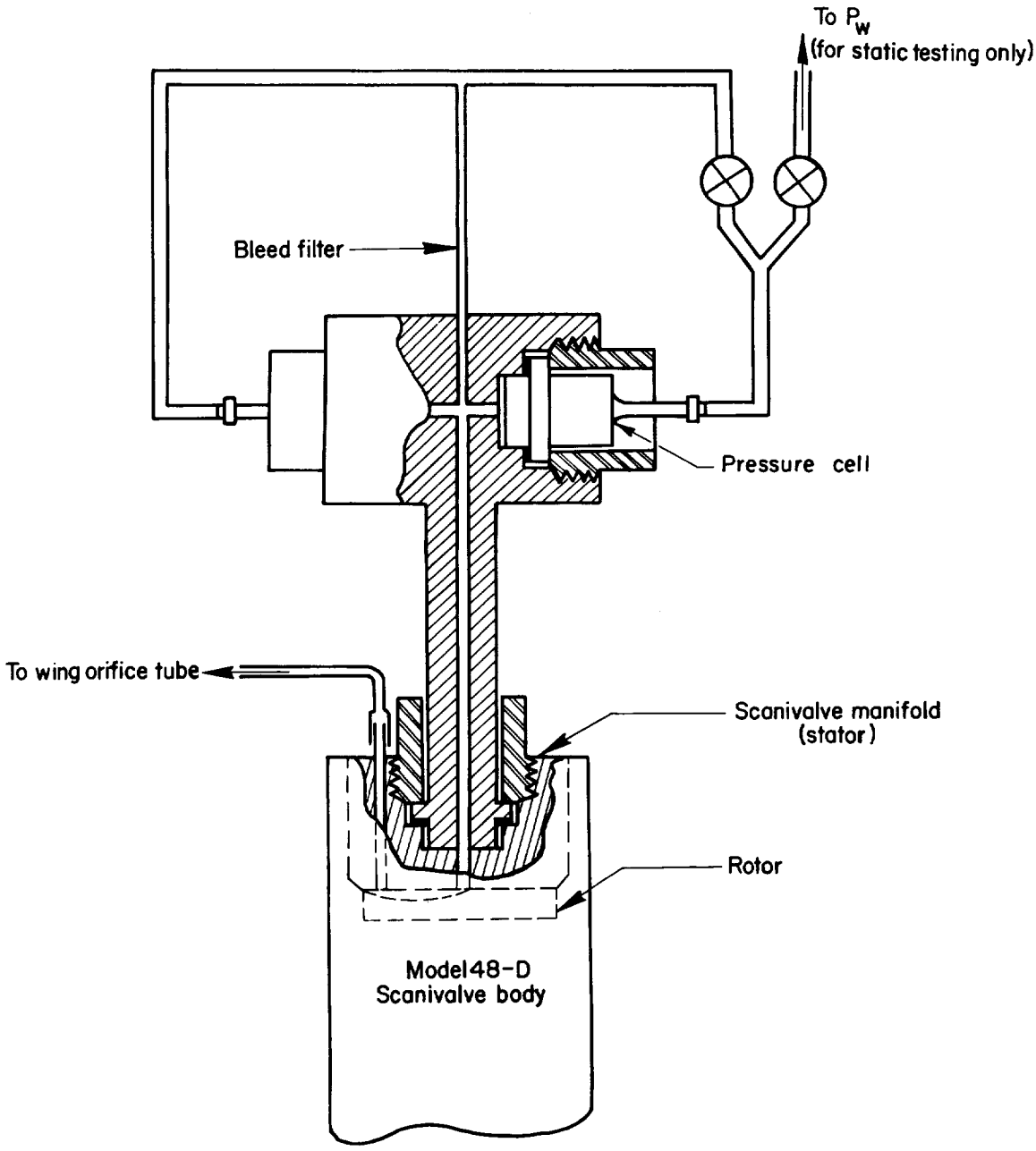


(f) Details of Scanivalve modification.

Figure 1.- Continued.

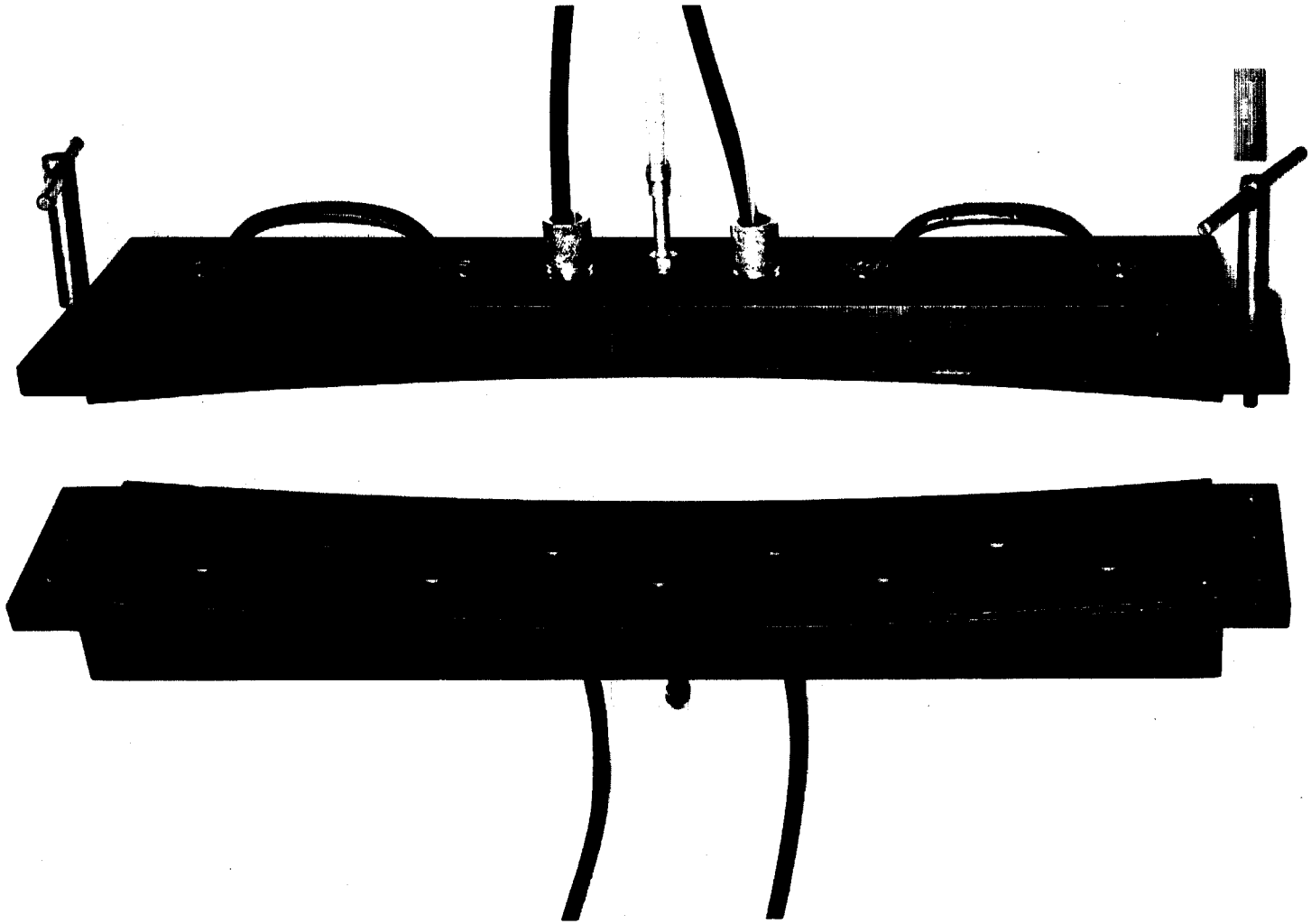

(g) Calibration block.

A-25915

Figure 1.- Concluded.

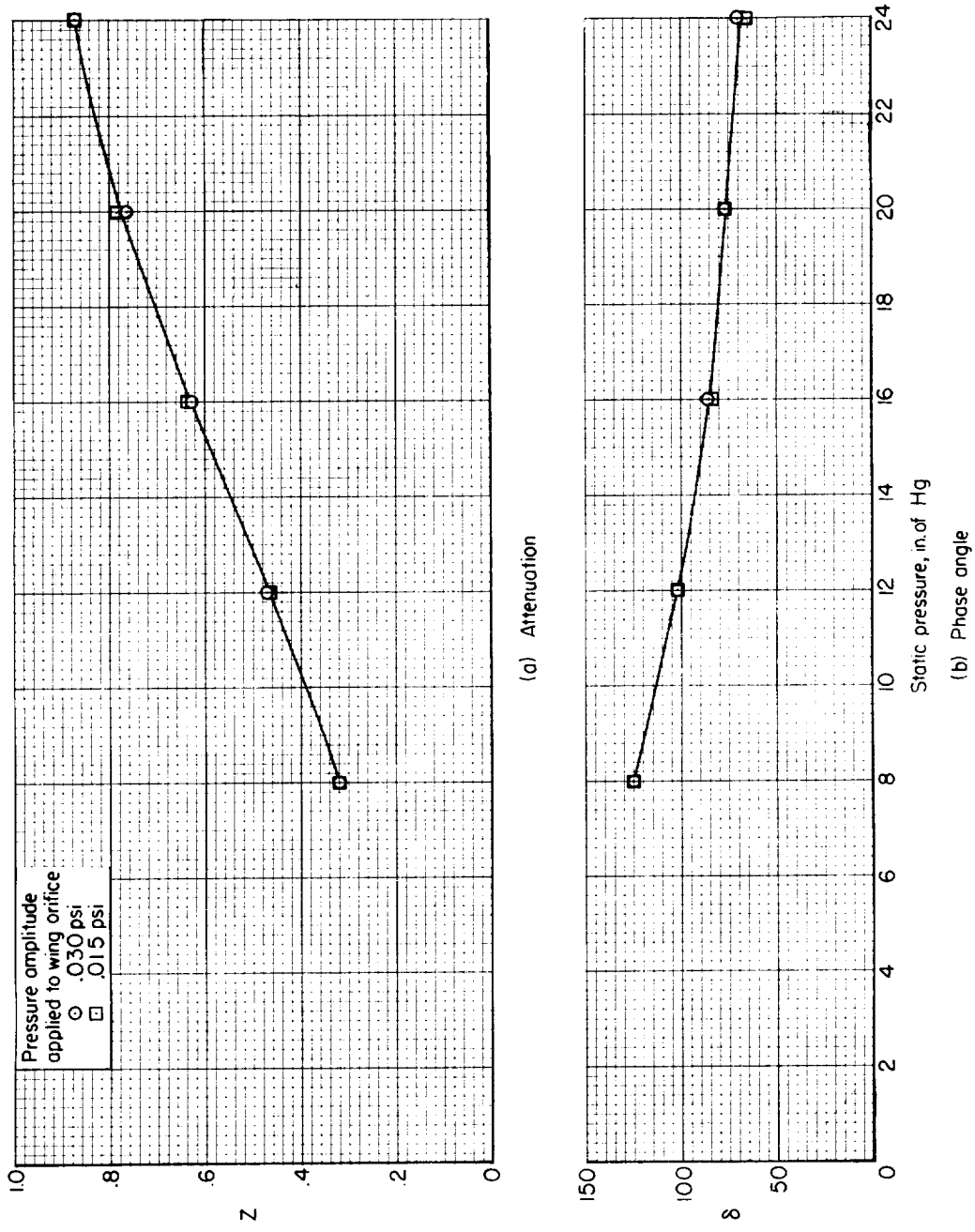


Figure 2.- Phase lag and attenuation typical of orifice tube at the 90-percent semispan station.

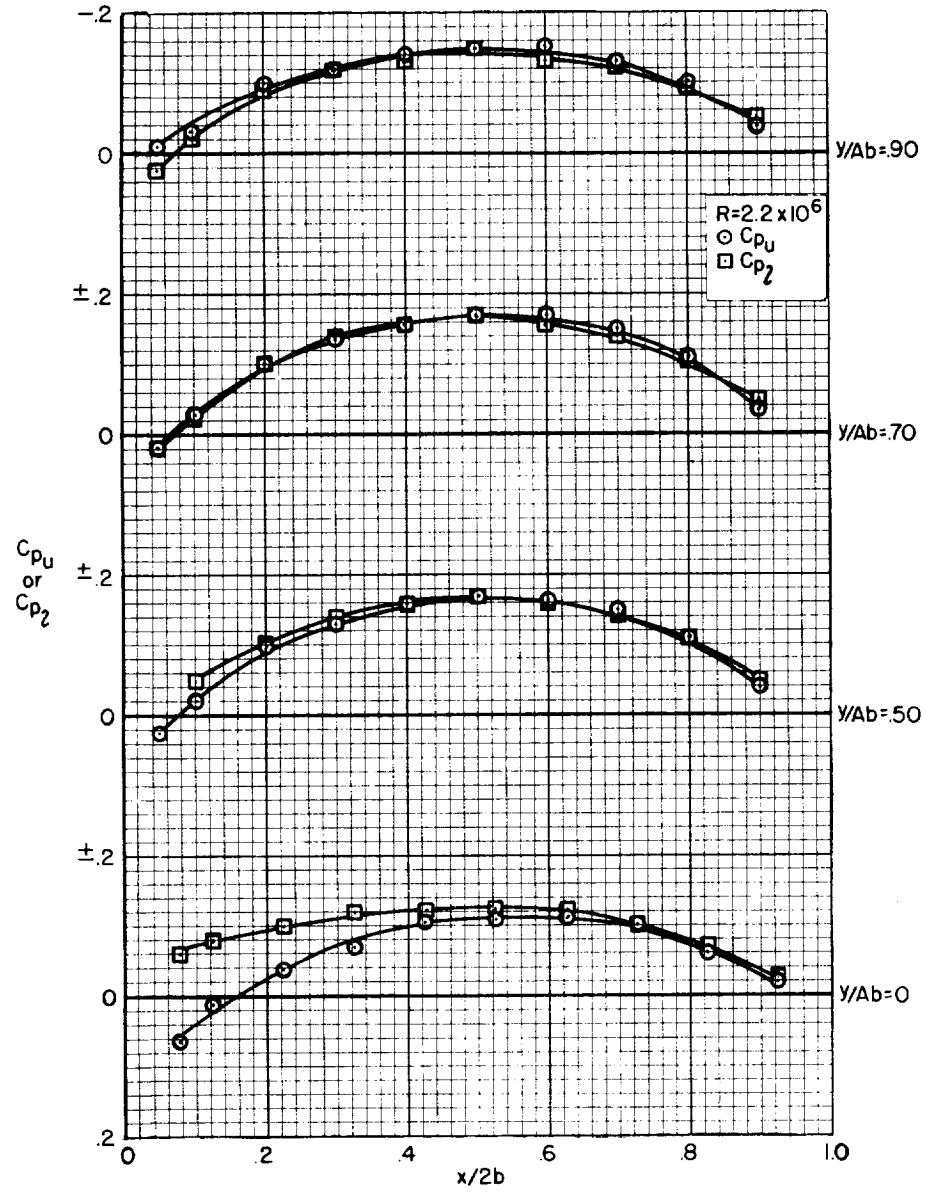


(a) Pressures on upper and lower surfaces; M = 0.24, $\alpha = 0^{\circ}$.

Figure 3.- Static-pressure distributions.

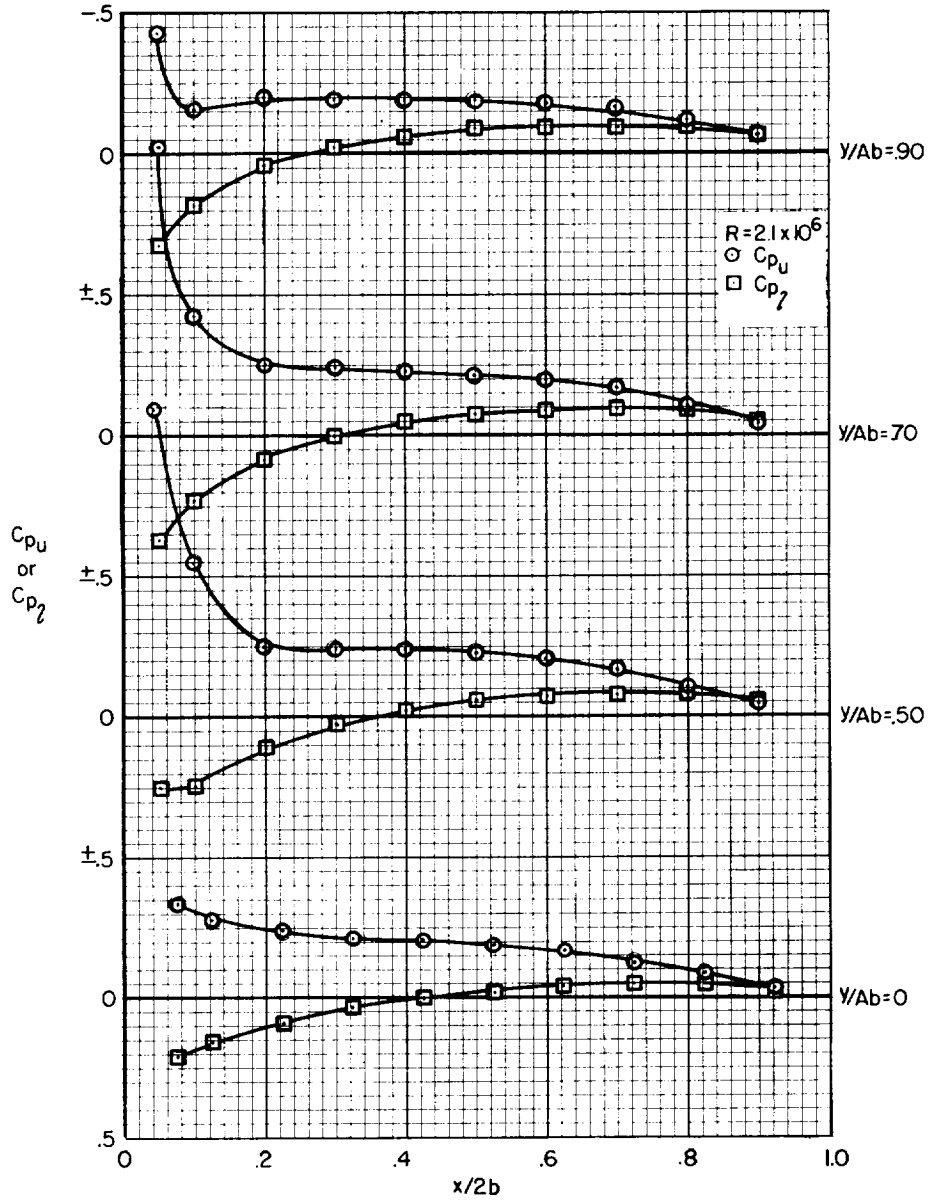


(b) Pressures on upper and lower surfaces; M = 0.24, $\alpha = 5^{\circ}$.

Figure 3.- Continued.

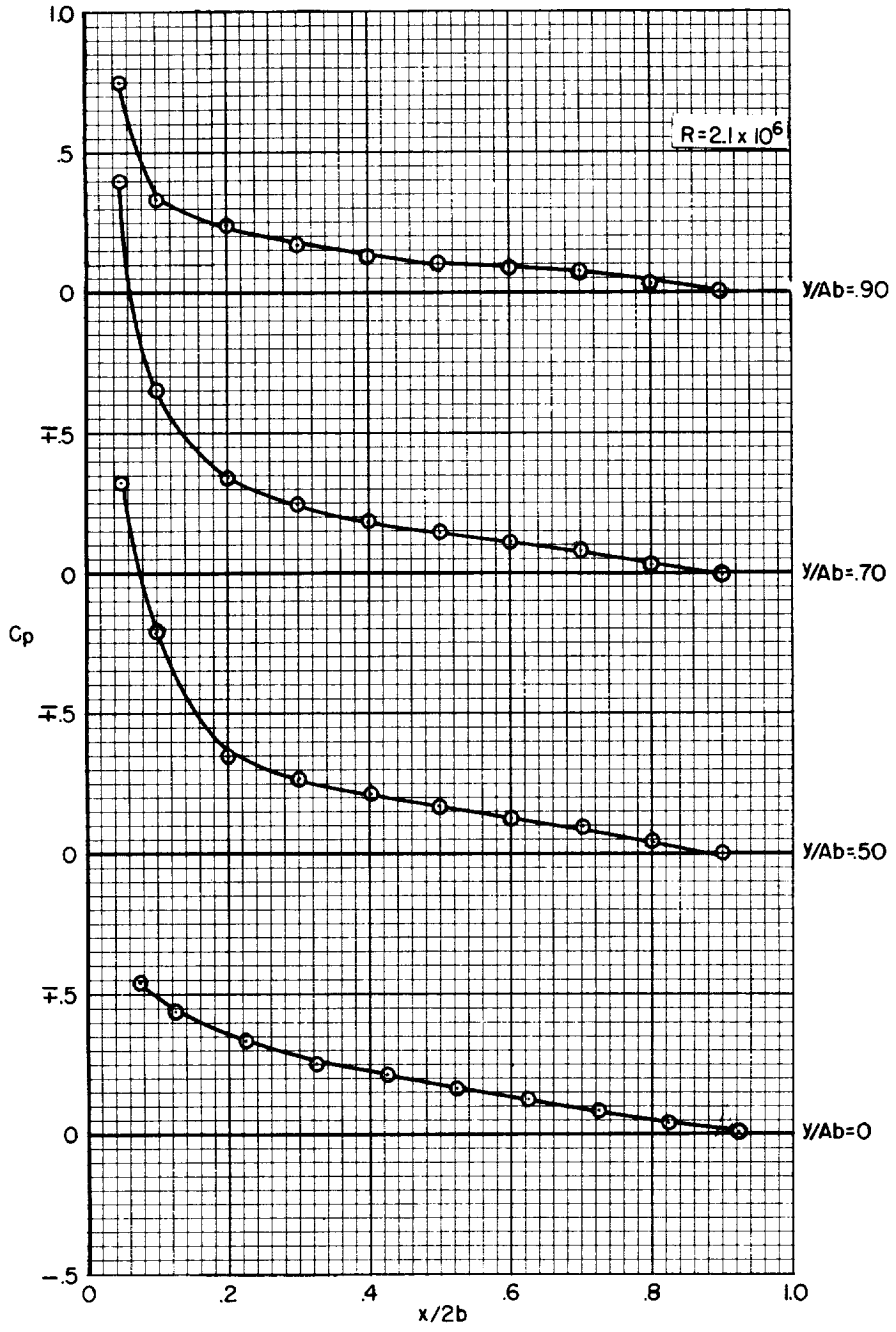


(c) Lifting pressures; M = 0.24, $\alpha = 5^{\circ}$.

Figure 3.- Continued.

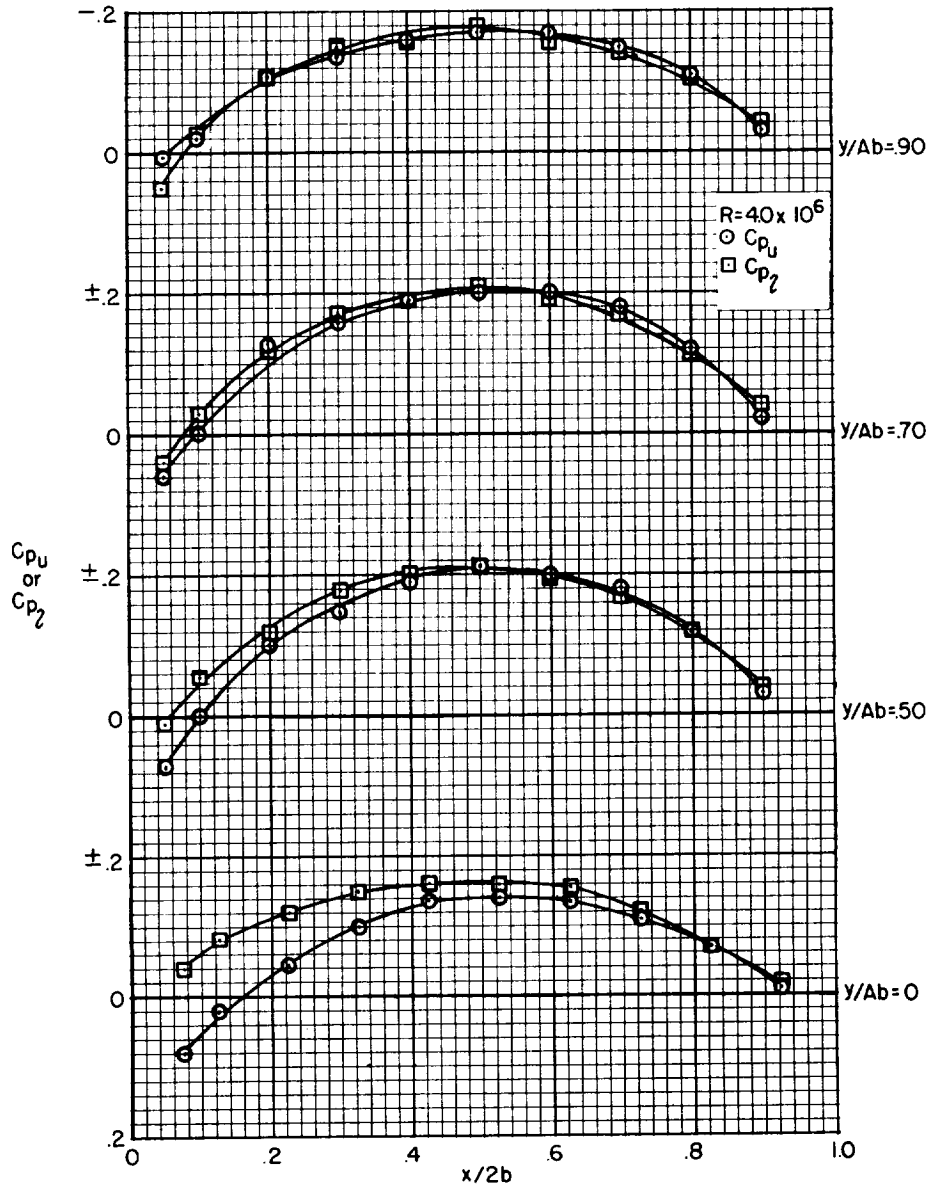


(d) Pressures on upper and lower surfaces; M = 0.70, $\alpha = 0^{\circ}$.

Figure 3.- Continued.

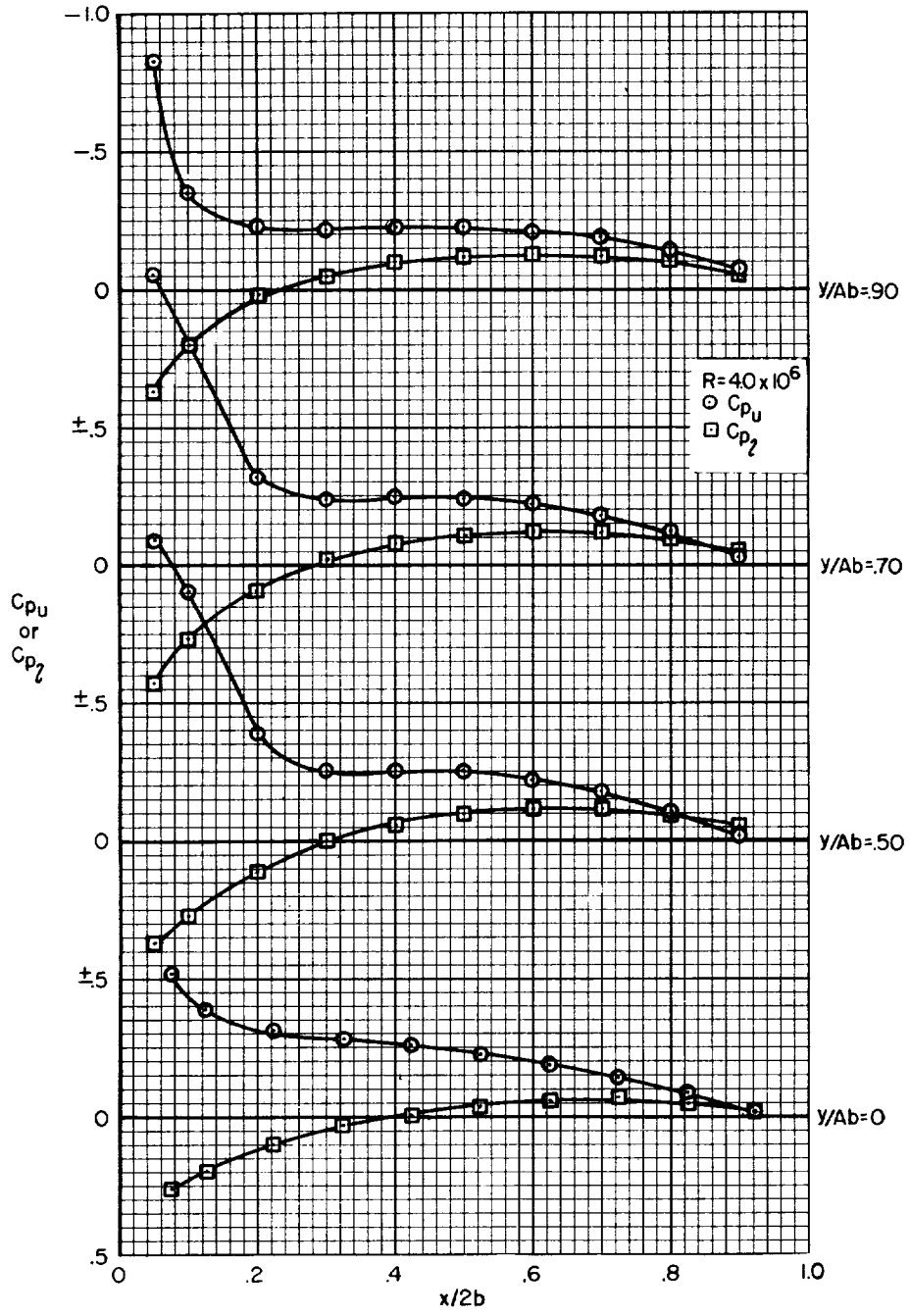


(e) Pressures on upper and lower surfaces; M = 0.70, $\alpha = 5^{\circ}$.

Figure 3.- Continued.

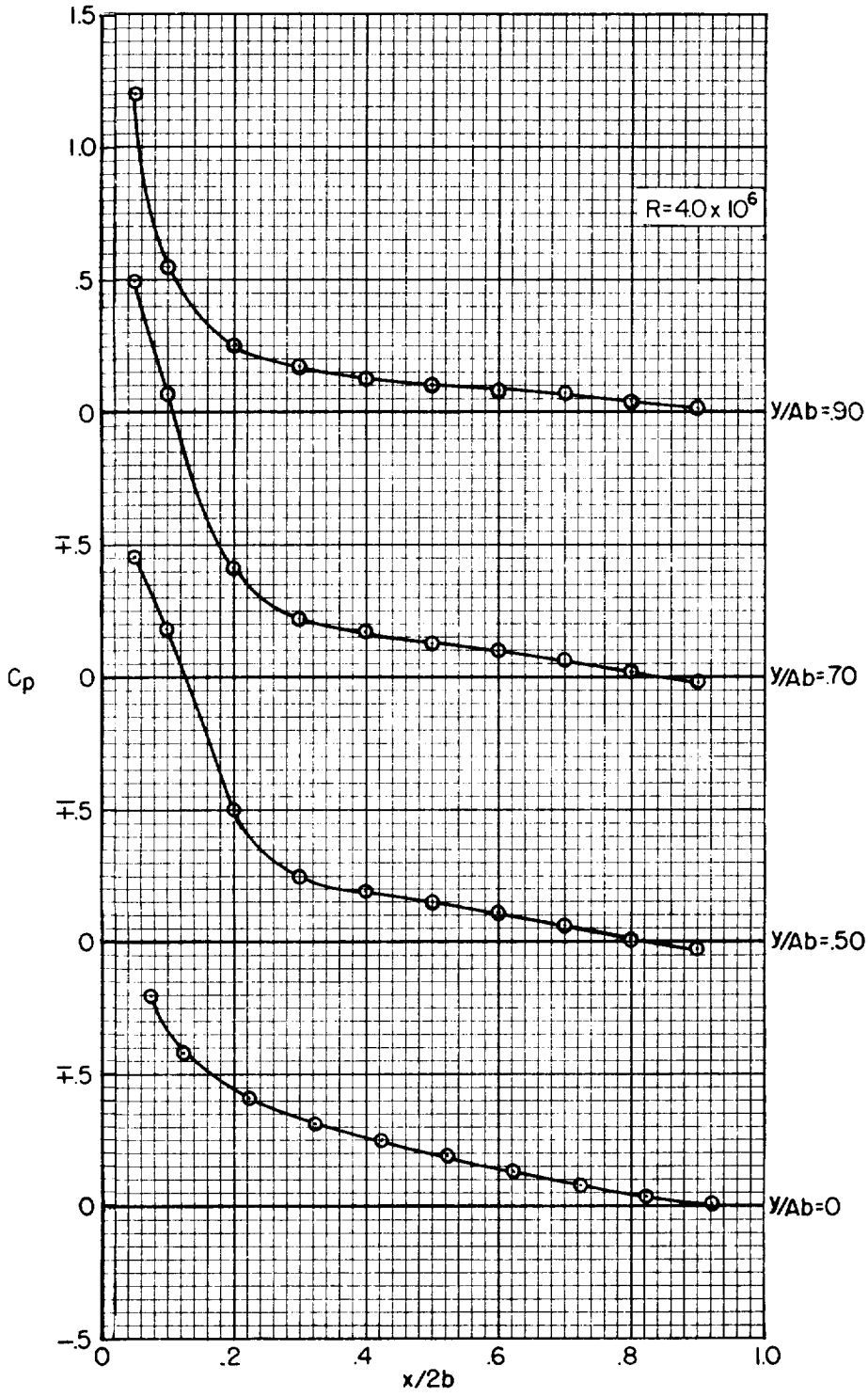


(f) Lifting pressures; M = 0.70, $\alpha = 5^{\circ}$.

Figure 3.- Continued.

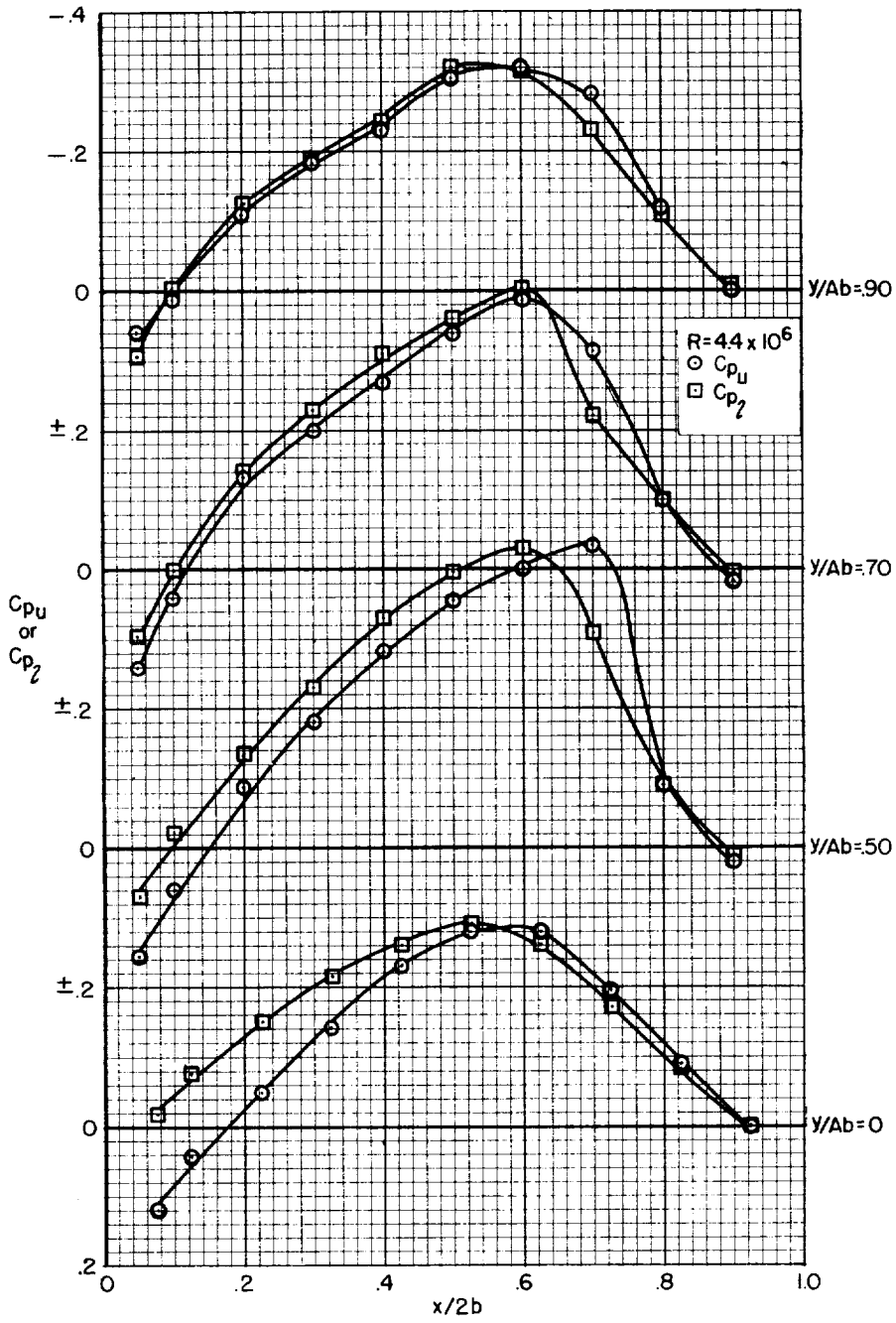


(g) Pressures on upper and lower surfaces; M = 0.90, $\alpha = 0^{\circ}$.

Figure 3.- Continued.

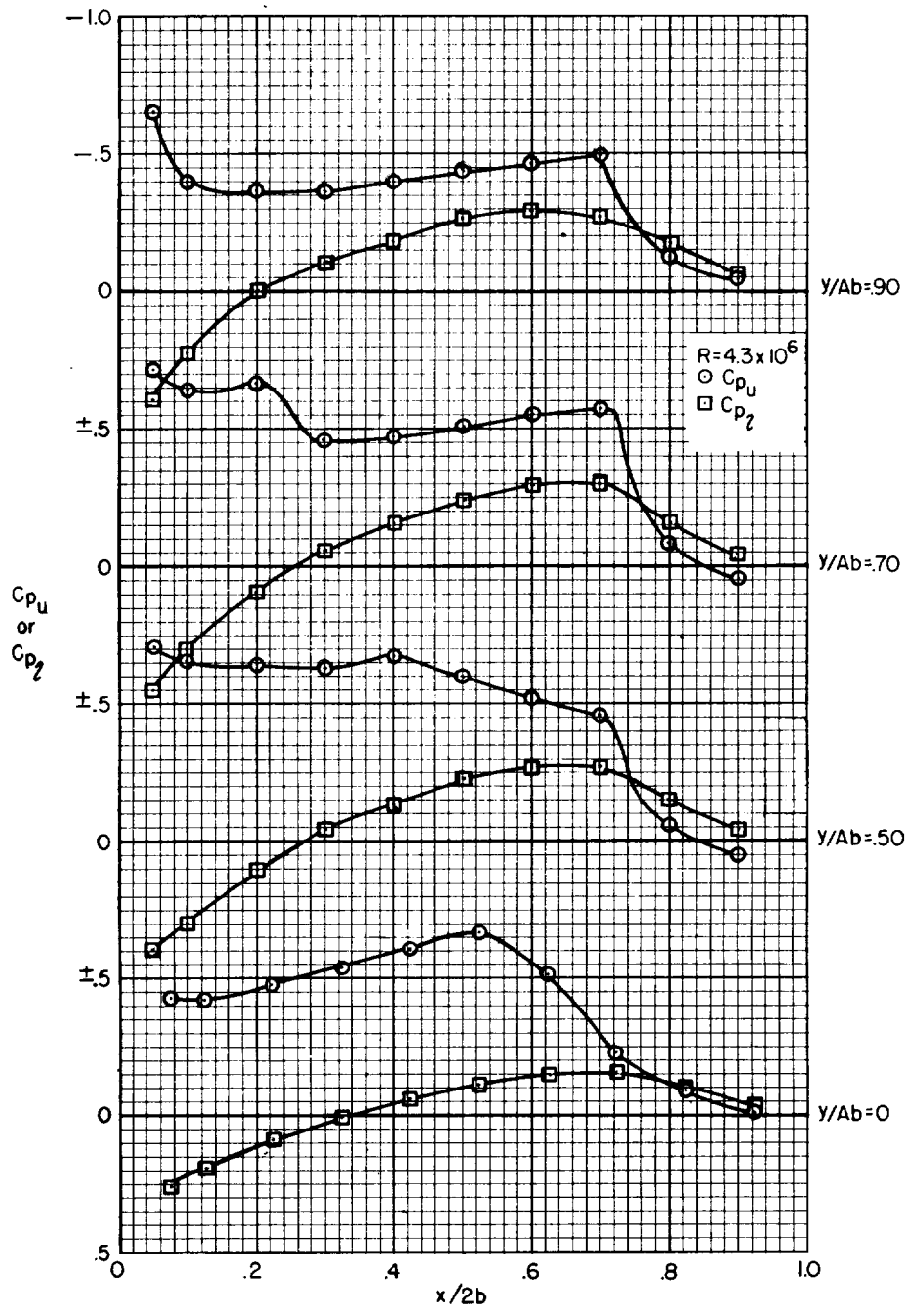


(h) Pressures on upper and lower surfaces; M = 0.90, $\alpha = 5^{\circ}$.

Figure 3.- Continued.

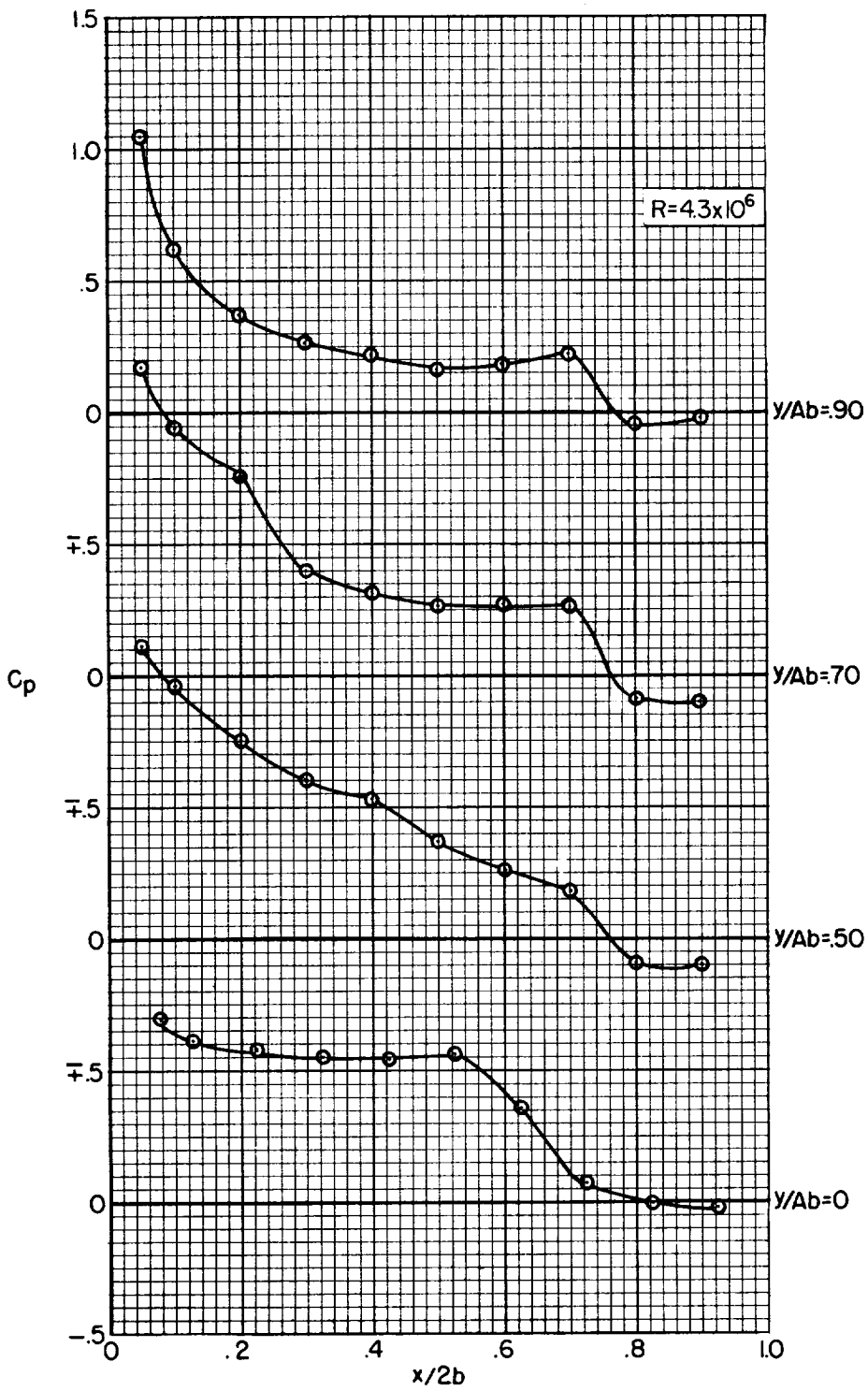


(i) Lifting pressures; M = 0.90, $\alpha = 5^{\circ}$.

Figure 3.- Continued.

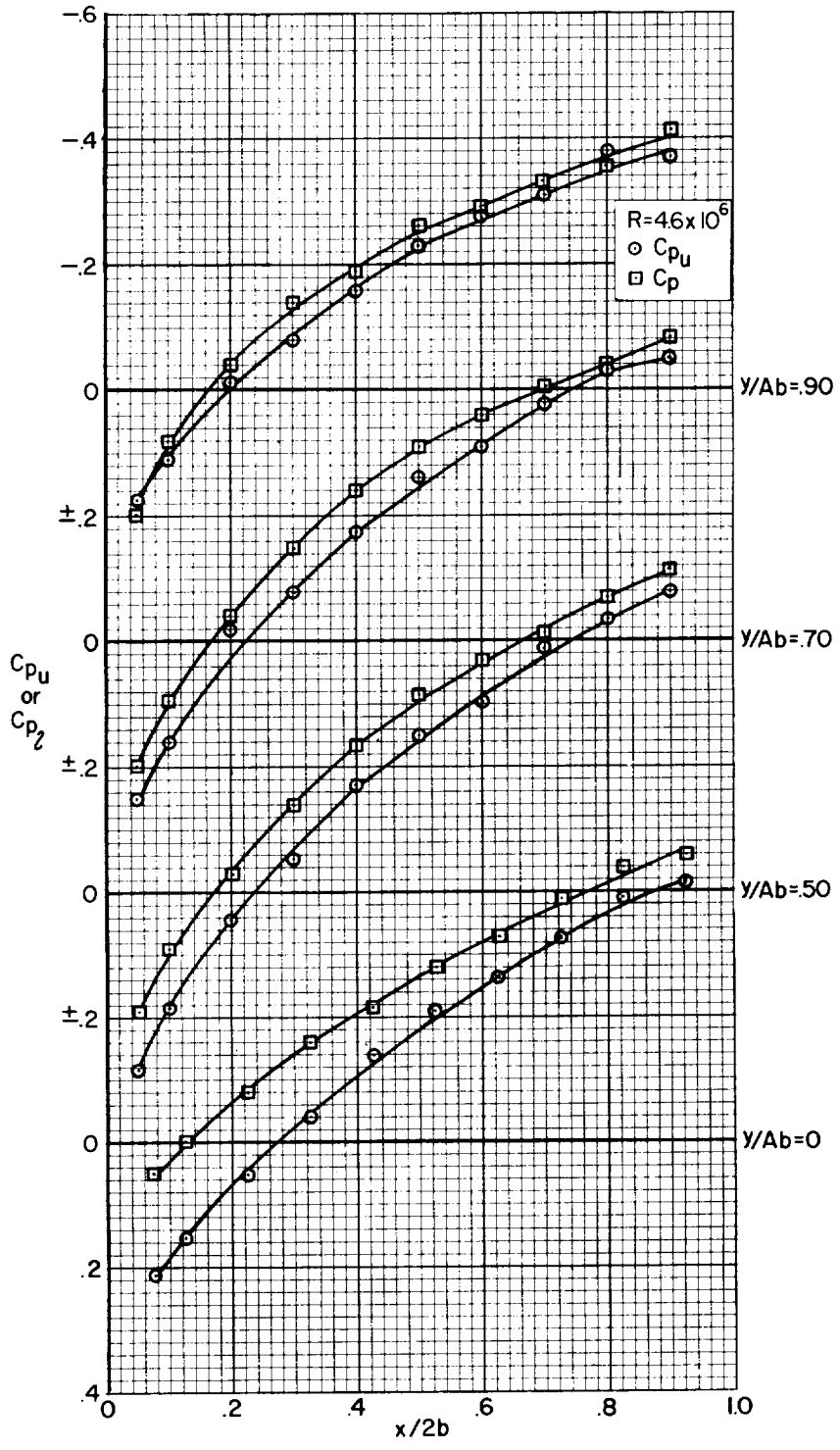


(j) Pressures on upper and lower surfaces; M = 1.00, $\alpha = 0^{\circ}$.

Figure 3.- Continued.

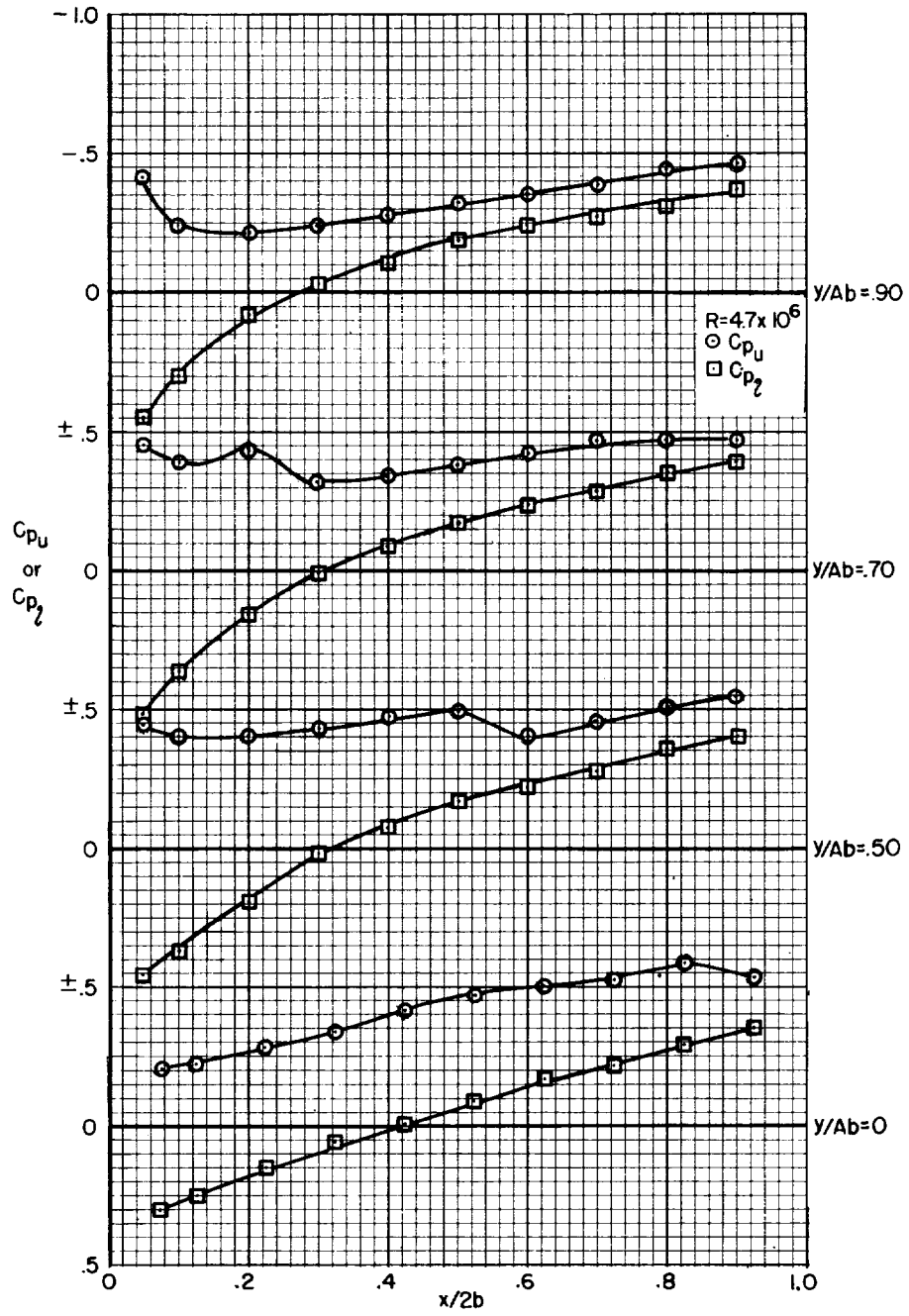


(k) Pressures on upper and lower surfaces; M = 1.00, $\alpha = 5^{\circ}$.

Figure 3.- Continued.

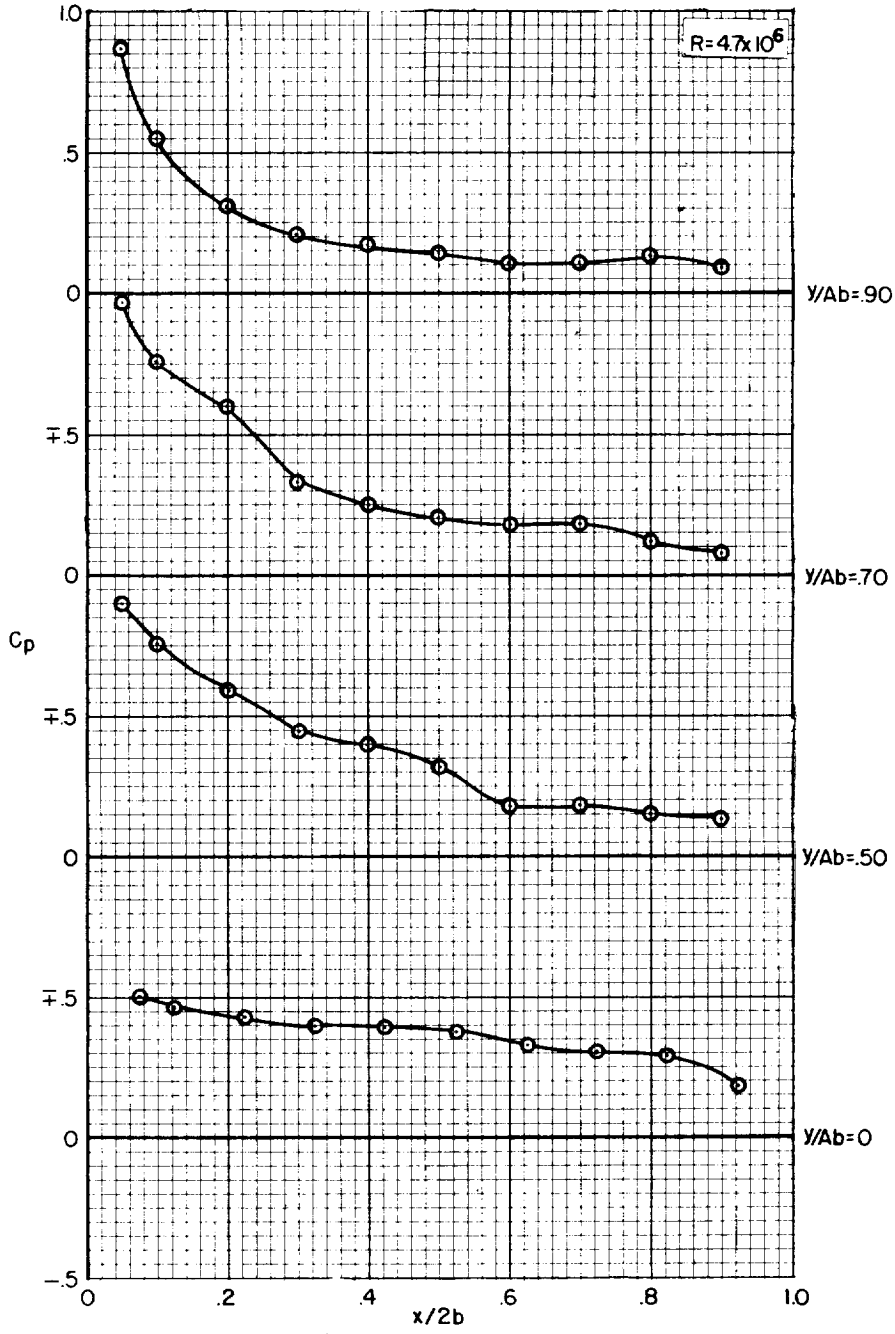


(*l*) Lifting pressures; M = 1.00, $\alpha = 5^{\circ}$.

Figure 3.- Continued.

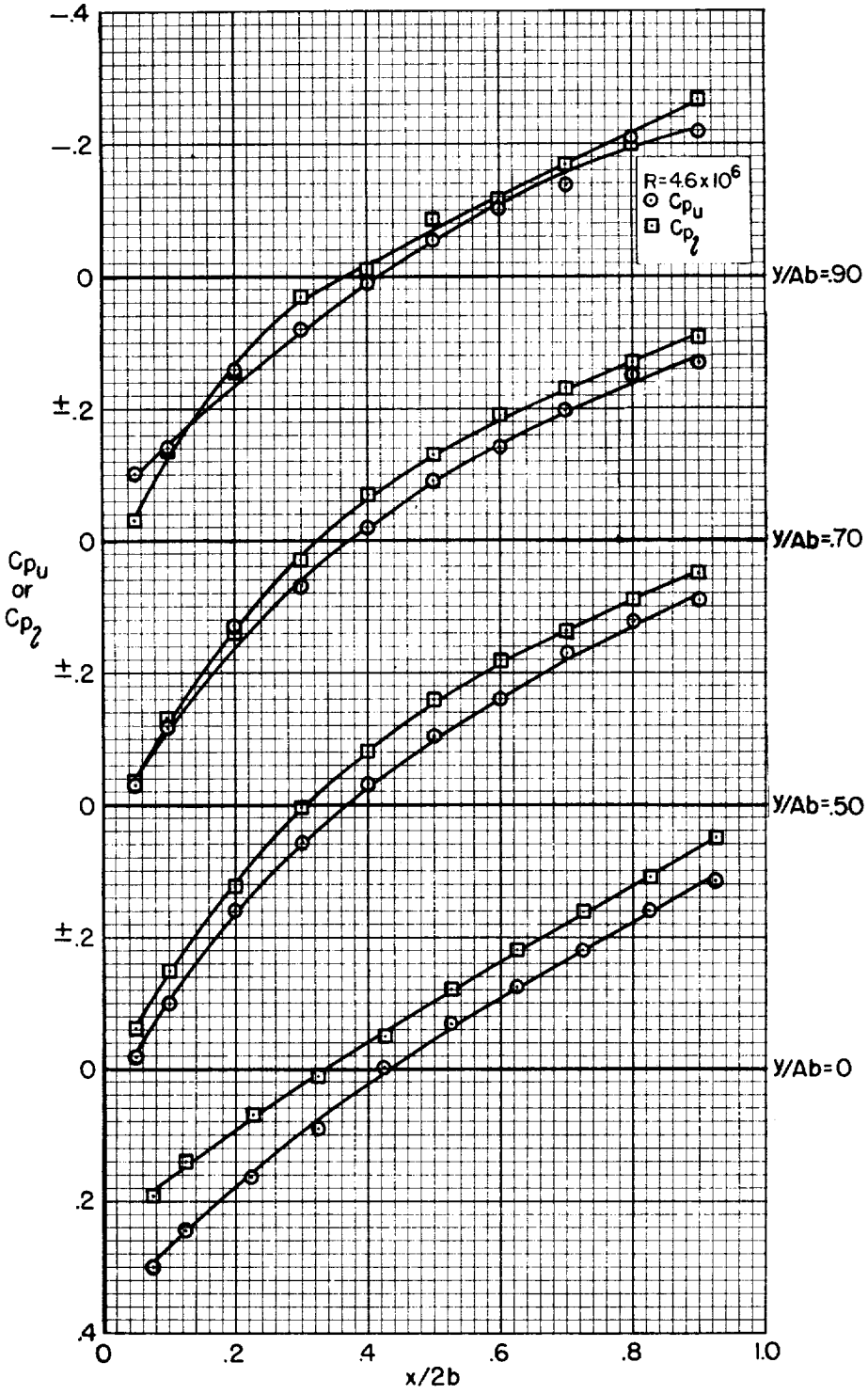


(m) Pressures on upper and lower surfaces; M = 1.10, $\alpha = 0^{\circ}$.

Figure 3.- Continued.

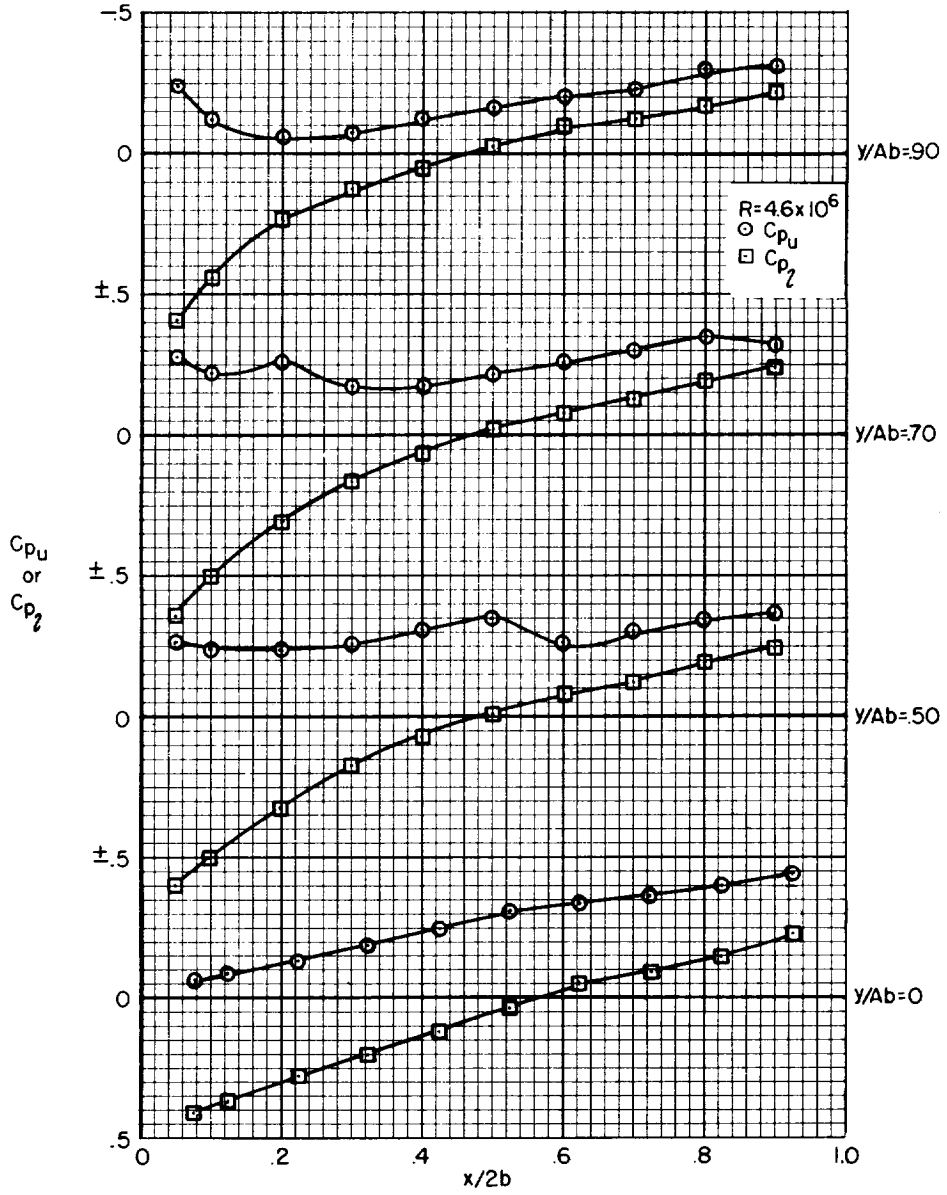


(n) Pressures on upper and lower surfaces; M = 1.10, $\alpha = 5^{\circ}$.

Figure 3.- Continued.

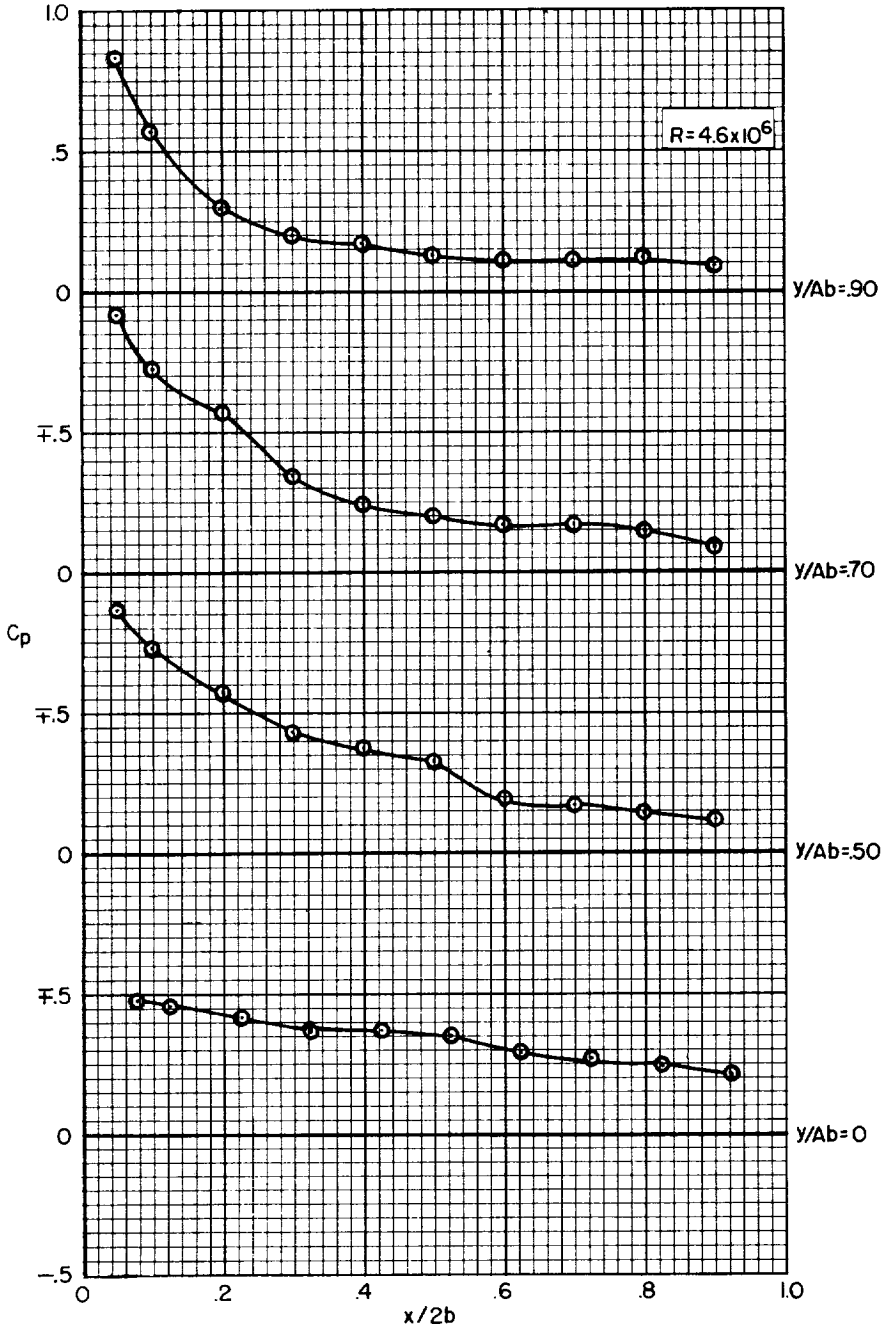


(o) Lifting pressures; M = 1.10, $\alpha = 5^{\circ}$.

Figure 3.- Continued.

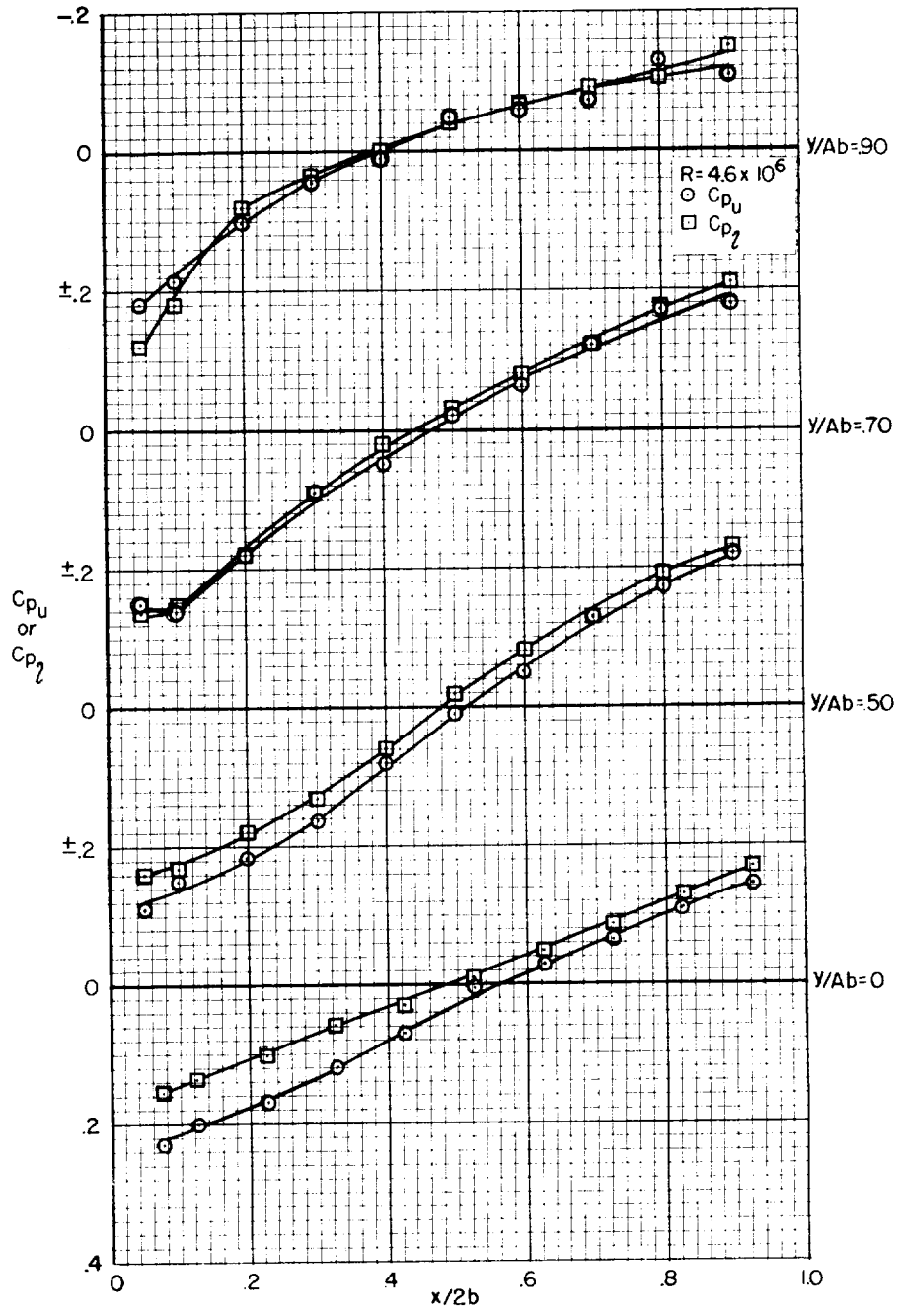


(p) Pressures on upper and lower surfaces; M = 1.30, $\alpha = 0^{\circ}$.

Figure 3.- Continued.

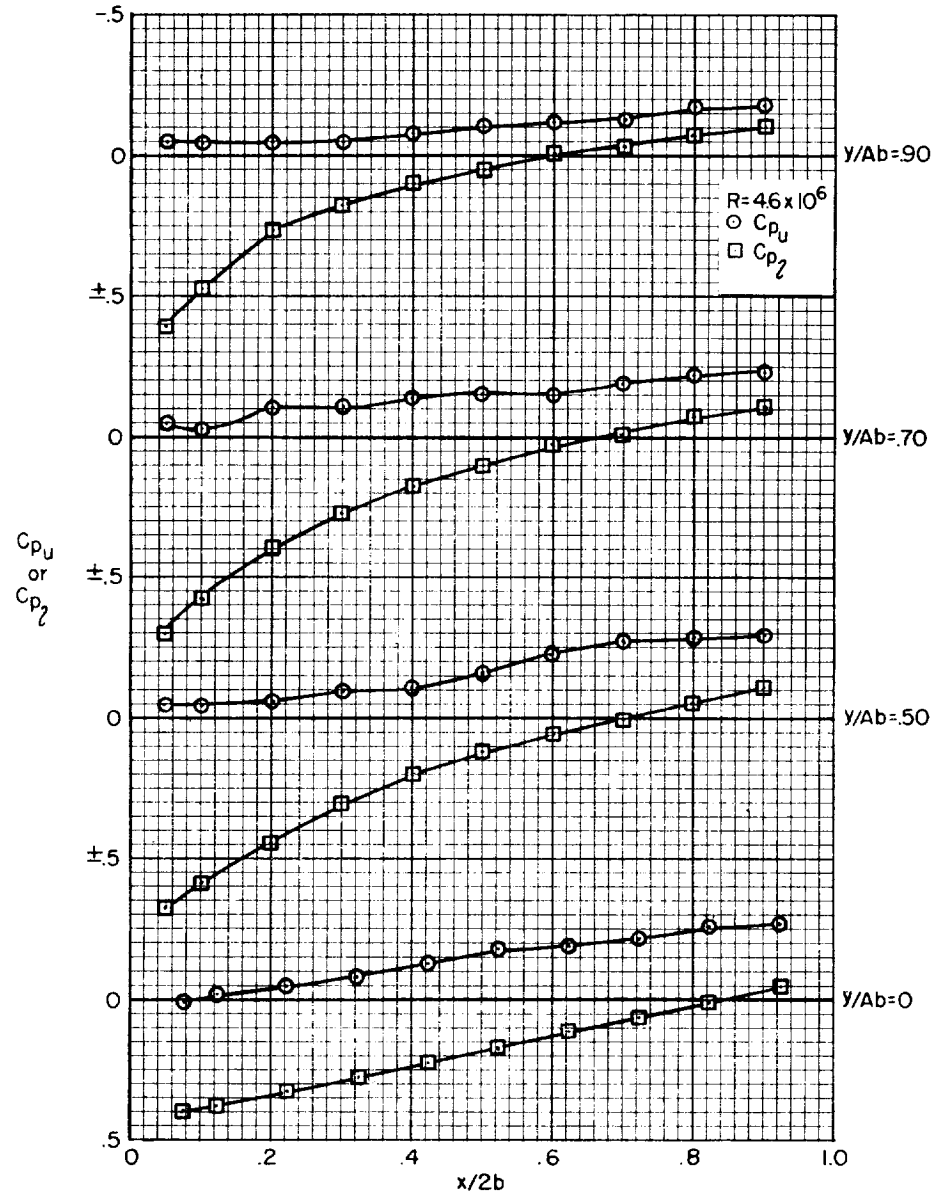


(q) Pressures on upper and lower surfaces; M = 1.30, $\alpha = 5^{\circ}$.

Figure 3.- Continued.

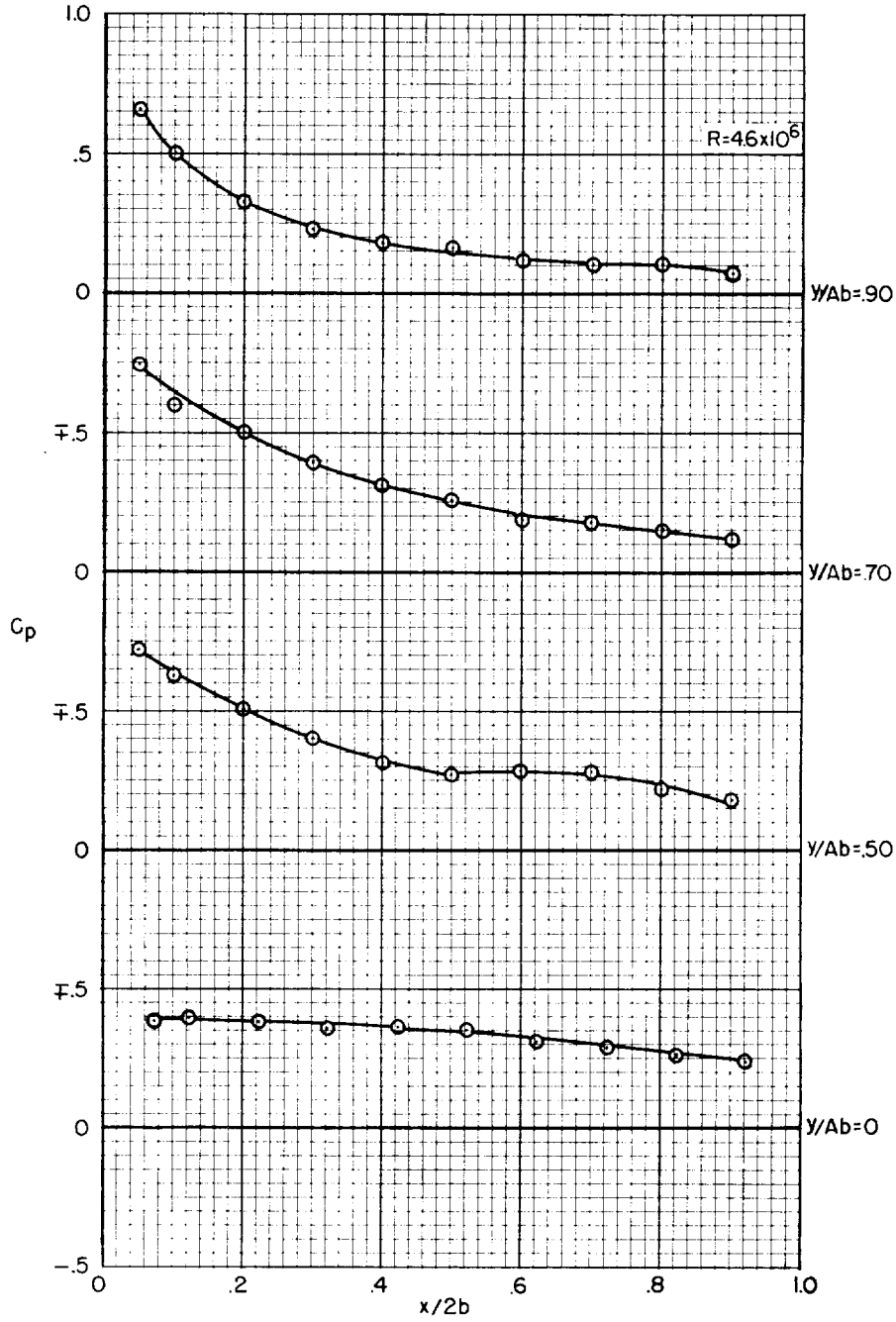


(r) Lifting pressures; M = 1.30, $\alpha = 5^{\circ}$.

Figure 3.- Concluded.

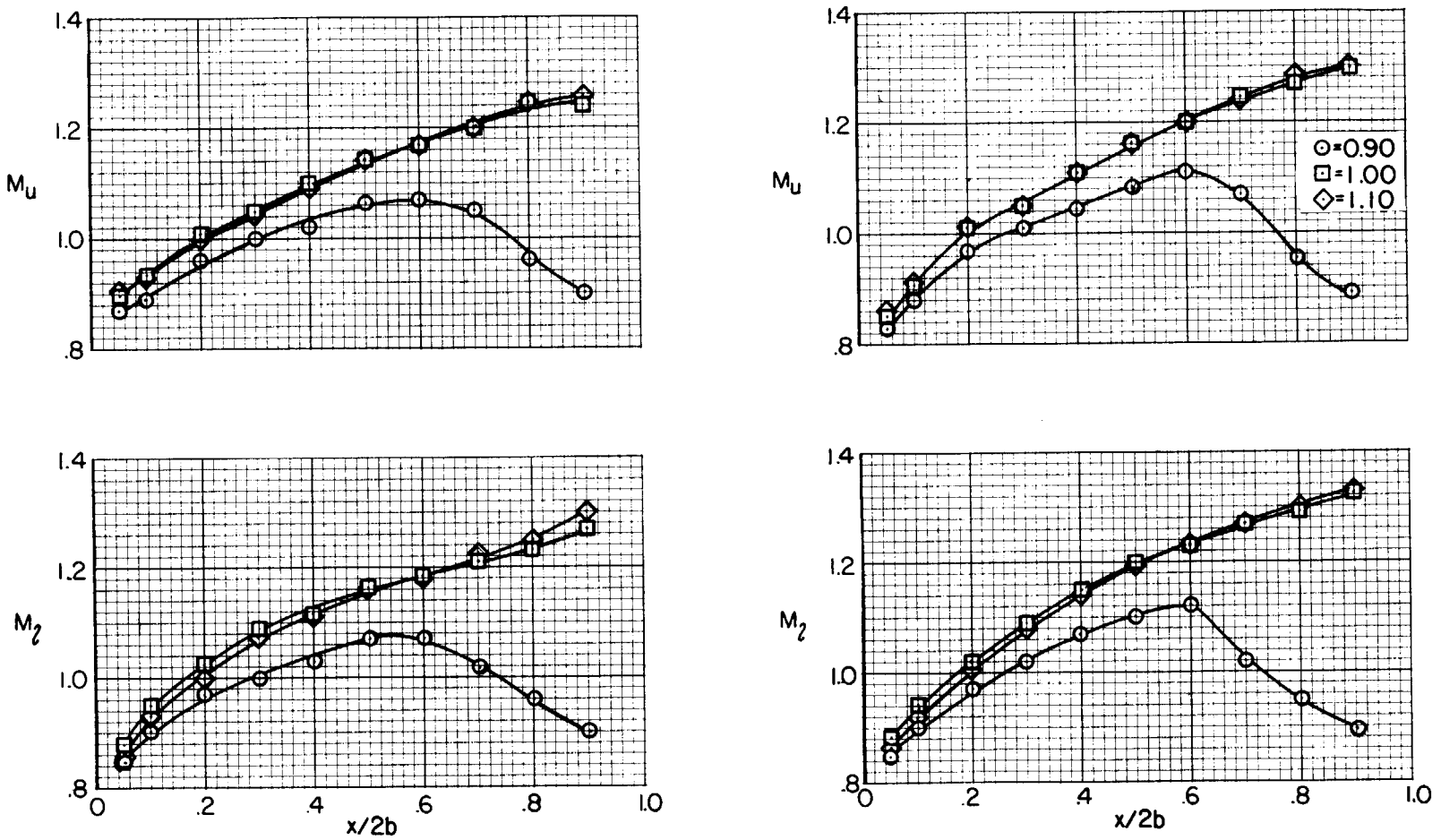


(a) y/Ab = 0.90, $\alpha = 0^\circ$

(b) y/Ab = 0.70, $\alpha = 0^\circ$

Figure 4.- Local Mach number distribution over surfaces of wing at transonic speeds.

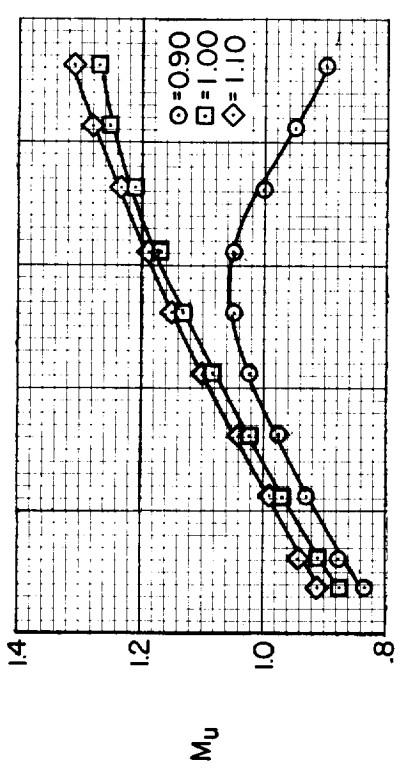


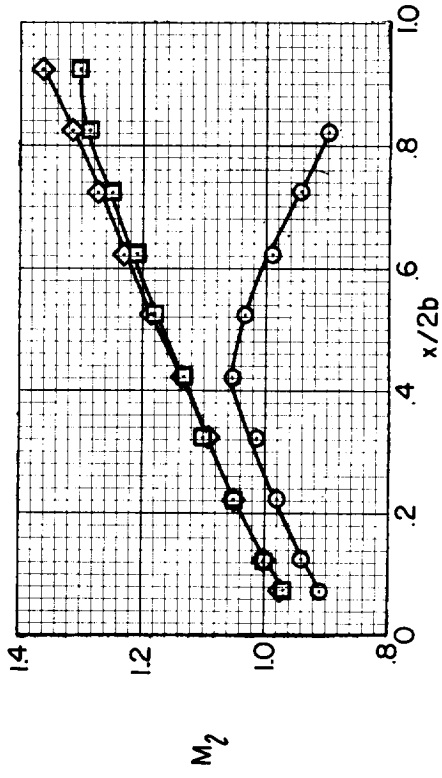


(d) y/Ab = 0, α = 0°

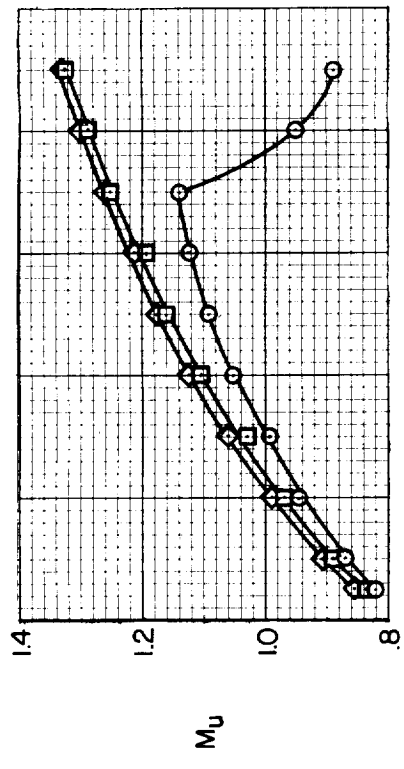


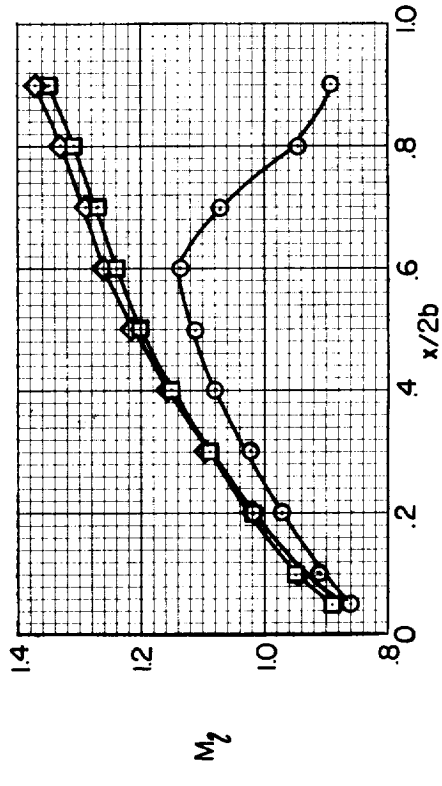


(c) y/Ab = 0.50, α = 0°

Figure 4.- Continued.

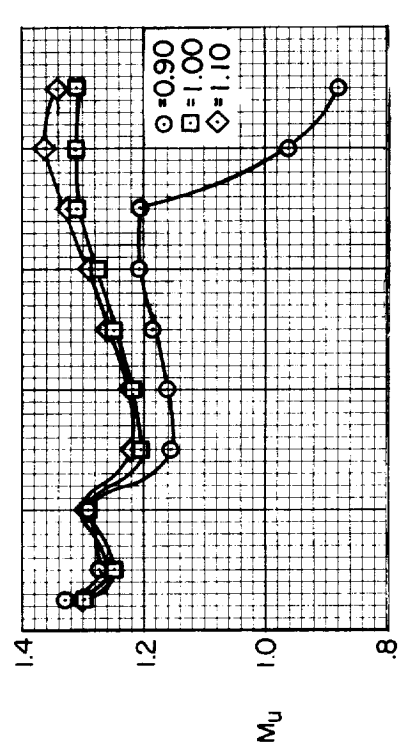


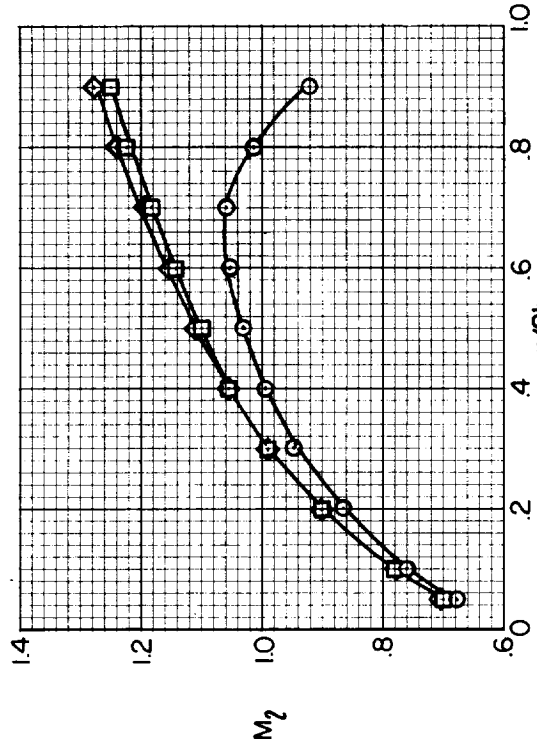


(f) $y/Ab = 0.70$, $\alpha = 5^\circ$

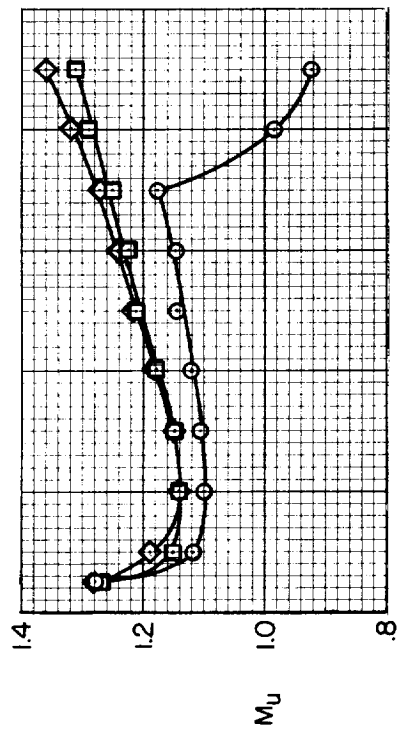


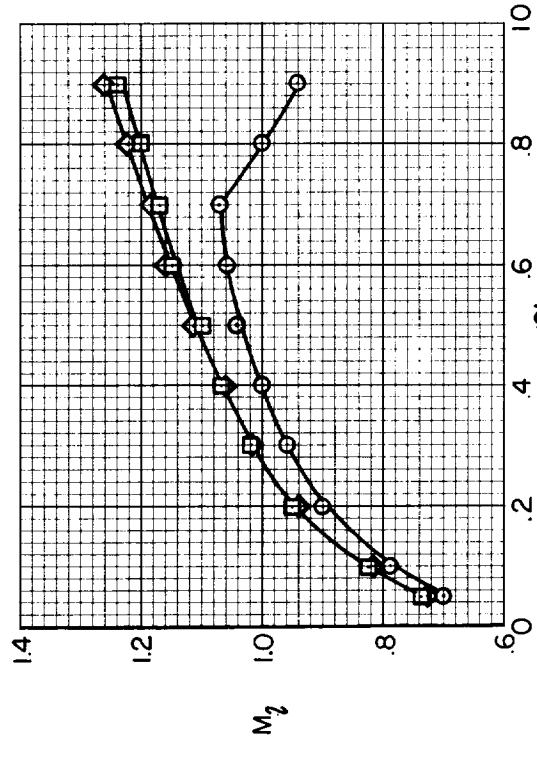


(e) $y/Ab = 0.90$, $\alpha = 5^\circ$

Figure 4.- Continued.

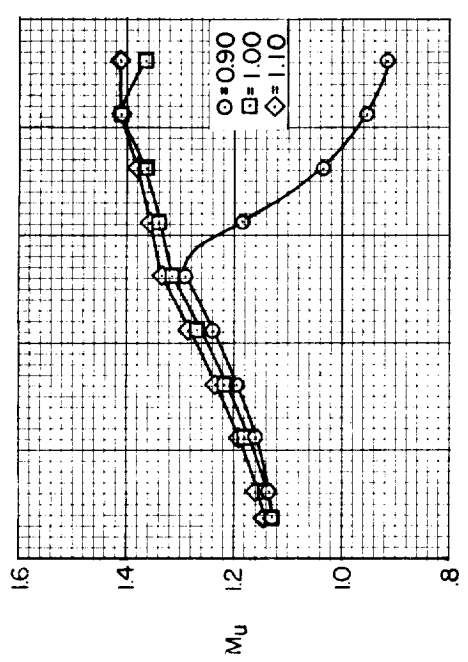


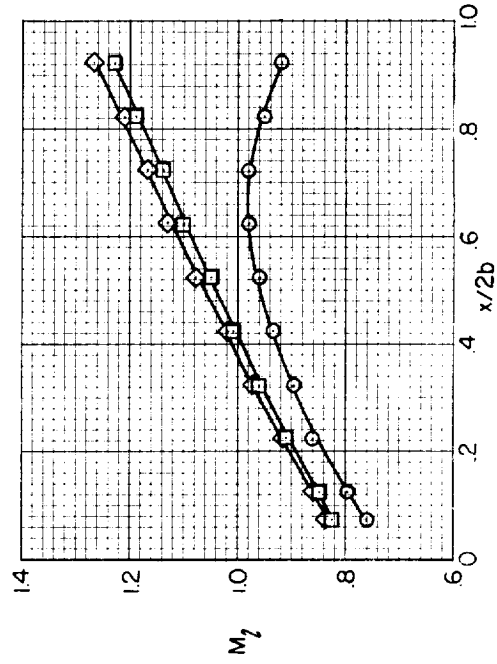


(h) $y/Ab = 0$, $\alpha = 5^\circ$

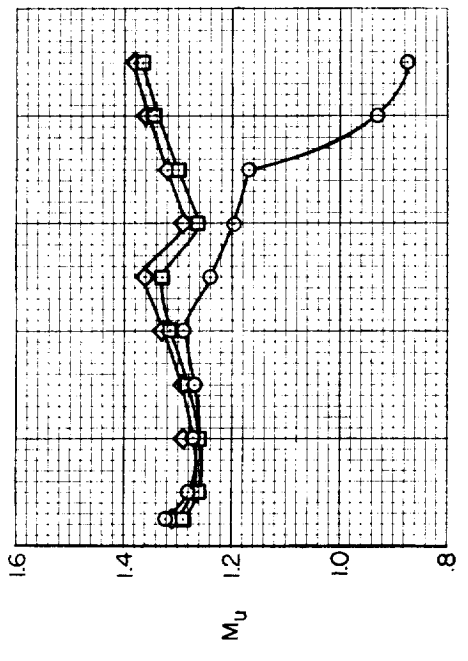


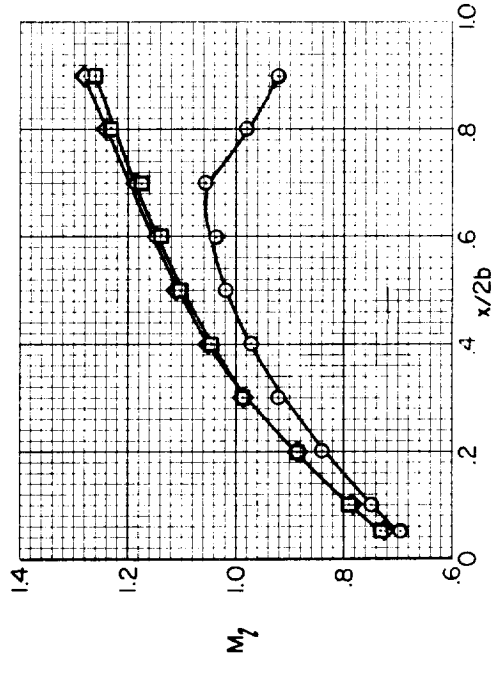


(g) $y/Ab = 0.50$, $\alpha = 5^\circ$

Figure 4.- Concluded.

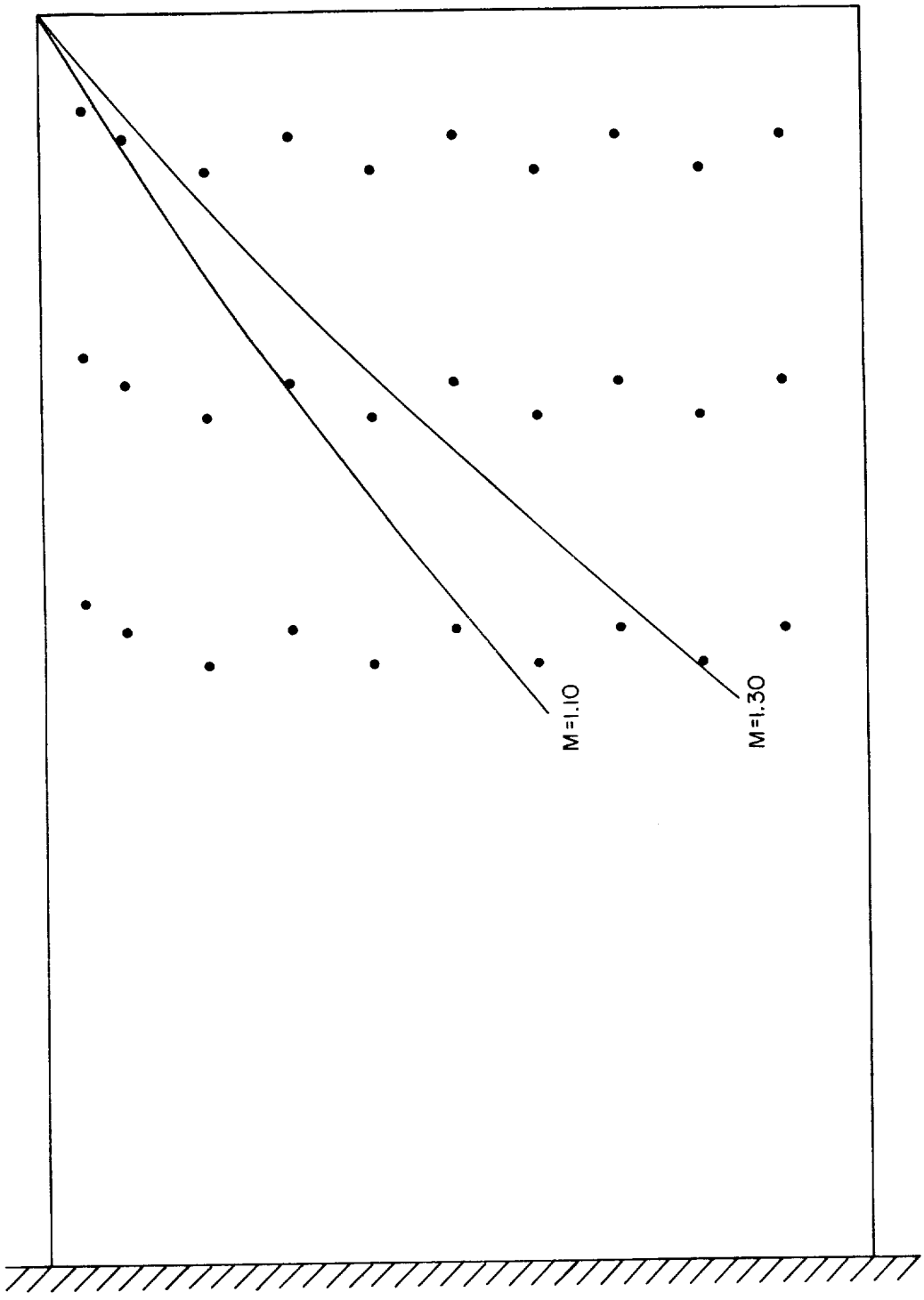


Figure 5.- Plot showing the approximate location of the curve bounding the wing-tip region of influence.

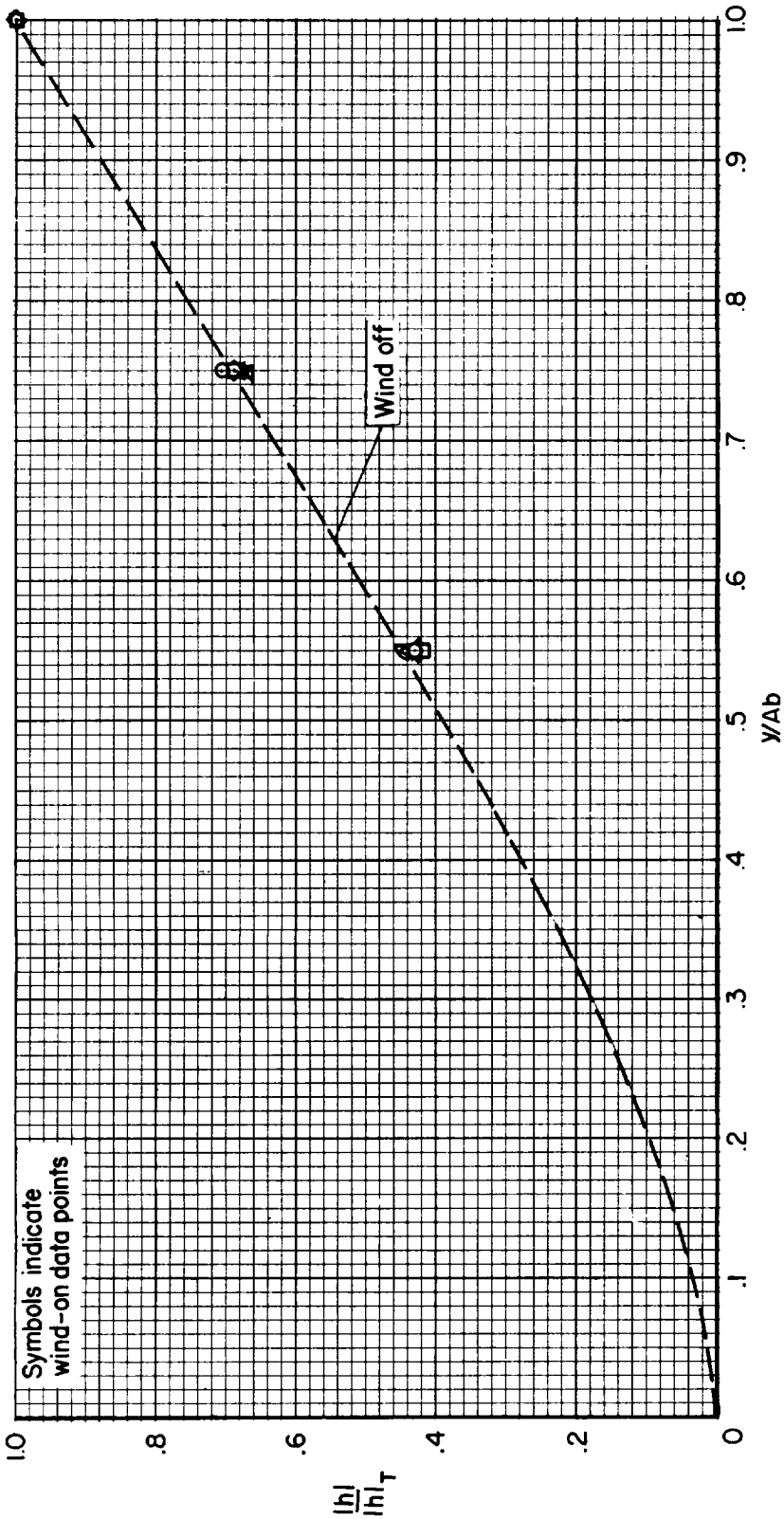


Figure 6.- Normalized mode shape.

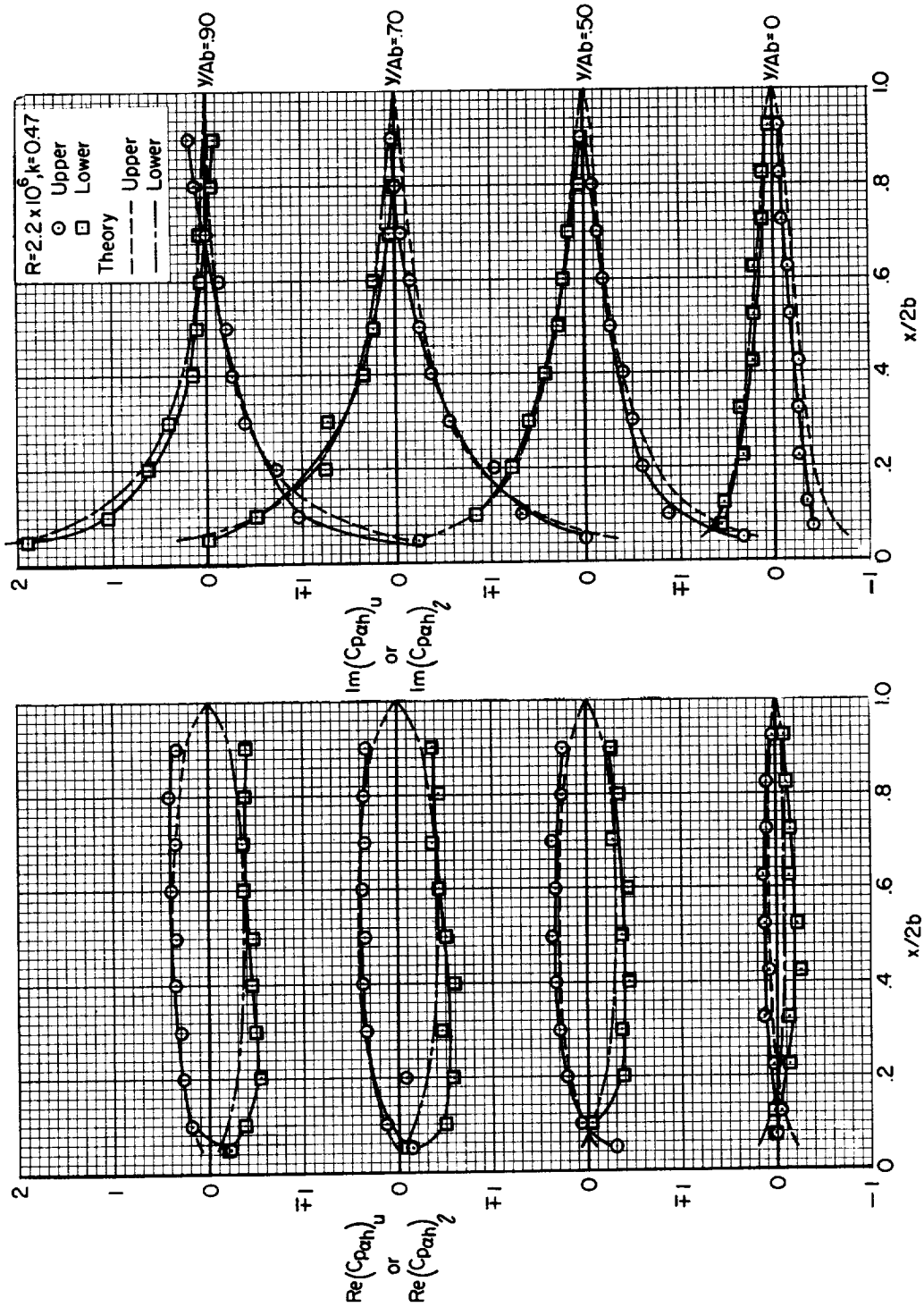


Figure 7.- In-phase and out-of-phase components of the surface pressure coefficient at $M = 0.24$, $\alpha = 0^{\circ}$.

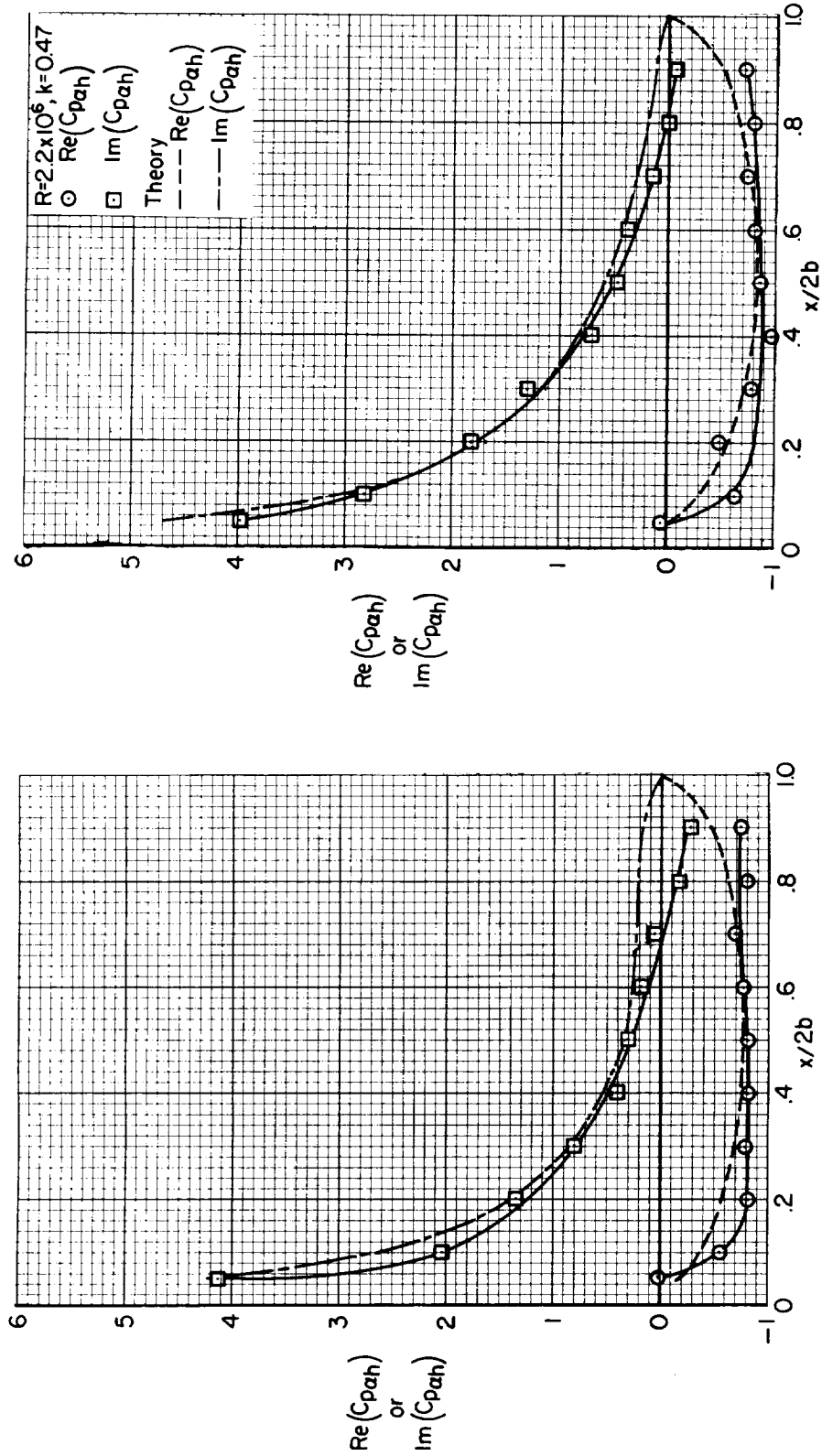


(a) y/Ab = 0.90

(b) y/Ab = 0.70

Figure 8.- In-phase and out-of-phase components of the lifting-pressure coefficient at M = 0.24, $\alpha = 0^{\circ}$.

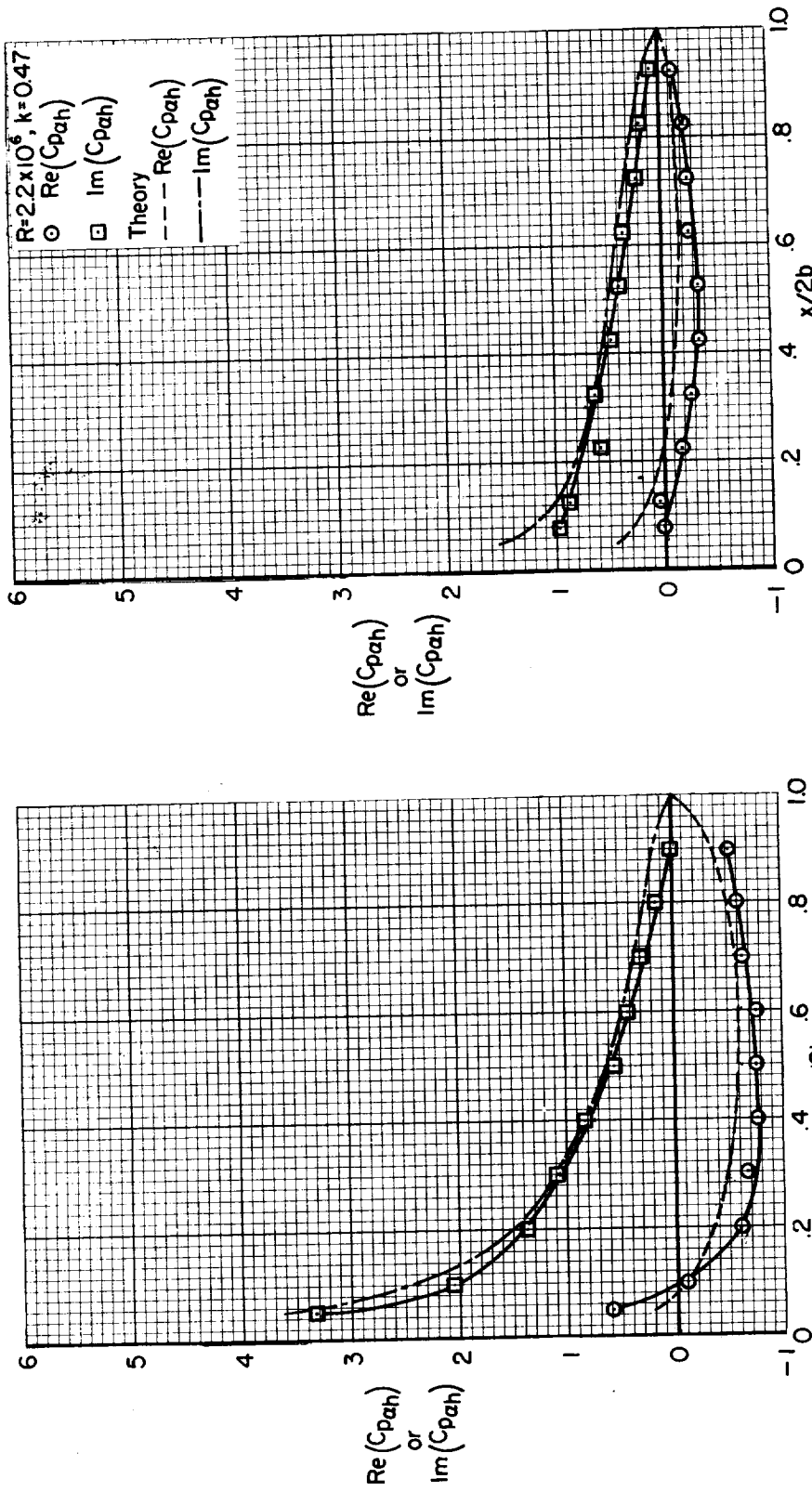


(c) y/Ab = 0.50

(d) y/Ab = 0

Figure 8.- Concluded.

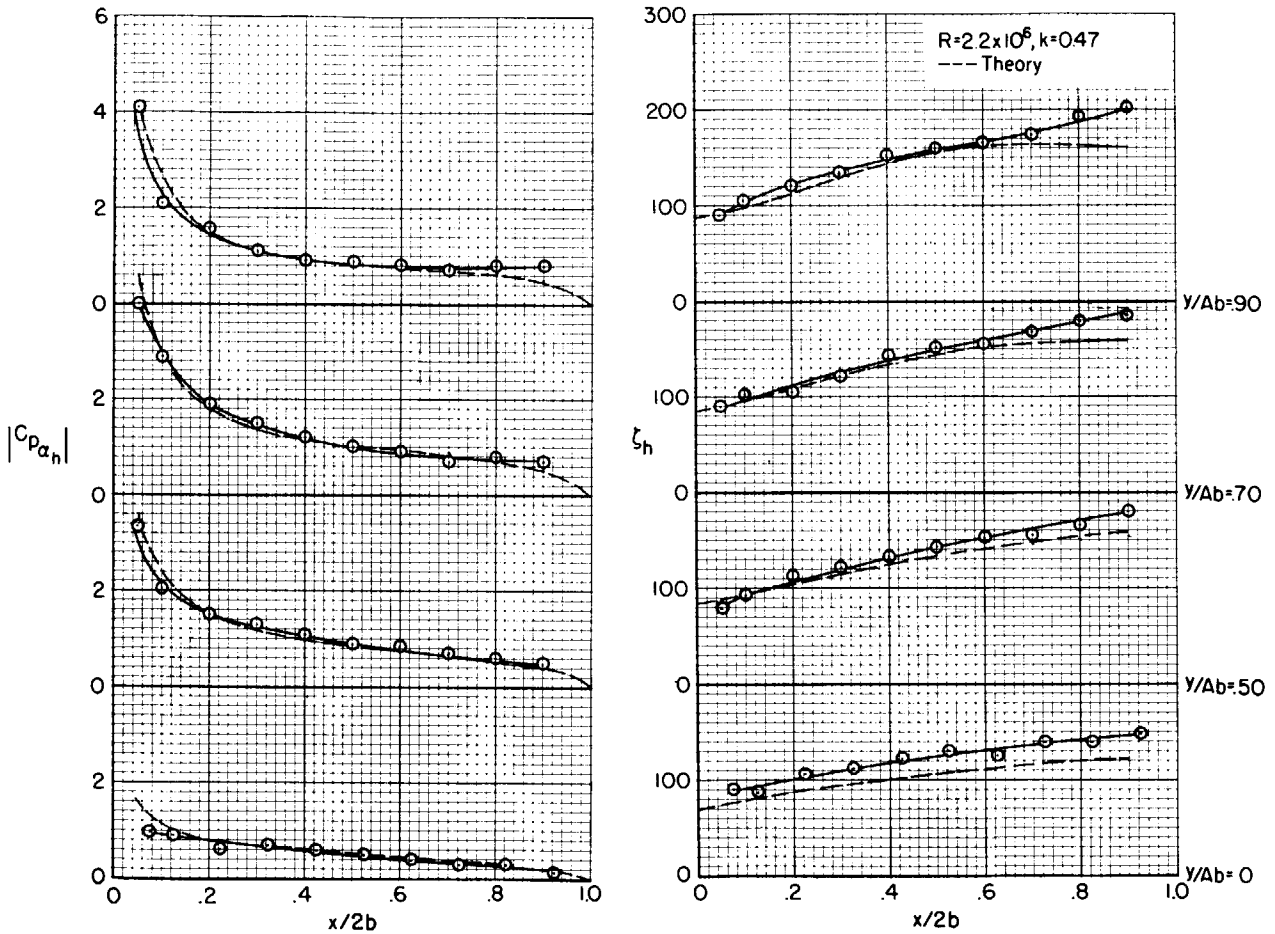


(a) M = 0.24

Figure 9.- Amplitudes and phase angles of the lifting-pressure coefficient at $\alpha = 0^{\circ}$.

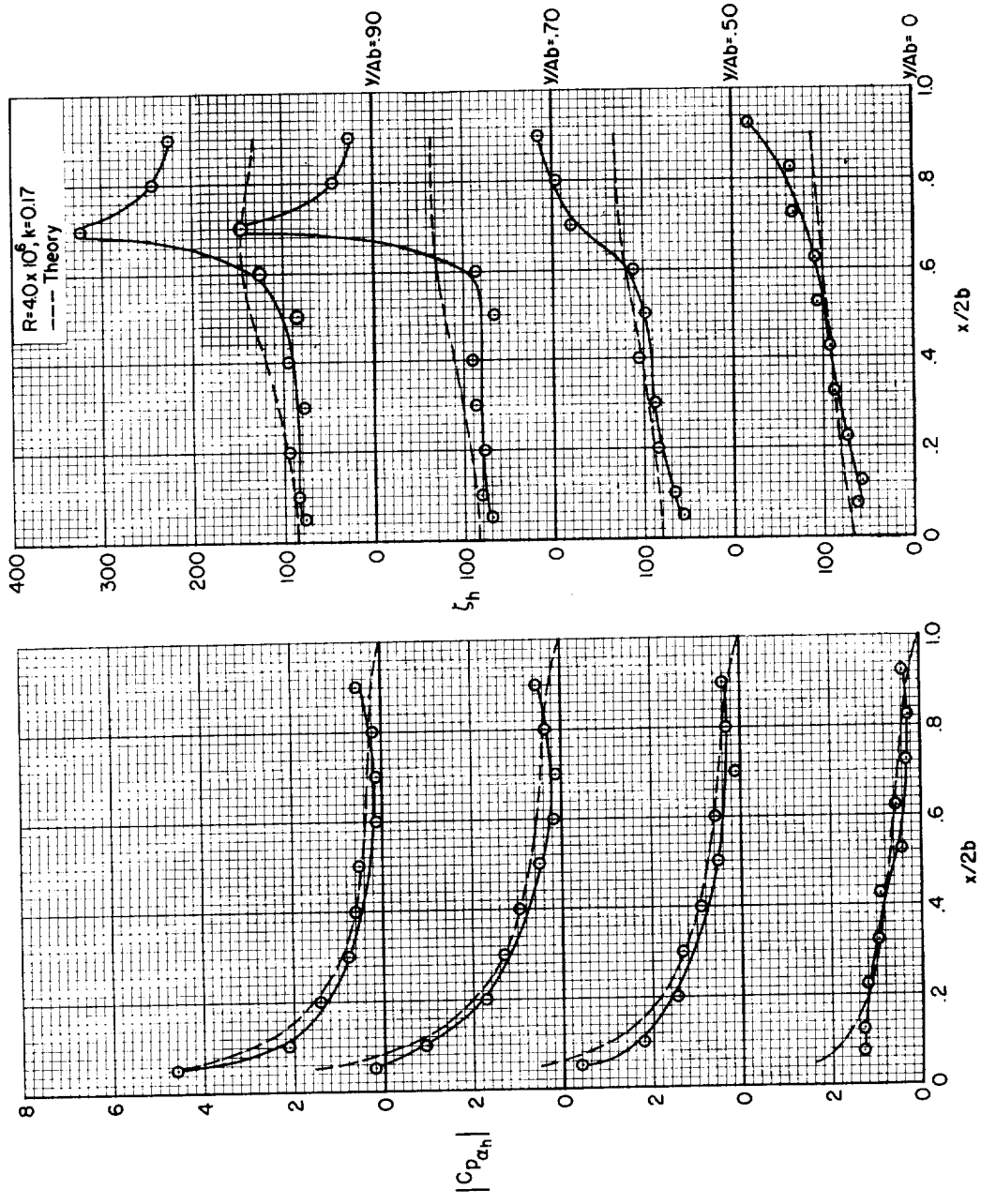


(b) M = 0.70

Figure 9.- Continued.

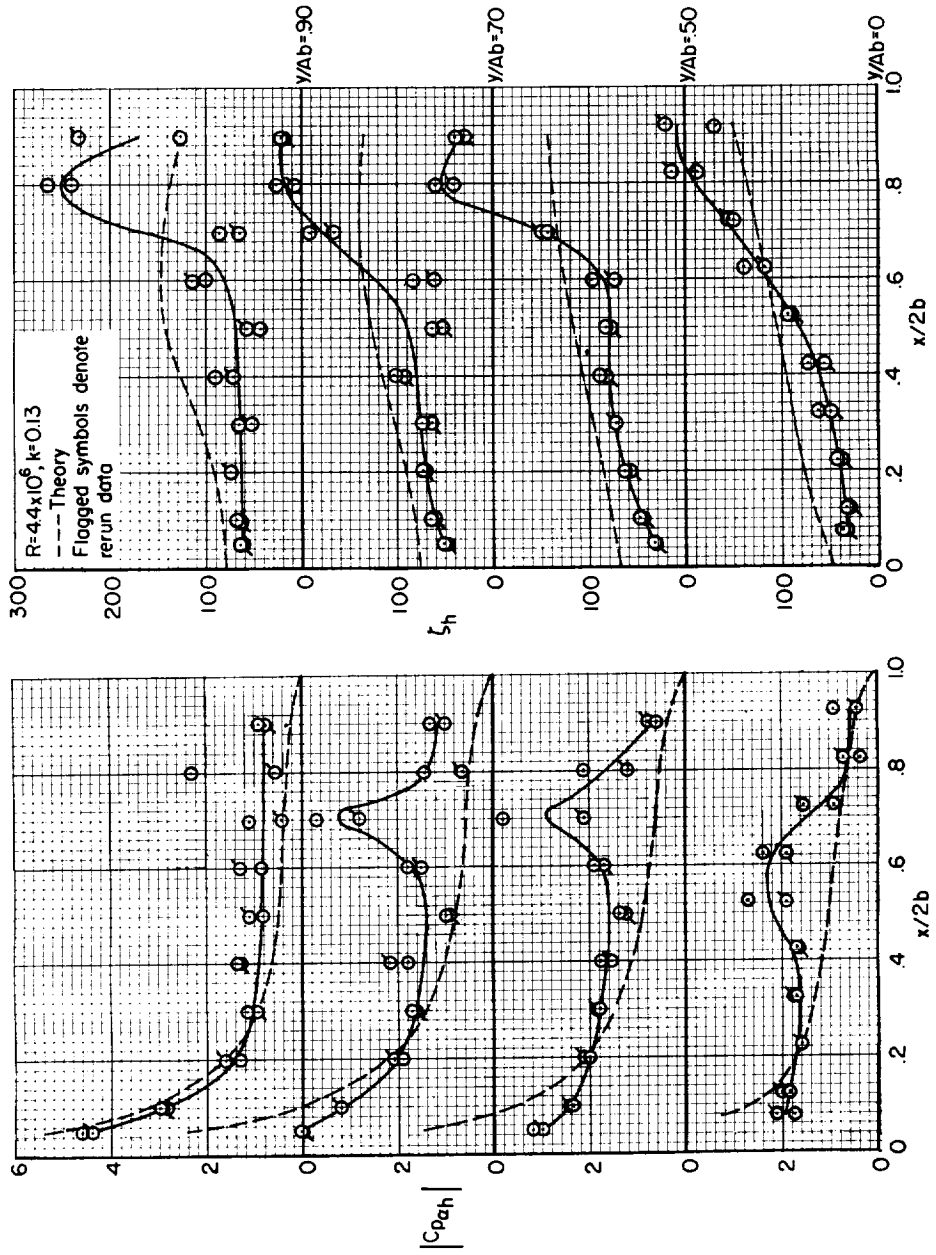


(c) M = 0.90

Figure 9.- Continued.

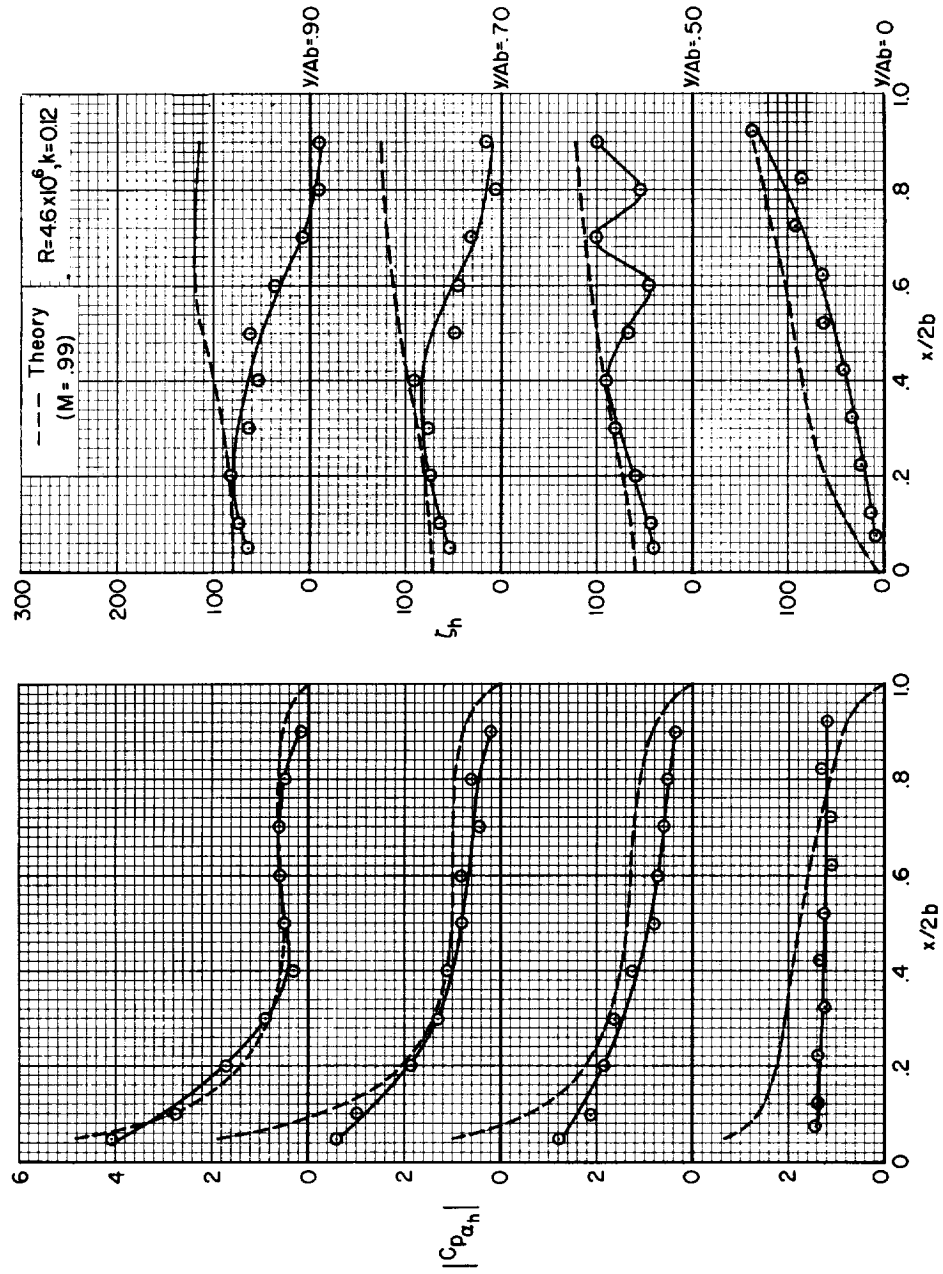


(d) M = 1.00

Figure 9.- Continued.

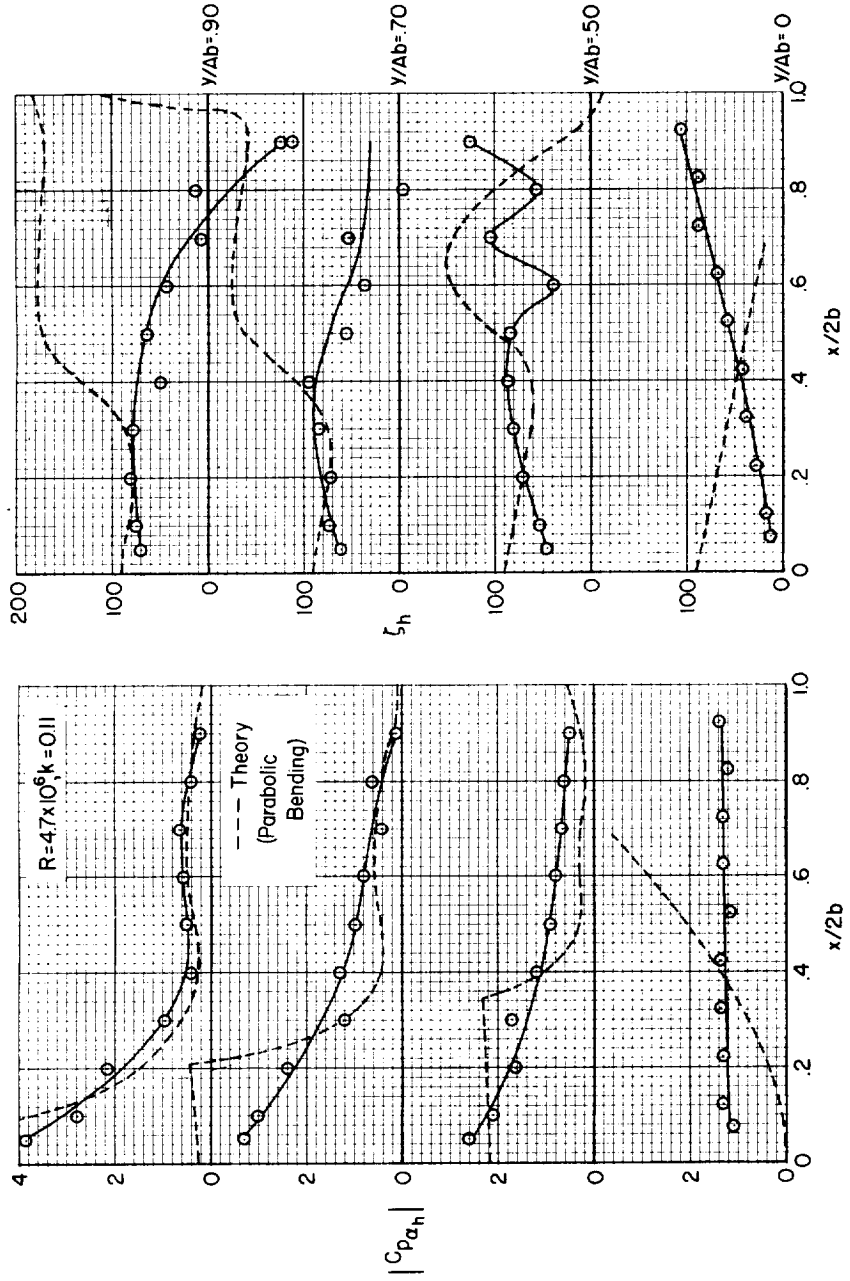


(e) M = 1.10

Figure 9.- Continued.

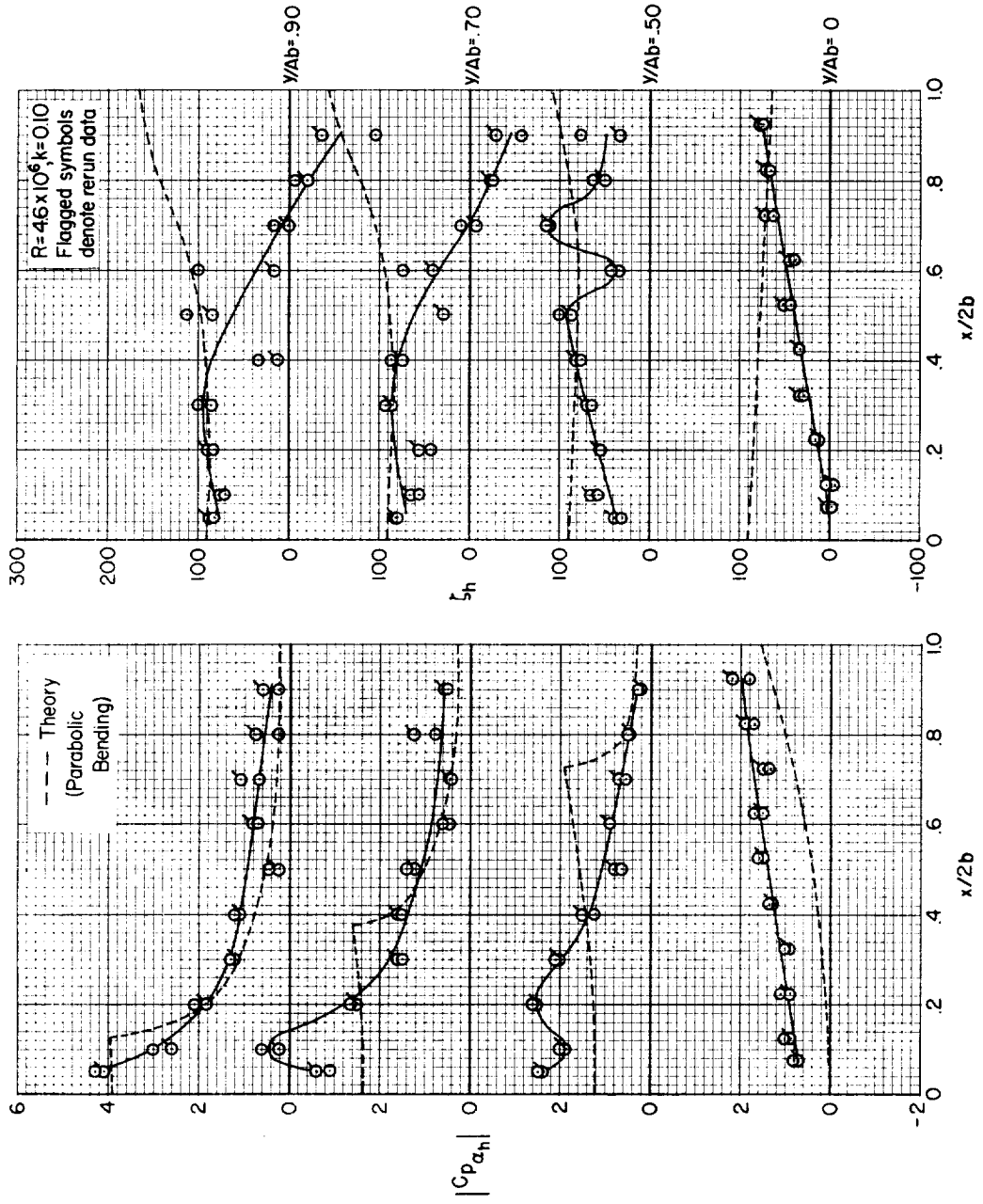


(f) M = 1.30

Figure 9.- Concluded.

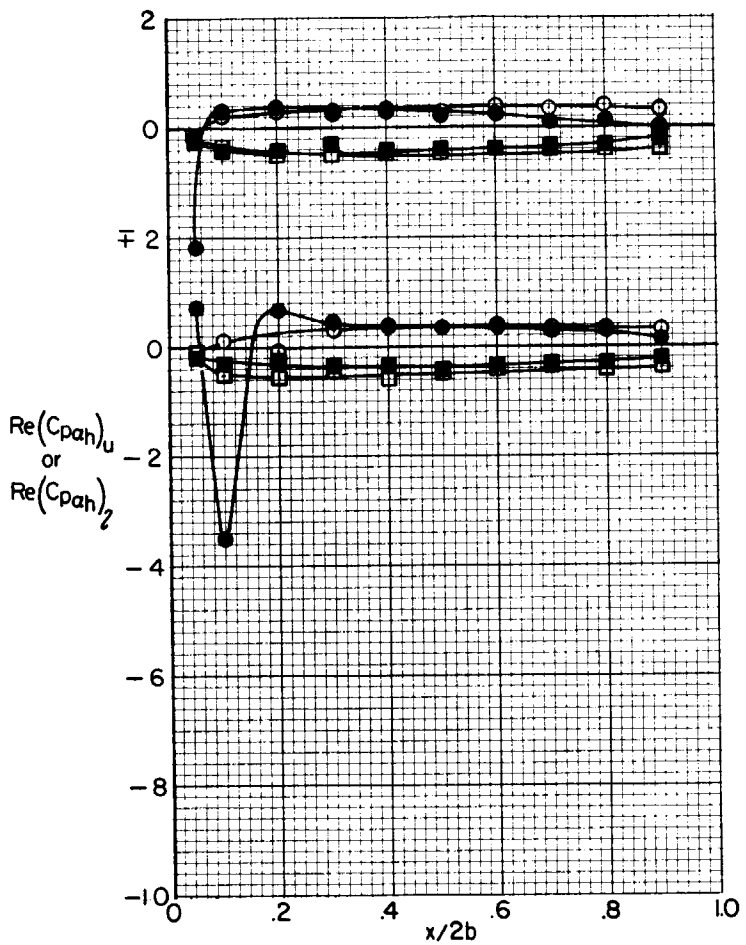


(a) y/Ab = 0.90

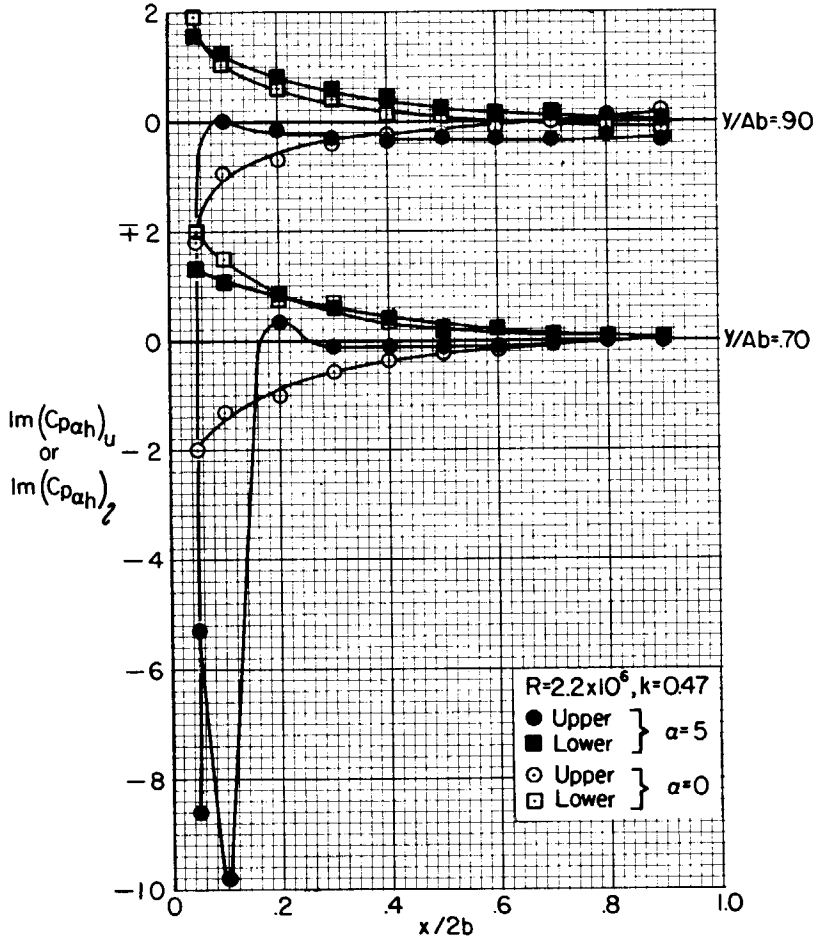


(b) y/Ab = 0.70

Figure 10.- In-phase and out-of-phase components of the surface pressure coefficient at M = 0.24, $\alpha = 0^{\circ}$, and $\alpha = 5^{\circ}$.

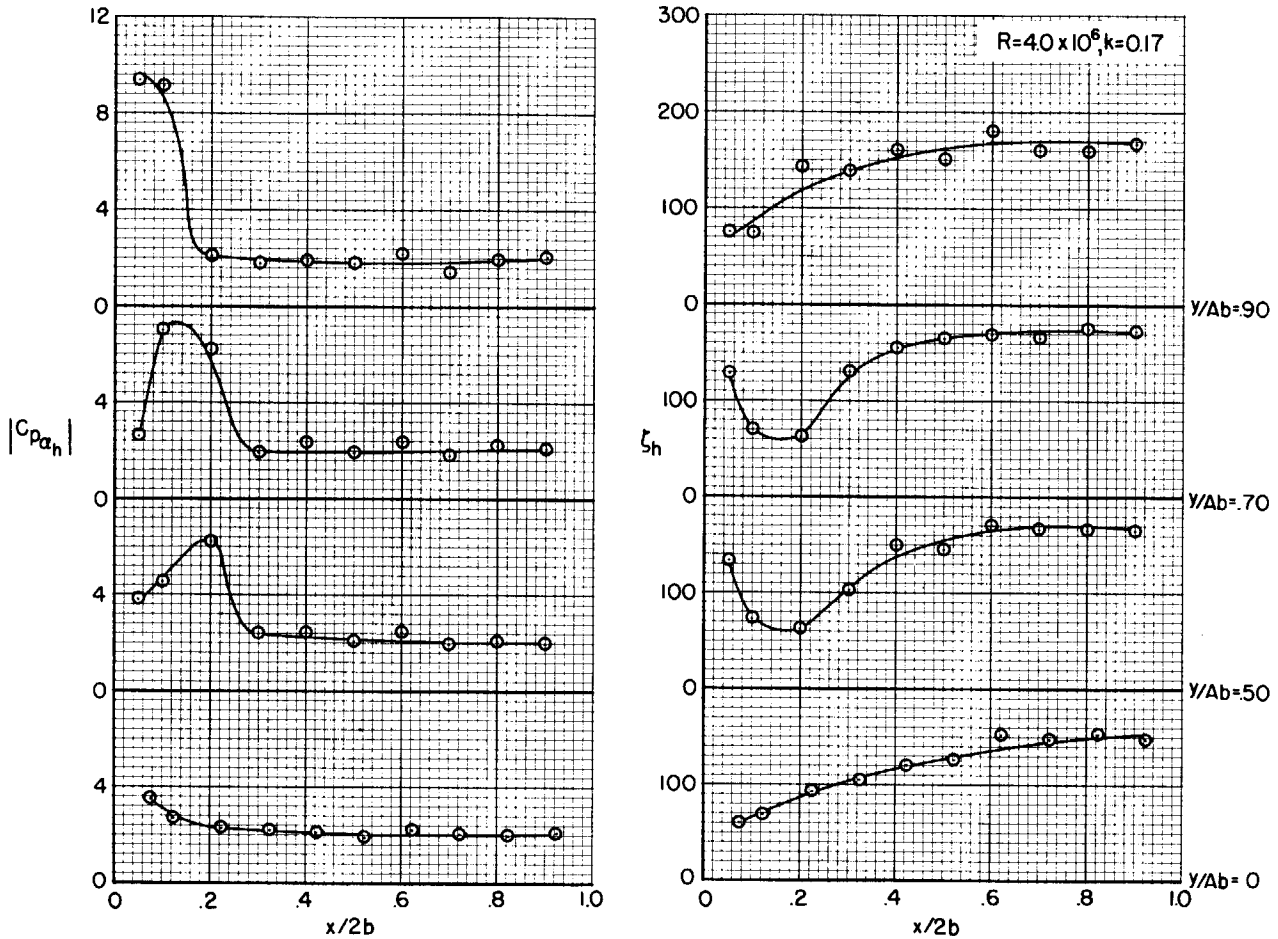


(b) M = 0.70

Figure 11.- Continued.

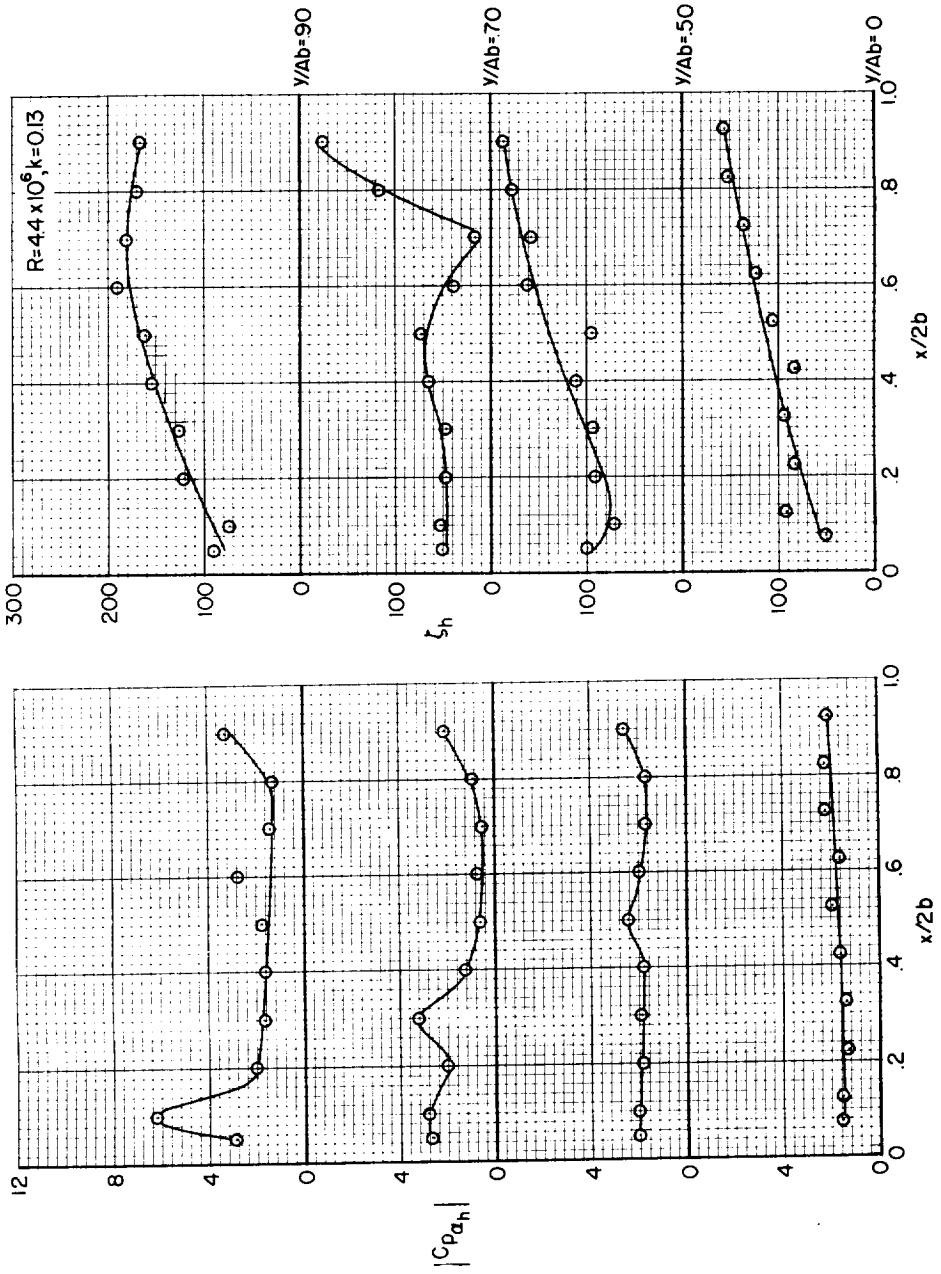


(c) M = 0.90

Figure 11.- Continued.

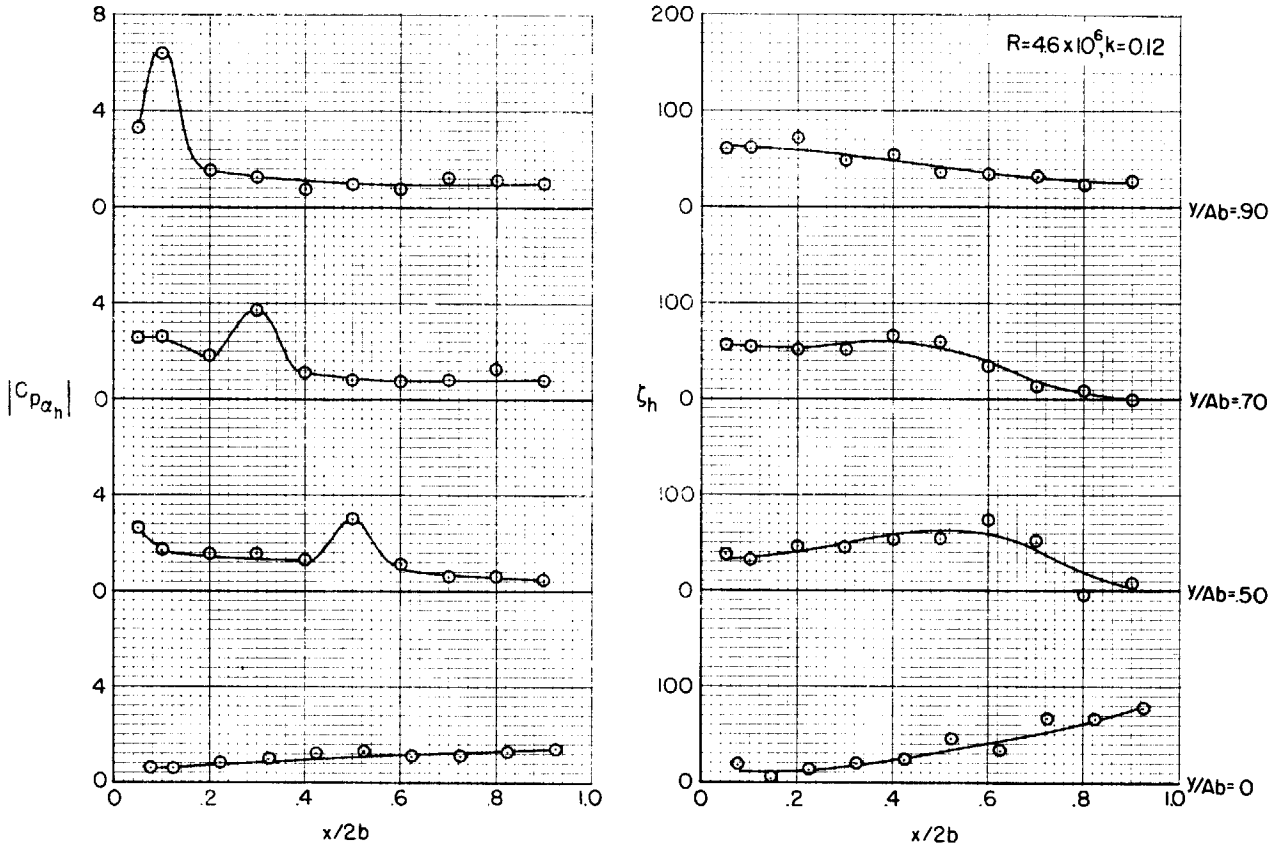


(d) M = 1.00

Figure 11.- Continued.

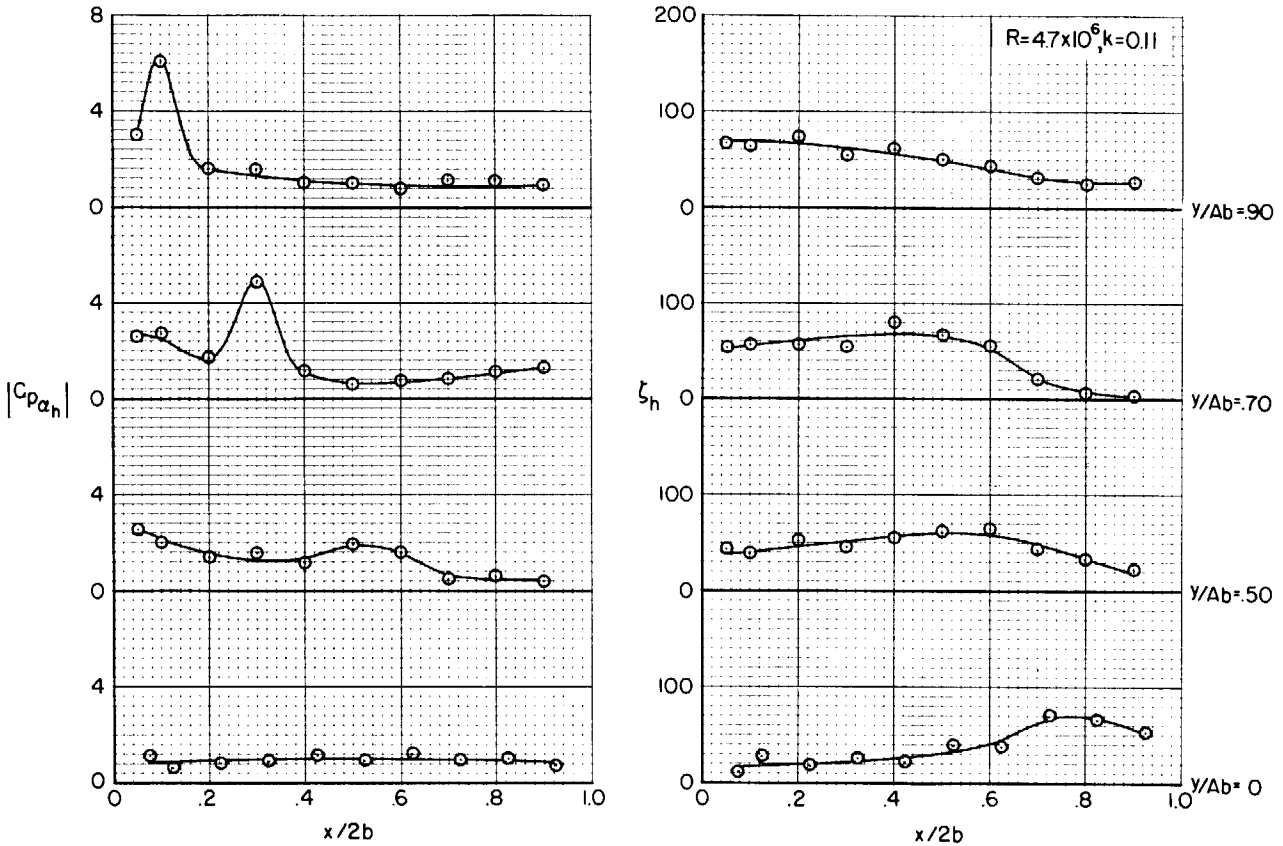


(e) M = 1.10

Figure 11.- Continued.

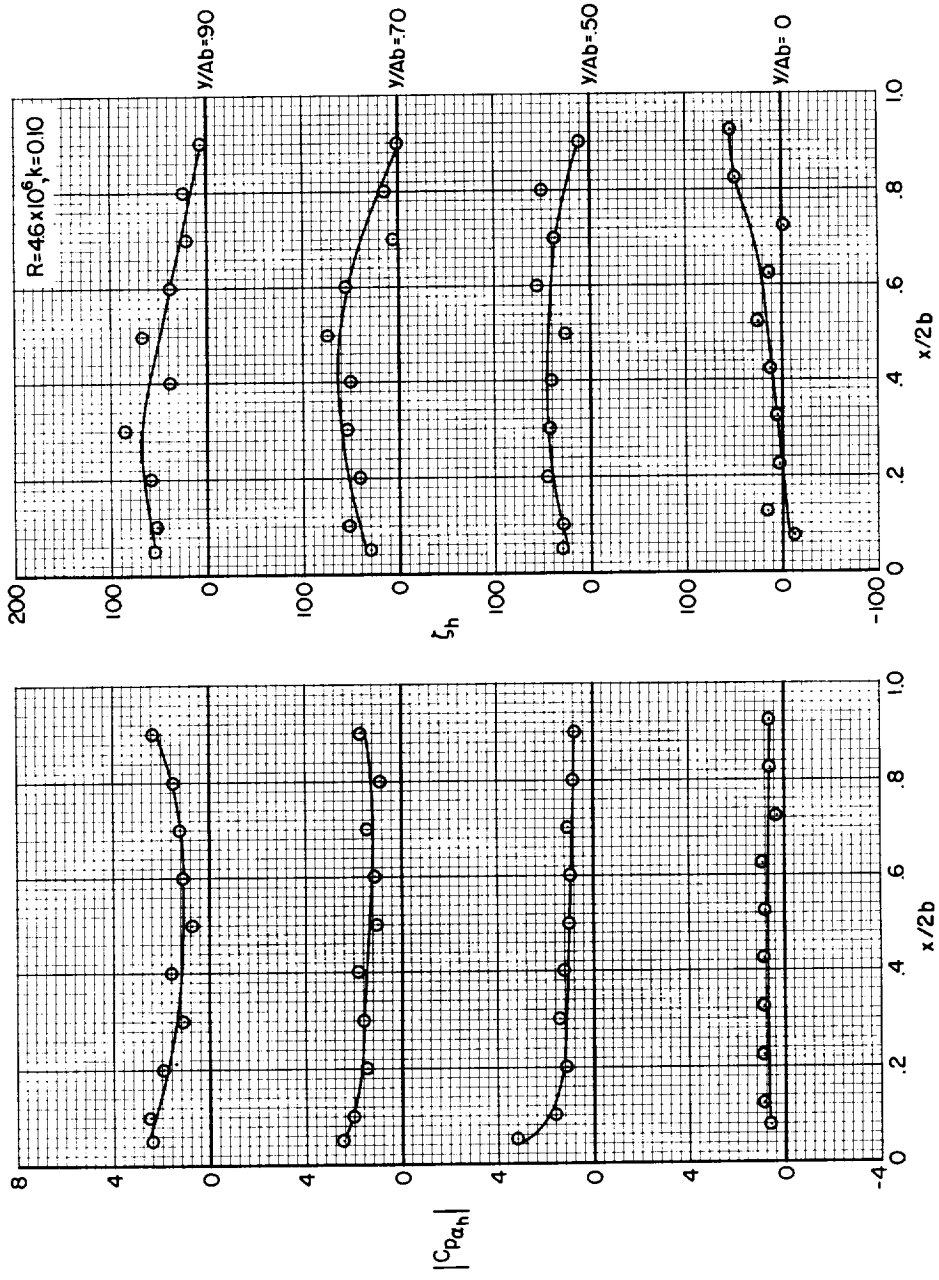


(f) M = 1.30

Figure 11.- Concluded.

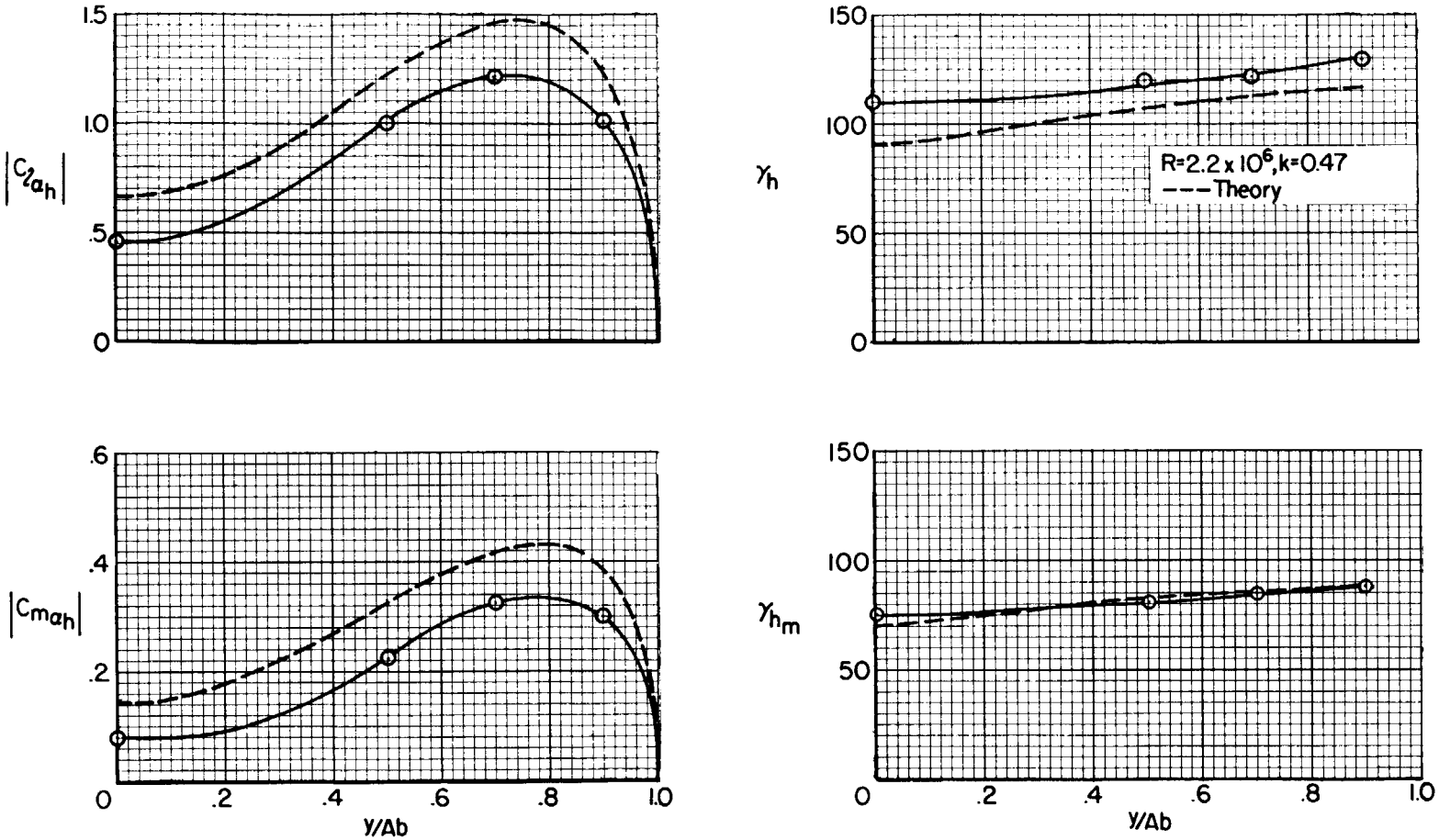


(a) M = 0.24

Figure 12.- Spanwise distributions of the amplitudes and phase angles of the section lift and moment coefficients at $\alpha = 0^{\circ}$.

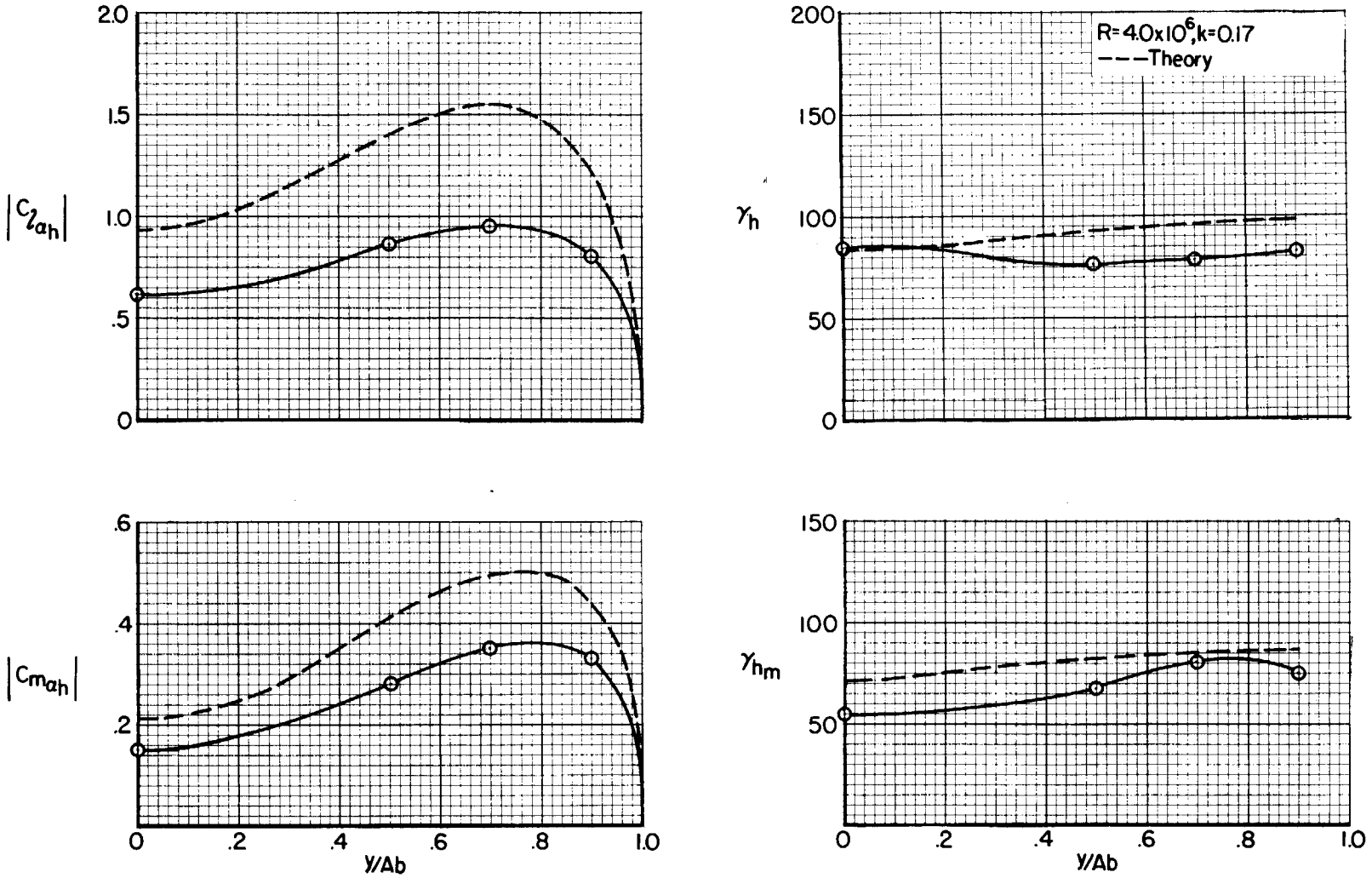


(b) M = 0.70

Figure 12.- Continued.

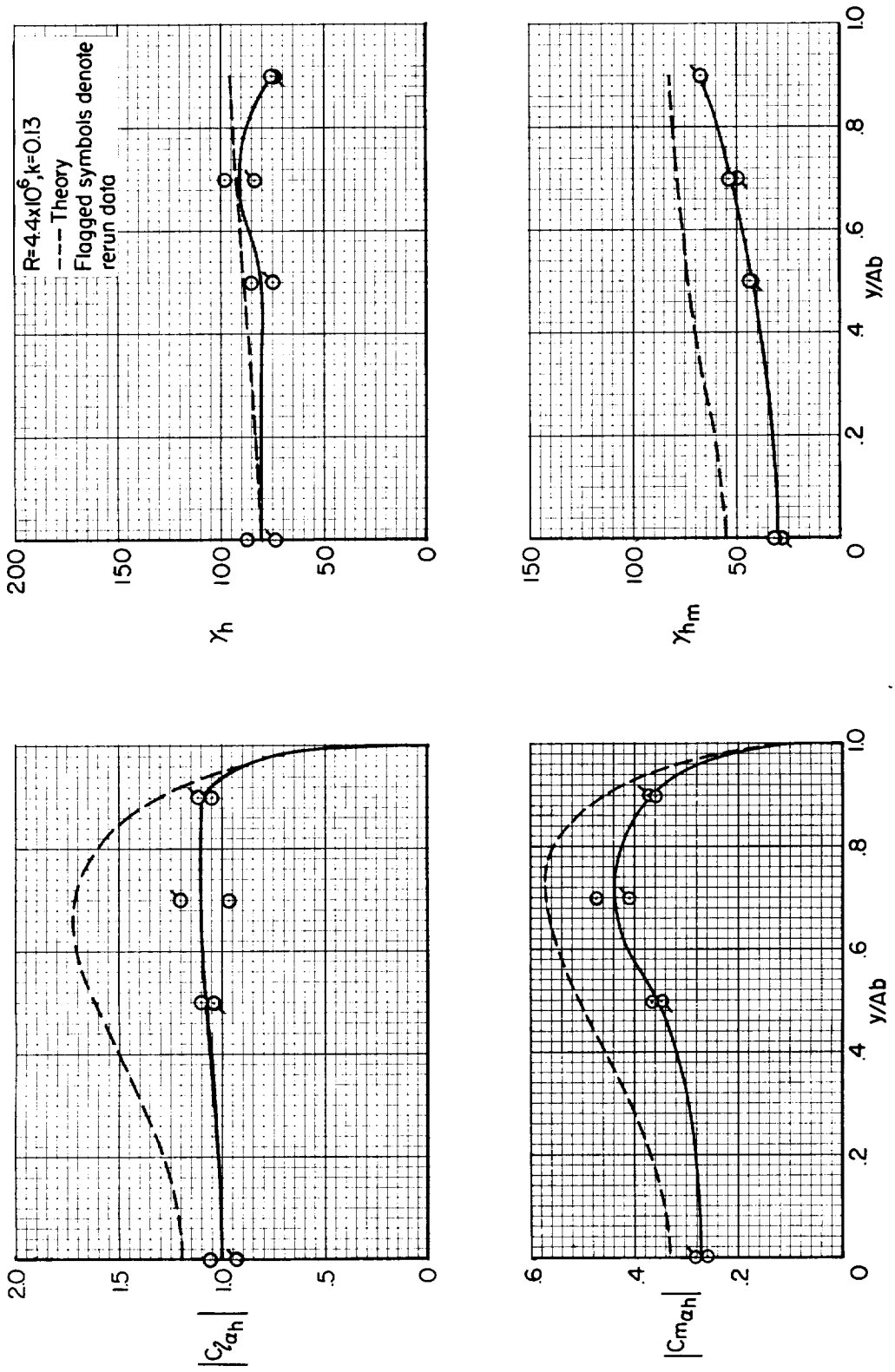


(c) M = 0.90

Figure 12.- Continued.

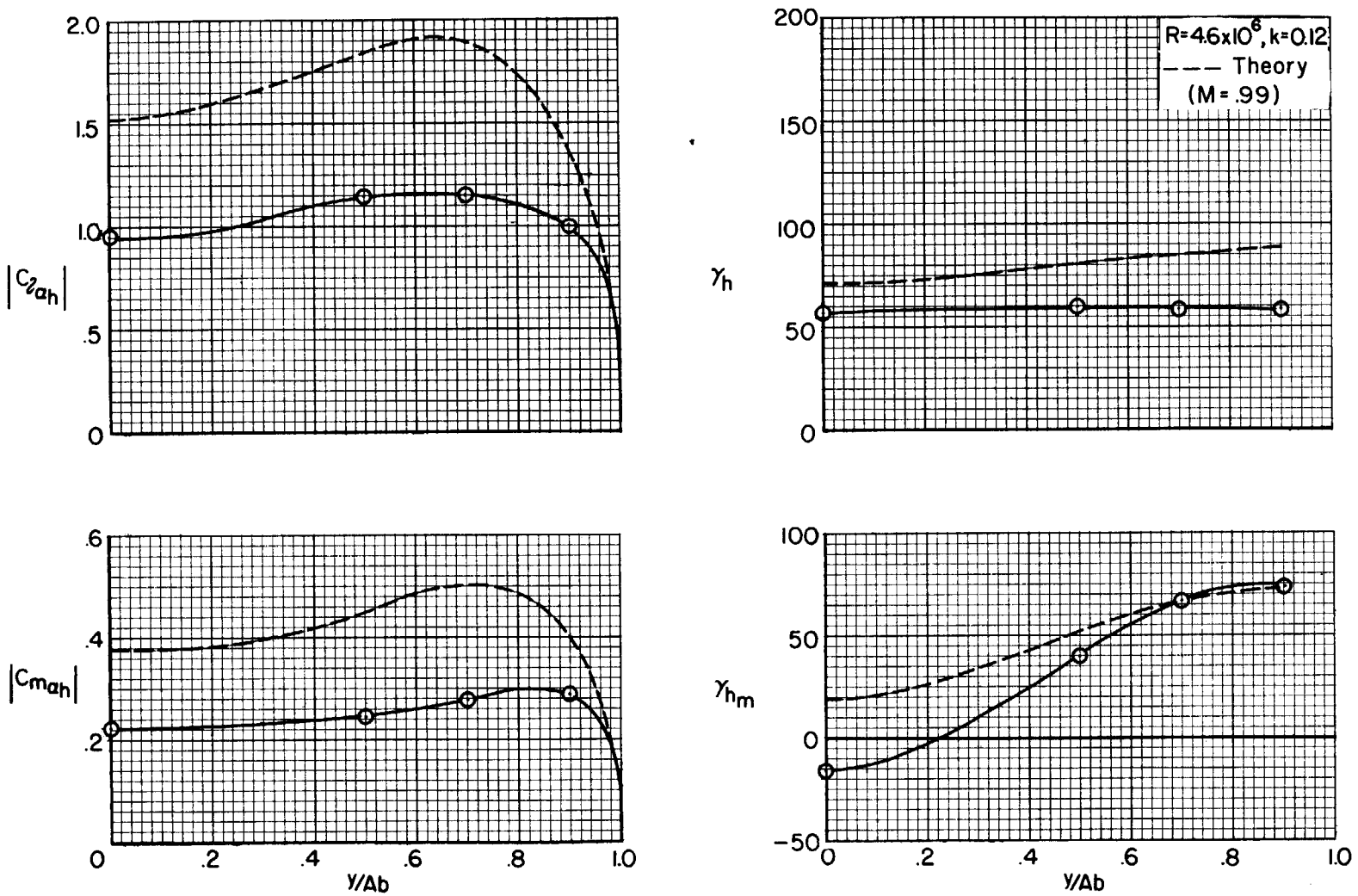


(d) M = 1.00

Figure 12.- Continued.

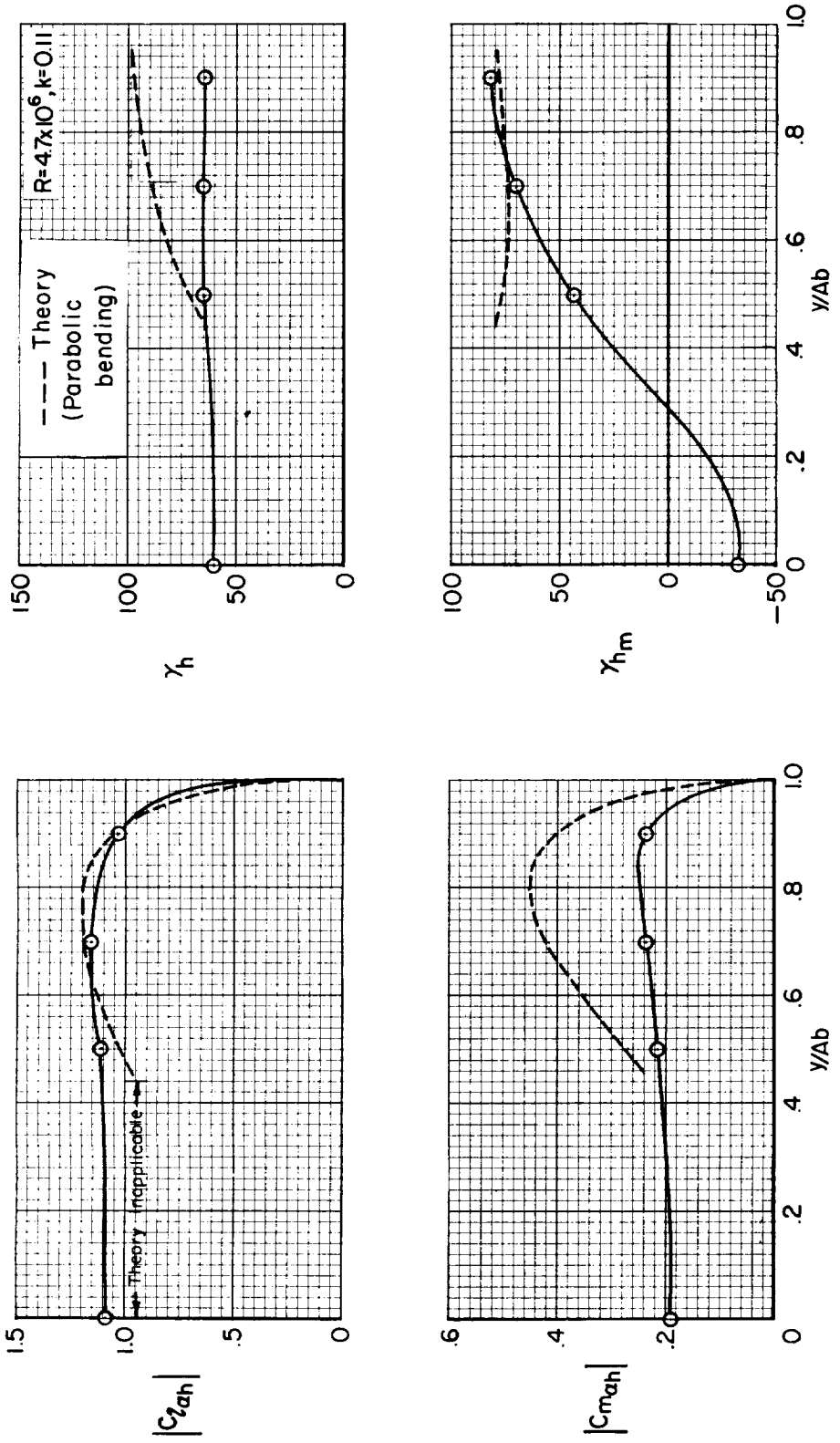


(e) M = 1.10

Figure 12.- Continued.

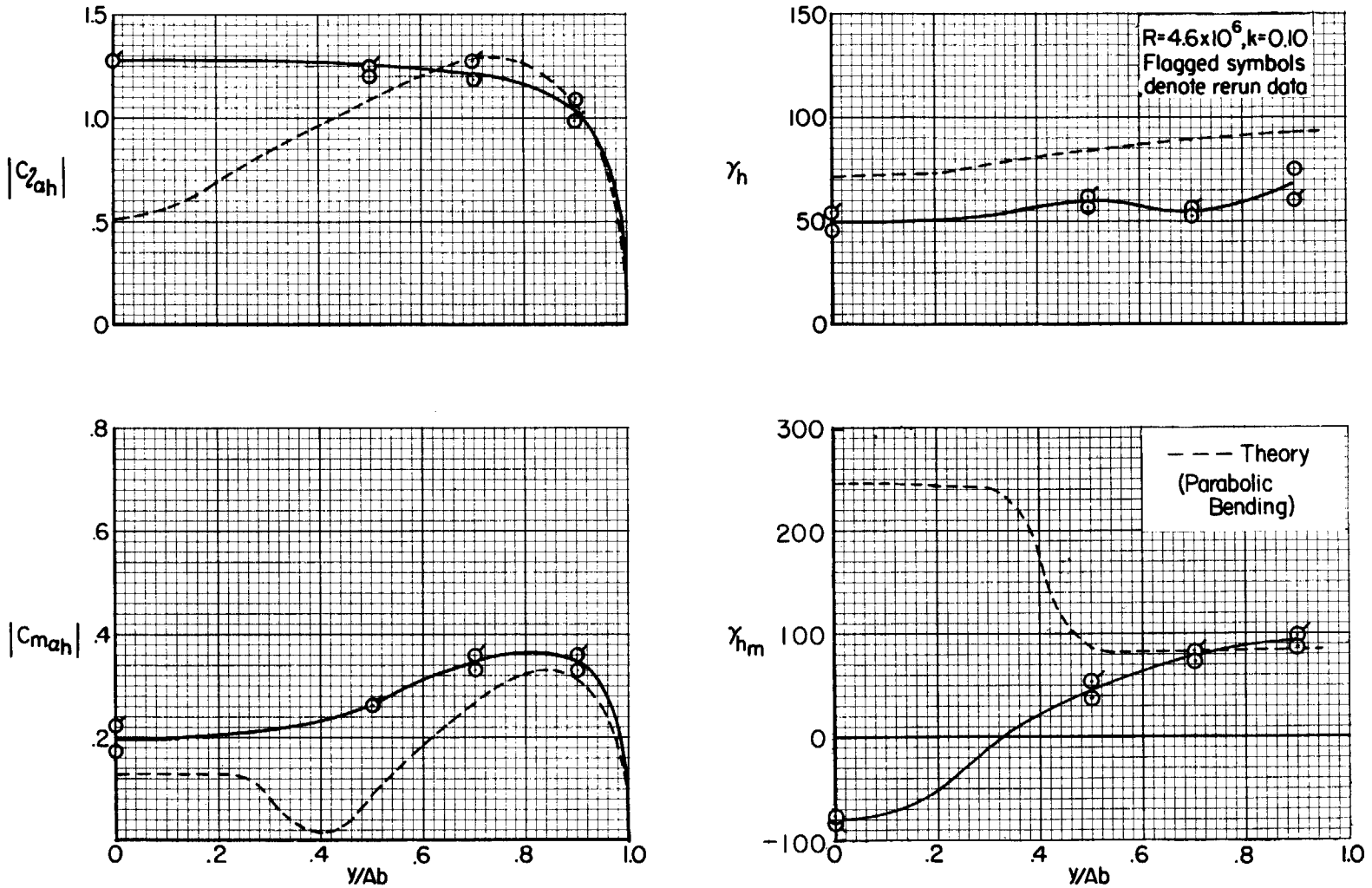


(f) M = 1.30

Figure 12.- Concluded.

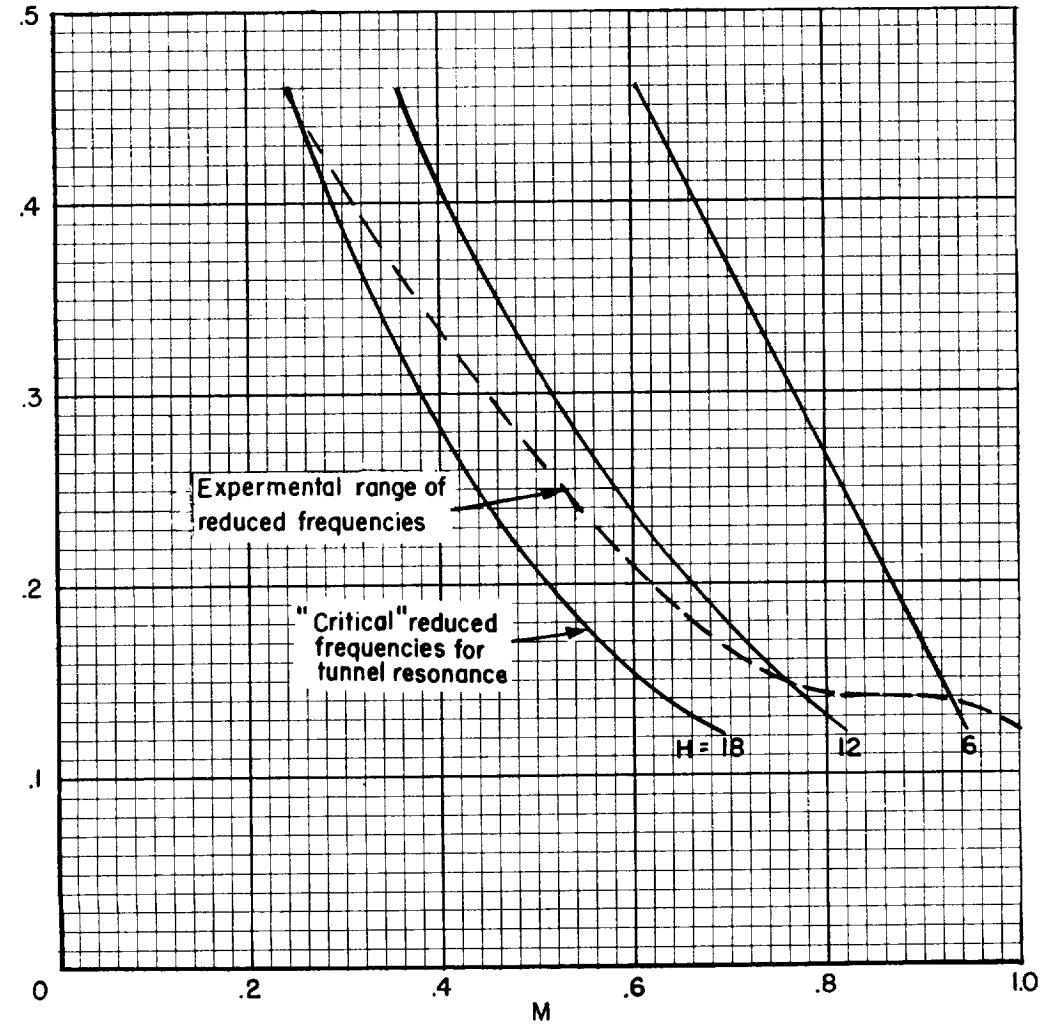


Figure 13.- Comparison of experimental reduced frequencies and theoretical reduced frequencies necessary for tunnel resonance for various effective tunnel heights.

NASA TN D-344
National Aeronautics and Space Administration.
EXPERIMENTAL DETERMINATION OF THE PRESSURE DISTRIBUTION ON A RECTANGULAR WING OSCILLATING IN THE FIRST BENDING MODE FOR MACH NUMBERS FROM 0.24 TO 1.30. Henry C. Lessing, John L. Troutman, and Gene P. Menees. December 1960. 91p. OTS price, $2.25.
(NASA TECHNICAL NOTE D-344)

The results of an experimental investigation in a wind tunnel to obtain the aerodynamic pressure distribution on an unswept rectangular wing oscillating in its first symmetrical bending mode are presented. The wing was of aspect ratio 3 with 5-percent-thick biconvex airfoil sections. Data were obtained at $0^{\circ}$ and $5^{\circ}$ angle of attack in the Mach number range from 0.24 to 1.30. The experimental data are compared with oscillatory pressure distributions computed by means of the most complete linearized theories available.

Copies obtainable from NASA, Washington

I. Lessing, Henry C.
II. Troutman, John L.
III. Menees, Gene P.
IV. NASA TN D-344

(Initial NASA distribution:
1, Aerodynamics, aircraft;
51, Stresses and loads.)

NASA

---

NASA TN D-344
National Aeronautics and Space Administration.
EXPERIMENTAL DETERMINATION OF THE PRESSURE DISTRIBUTION ON A RECTANGULAR WING OSCILLATING IN THE FIRST BENDING MODE FOR MACH NUMBERS FROM 0.24 TO 1.30. Henry C. Lessing, John L. Troutman, and Gene P. Menees. December 1960. 91p. OTS price, $2.25.
(NASA TECHNICAL NOTE D-344)

The results of an experimental investigation in a wind tunnel to obtain the aerodynamic pressure distribution on an unswept rectangular wing oscillating in its first symmetrical bending mode are presented. The wing was of aspect ratio 3 with 5-percent-thick biconvex airfoil sections. Data were obtained at $0^{\circ}$ and $5^{\circ}$ angle of attack in the Mach number range from 0.24 to 1.30. The experimental data are compared with oscillatory pressure distributions computed by means of the most complete linearized theories available.

Copies obtainable from NASA, Washington

I. Lessing, Henry C.
II. Troutman, John L.
III. Menees, Gene P.
IV. NASA TN D-344

(Initial NASA distribution:
1, Aerodynamics, aircraft;
51, Stresses and loads.)

NASA

---

NASA TN D-344
National Aeronautics and Space Administration.
EXPERIMENTAL DETERMINATION OF THE PRESSURE DISTRIBUTION ON A RECTANGULAR WING OSCILLATING IN THE FIRST BENDING MODE FOR MACH NUMBERS FROM 0.24 TO 1.30. Henry C. Lessing, John L. Troutman, and Gene P. Menees. December 1960. 91p. OTS price, $2.25.
(NASA TECHNICAL NOTE D-344)

The results of an experimental investigation in a wind tunnel to obtain the aerodynamic pressure distribution on an unswept rectangular wing oscillating in its first symmetrical bending mode are presented. The wing was of aspect ratio 3 with 5-percent-thick biconvex airfoil sections. Data were obtained at $0^{\circ}$ and $5^{\circ}$ angle of attack in the Mach number range from 0.24 to 1.30. The experimental data are compared with oscillatory pressure distributions computed by means of the most complete linearized theories available.

Copies obtainable from NASA, Washington

I. Lessing, Henry C.
II. Troutman, John L.
III. Menees, Gene P.
IV. NASA TN D-344

(Initial NASA distribution:
1, Aerodynamics, aircraft;
51, Stresses and loads.)

NASA

---

NASA TN D-344
National Aeronautics and Space Administration.
EXPERIMENTAL DETERMINATION OF THE PRESSURE DISTRIBUTION ON A RECTANGULAR WING OSCILLATING IN THE FIRST BENDING MODE FOR MACH NUMBERS FROM 0.24 TO 1.30. Henry C. Lessing, John L. Troutman, and Gene P. Menees. December 1960. 91p. OTS price, $2.25.
(NASA TECHNICAL NOTE D-344)

The results of an experimental investigation in a wind tunnel to obtain the aerodynamic pressure distribution on an unswept rectangular wing oscillating in its first symmetrical bending mode are presented. The wing was of aspect ratio 3 with 5-percent-thick biconvex airfoil sections. Data were obtained at $0^{\circ}$ and $5^{\circ}$ angle of attack in the Mach number range from 0.24 to 1.30. The experimental data are compared with oscillatory pressure distributions computed by means of the most complete linearized theories available.

Copies obtainable from NASA, Washington

I. Lessing, Henry C.
II. Troutman, John L.
III. Menees, Gene P.
IV. NASA TN D-344

(Initial NASA distribution:
1, Aerodynamics, aircraft;
51, Stresses and loads.)

NASA